Nebraska Specific Slope Design Manual

Chung R. Song, Ph.D., A.E.
Associate Professor
Department of Civil Engineering
University of Nebraska-Lincoln

Yong-Rak Kim, Ph.D.
Professor
Hossein Bahmyari
Graduate Research Assistant
Layal Bitar
Graduate Research Assistant
Soroosh Amelian
Graduate Research Assistant

Nebraska Specific Slope Design Manual

Chung R. Song, Ph.D., A.E.
Associate Professor
Department of Civil Engineering
University of Nebraska-Lincoln

Yong-Rak Kim, Ph. D.
Professor
Department of Civil Engineering
University of Nebraska-Lincoln

Hossein Bahmyari
Graduate Research Assistant
Department of Civil Engineering
University of Nebraska-Lincoln

Layal Bitar
Graduate Research Assistant
Department of Civil Engineering
University of Nebraska-Lincoln

Soroosh Amelian
Graduate Research Assistant
Department of Civil Engineering
University of Nebraska-Lincoln

A Report on Research Sponsored by

December 2018

Technical Report Documentation Page

1. Report No. NDOT: SPR-1(17) M061 NTC: 26-1121-4036-001	2. Government Accession No.	3. Recipient's Catalog No.	
4. Title and Subtitle Nebraska Specific Slope Design Manual		5. Report Date December 2018	
		6. Performing Organization Code	
7. Author(s) Chung R. Song, Ph.D., Hossein Bahmyari, and Layal Bitar		8. Performing Organization Report No. 26-1121-4036-001	
9. Performing Organization Name and Address Nebraska Department of Transportation 2200 Vine St. P.O. Box 830851 Lincoln, NE 68583-0851		10. Work Unit No.	
		11. Contract or Grant No.	
12. Sponsoring Agency Name and Address Nebraska Transportation Center 2200 Vine Street PO Box 830851 Lincoln, NE 68583-0851		13. Type of Report and Period Covered Final Report (July, 2016 – Dec. 2018)	
		14. Sponsoring Agency Code	
15. Supplementary Notes			

16. Abstract

This study introduces proper design and retrofitting techniques to mitigate slope failure in Nebraska based on experimental and analytical research. The geological history, unique soil properties, failure mechanisms and potential new design/retrofitting methods are accounted for in this study. The following are the key findings.

Nebraska is covered by glacial tills, loess/sands, and shales with expansive clay minerals. Loess and shales are often highly overconsolidated due to the high overburden from Laurentide ice sheet which covered North America between 0.1 M to 0.02 M years ago. Overconsolidated expansive shale clays often exhibit time dependent strength reduction, and collapsible loess often exhibit much lower residual strength than the peak strength. The test results showed the presence of overconsolidated conditions and expansive clays. Test specimens show that the unconfined compression strength and the consolidated undrained strength are higher than the consolidated drained shear strength for clayey soils; typical behavior of overconsolidated conditions. Also, test specimens showed that the residual strength of unconfined compression and the consolidated drained shear strength were substantially lower than that of unconfined compression and consolidated undrained shear strength; typical behavior of clays containing expansive clay minerals. Some test specimens even showed volume expansion during consolidation.

XRD (X-ray Diffraction) tests showed montmorillonite clay minerals (as high as 11%) in specimens, explaining the expansive behavior and lower residual drained shear strength. Although unconfined compression tests are easy and inexpensive, this method may overestimate the long term strength of Nebraska soils. This study recommends that the consolidated drained strength be used for the design of new slopes and retrofitting techniques. Among several retrofitting techniques, earth anchor and biopolymer based reinforcement are recommended. Earth anchors are recommended because the resisting force is provided by deep soil layers which are free from weathering and associated strength reduction. Biopolymer based soil treatment is recommended because the technique showed promising weathering resistance in this research. However, biopolymer based soil treatment technique is not thoroughly verified, further verification research may be needed.

17. Key Words Slope stability, expansive soils, Pierre shale, Loess, Glacial Till		18. Distribution Statement No restrictions.		
19. Security Classif. (of this report) Unclassified		20. Security Classif. (of this page) Unclassified	21. No. of Pages 176	22. Price

Form DOT F 1700.7 (8-72)   Reproduction of completed page authorized

Table of Contents

List of Figures

List of Tables

Abstract

This study introduces design and retrofitting techniques to mitigate slope failure in Nebraska based on experimental and analytical research. The geological history, unique soil properties, failure mechanisms and potential new design/retrofitting methods are accounted for in this study. The following are the key findings.

Nebraska is covered by glacial tills, loess/sands, and shales with expansive clay minerals. Loess and shales are often highly overconsolidated due to the high overburden from Laurentide ice sheet which covered North America between 0.1 M to 0.02 M years ago. Overconsolidated expansive shale clays often exhibit time dependent strength reduction, and collapsible loess often exhibit much lower residual strength than the peak strength.

The test results showed 1) the presence of overconsolidated conditions and expansive clays; 2) higher unconfined compression strength and the consolidated undrained strength than the consolidated drained shear strength for clayey soils, a typical behavior of overconsolidated conditions. Also, test specimens showed that the residual strength of unconfined compression and the consolidated drained shear strength were substantially lower than that of unconfined compression and consolidated undrained shear strength; typical behavior of clays containing expansive clay minerals. Some test specimens even showed volume expansion during consolidation.

XRD (X-ray Diffraction) tests showed montmorillonite clay minerals (as high as 11%) in specimens, explaining the expansive behavior and lower residual drained shear strength. Although unconfined compression tests are easy and inexpensive, this method may overestimate the long term strength of Nebraska soils. This study, therefore, recommends that the consolidated drained strength be used for the design of new slopes and retrofitting techniques.

Among several retrofitting techniques, earth anchor and biopolymer based reinforcement are recommended. Earth anchors are recommended because the resisting force is provided by deep soil layers which are free from weathering and associated strength reduction. Biopolymer based soil treatment is recommended because the technique showed promising weathering resistance in this research. However, biopolymer based soil treatment technique is not thoroughly verified, further verification research may be needed.

Chapter 1 Introduction

1.1 Geological History or Nebraska

It is helpful to review the geological history of Nebraska in order to better understand the uniqueness of slope failure pattern in Nebraska. Based on research by Frank (2018), Nebraska had been inundated by the sea several times. Modern surface rocks and soils are mostly formed after Mid Cretaceous era or Late Mesozoic era. Around this time, around 100 M years ago, Nebraska was completely under the sea called "Western Interior Seaway" also known as "Niobraran Sea". During this time, shales, chalks and sandstones belong to Dakota group were formed. Many rocks such as Pierre Shales (containing shales with occasional bentonite layers) and Niobrara formation (mostly containing chalks and marls) were formed as well. From about 50 M years ago, the water in Western Interior Seaway receded and Nebraska became a dry land. From about 8 M years ago, volcanic deposit such as loess and sand became abundant due to frequent volcanic activities in the west. From about 2.5 M years ago, glaciation caused the climate of Nebraska to be arid and resulted in the formation of sand hills and sand dunes. Subsequent melting of ice sheets brought glacial deposits to Nebraska. The Laurentide ice sheet that covered North America between 0.1 M to 0.02 M years ago, ranged to East Nebraska, brought glacial deposit called "Tills" or "Glacial Tills".

In summary, modern Nebraska soils are shales, chalks, and sand stones formed about 100 M years ago, volcanic deposits and sand formed about 8 M years, and glacial deposit formed about 0.1 M to 0.02 M years ago.

1.2 Geotechnical Implications

Geotechnically, shales are known to become slippery along cracks or open joints when subjected to ground water infiltration and weathering. The weathered shales with occasional bentonite layers can cause a particular geotechnical problem called "expansive soils" or "swelling

soils". Expansive soils have unbalanced Na^+ or Ca^{++} ions in its structure and tend to absorb polarized water molecules. This absorption of water causes the clays to expand and lose strength. When expansive soils lose water by evaporation, they shrink and become strong; causing seasonal high strength.

Loesses are wind-blown volcanic deposits. They are light weight and possess loose structure. Loesses are known to lose strength and become collapsible when they are saturated and exposed to stresses greater than its strength.

Glacial tills are usually known to be fertile for farming purposes. They are slowly sedimented particles from melting ice and are weak in strength. Glacial tills also implies the release of overburden pressure from the disappearing glacier that was 400 m to 32 m thick. The melting ice caused enormous stress release to the underlain soils which are loesses and shales. The release of overburden pressure sometimes caused expansion, cracked underlain soils, and accelerated degradation of strength of underlain soils.

Distribution of these problematic soils in Nebraska and other Midwestern states can be anticipated by the geological history. The distribution of shales and expansive soils closely match the range of the Old Western Interior Seaway as shown in Figure 1.1.
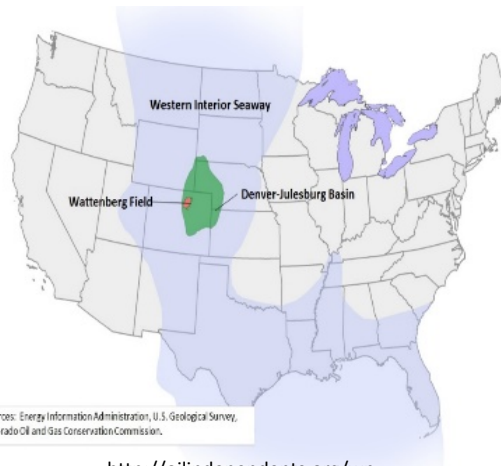
Figure 1.1 (a) Location of Western Interior Sea (Wikipedia, 2018); (b) Distribution of Expansive Soils (Oilindepents.org, 2018)

Loess is state-widely distributed except central Nebraska where thick and widely distributed sand dunes are distributed.
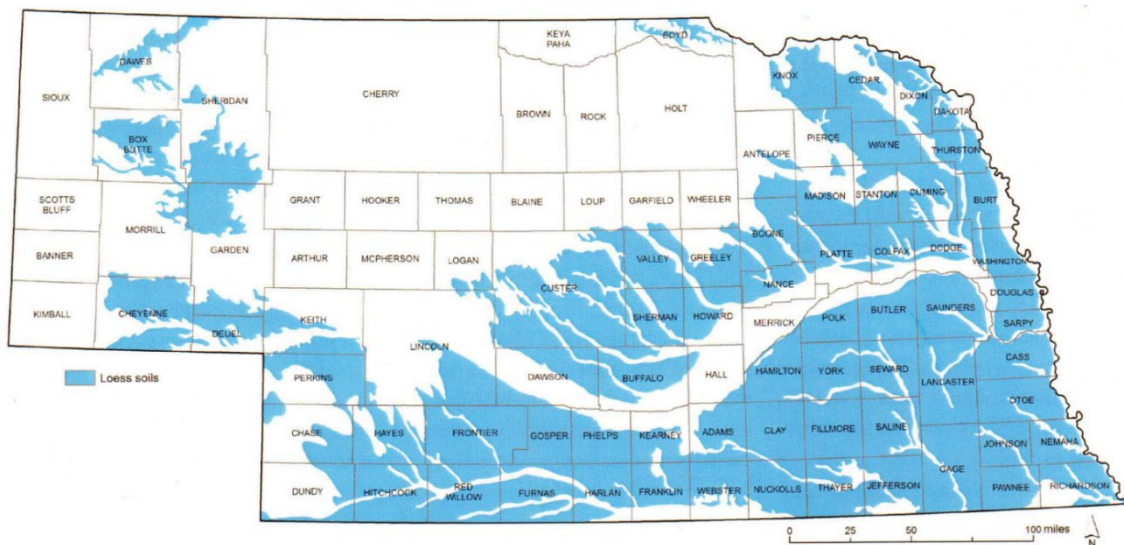
Figure 1.2 Distribution of Loess (Eversoll)

3

Distribution of glacial till is mostly on the east and north east of Nebraska as shown in Figure 1.3 due to the extent of Laurentide ice sheet during the last ice age.
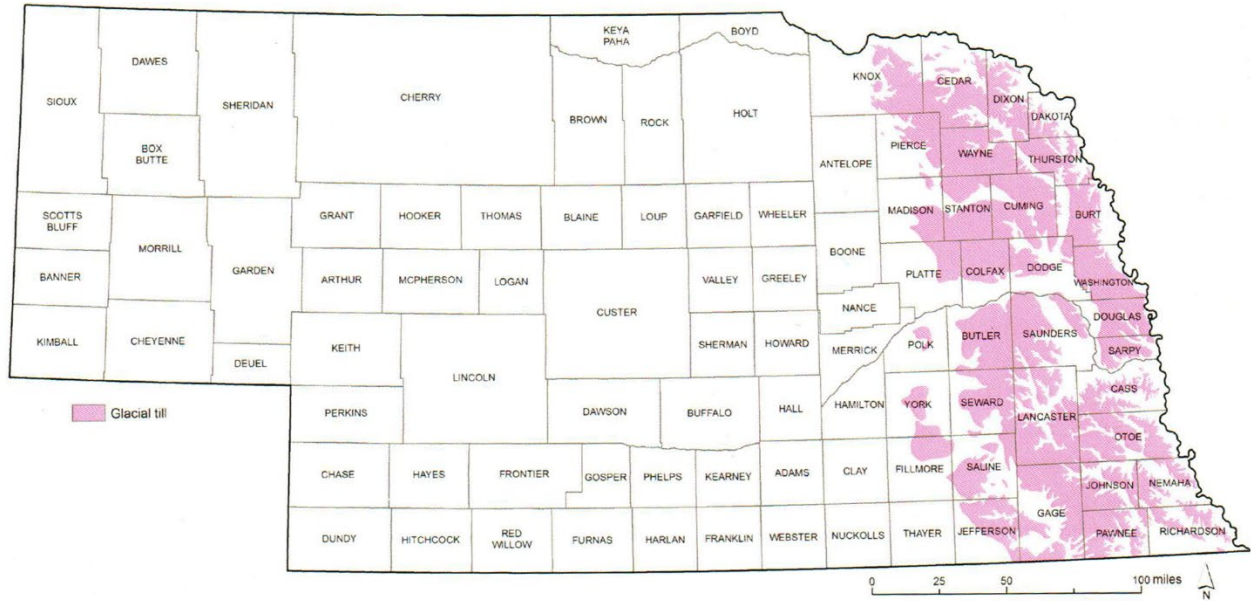
Figure 1.3 Distribution of glacial tills (Eversoll, 2013)

1.3 Surface Topography

With all the geological conditions discussed earlier, the slopes may not fail if the slope angles are gentle enough. Figure 1.4 shows the surface slope in percentile. The slopes along the Niobrara River, Missouri River, and small tributary rivers to the Platte River appear high. The combination of steep slope, Loess, and rainfall may create conditions susceptible to landslides in these areas.
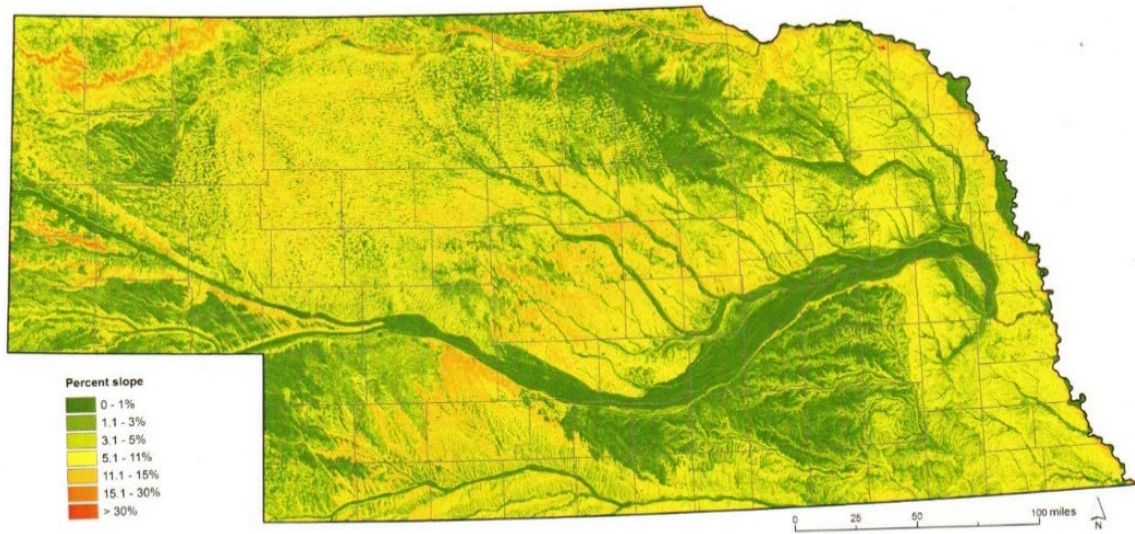
Figure 1.4 Surface topographic slope (After Eversoll, 2013)

1.4 Precipitation

Rain fall affects the ground water Table, usually increasing the driving force while reducing resisting force. The yearly precipitation recorded by Eversoll (2013) in Figure 1.5 shows that East Nebraska has high to extremely high rainfall, indicating that the precipitation may be another factor leading to slope failure.
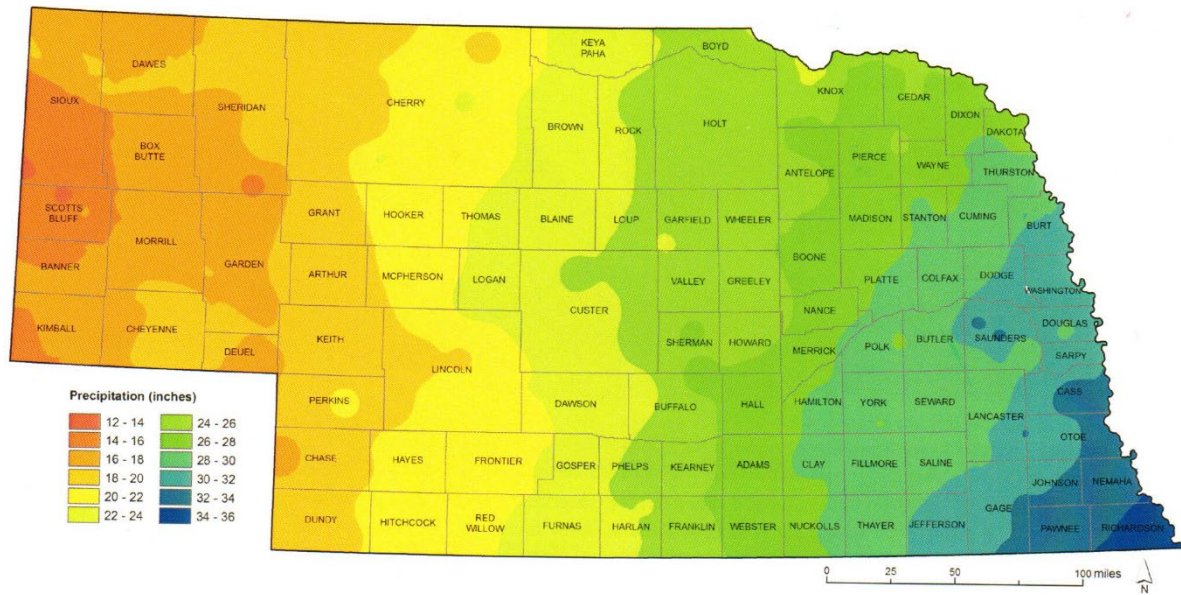
Figure 1.5 Annual precipitation record (After Eversoll, 2013)

1.5 Temperature

The temperature of Nebraska is high in the summer and particularly cold in the winter. The temperature pattern during Jan. 2016 is shown in Figure 1.6 A special weather pattern that may affect the rock slope stability is the repeated freeze and thaw pattern. This weather pattern will allow precipitation to infiltrate into rocks through cracks and joints. Then this water can freeze, applying high expansion pressure resulting in new cracks or expanding existing cracks. The repeated cycle of freeze and thaw is one of the potential factors which can cause rock fall or rock slope sliding.

This research team has found common and regionally unique reasons for slope failure in Nebraska through summarizing the geological, topographical and precipitation conditions. Many times, however, a standard slope design (FHWA, 2007; FHWA; NDOR, 2006; NDOR, 2010) does not provide enough details to consider these localities. This research team will study detailed mechanisms of these landslides in Nebraska through additional investigations and tests.

6
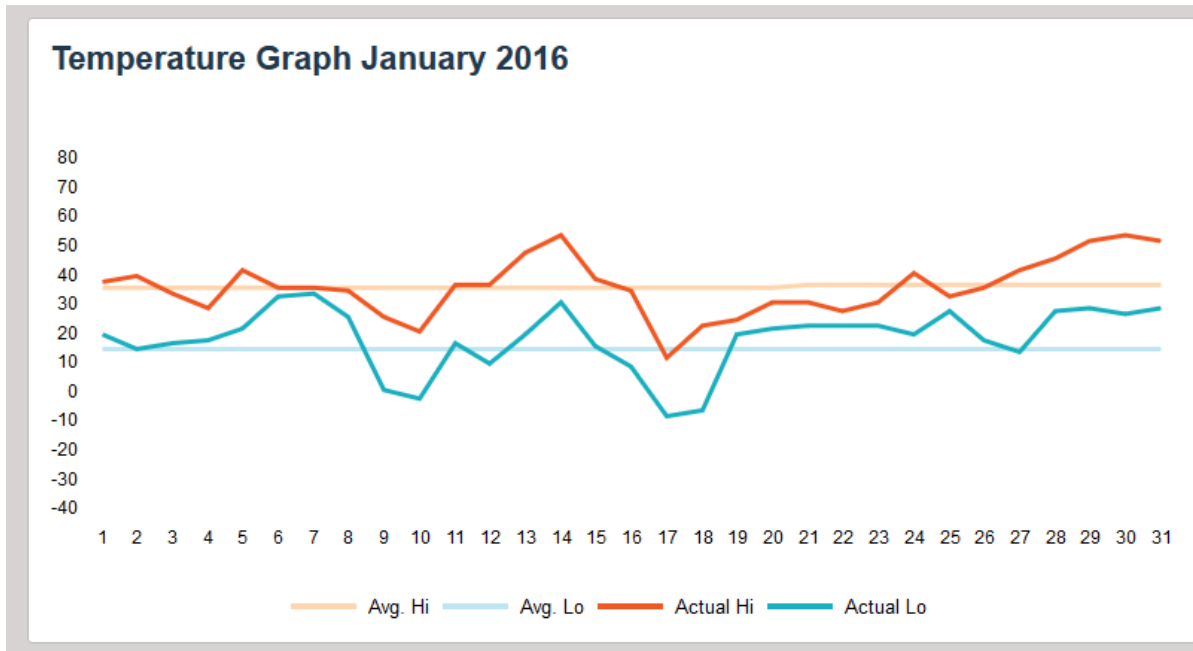
Figure 1.6 Temperature pattern of Lincoln, NE for Jan. 2016 (Accuweather, 2016)

1.6 Summary

Based on the landslide map by Eversoll (2013), it is clear that the landslides in Nebraska are concentrated in the Eastern and North Eastern part of Nebraska where it has thicker deposit of glacial tills, exposed loess/shales that could lose strength by severe weathering, and steeper surface grade.
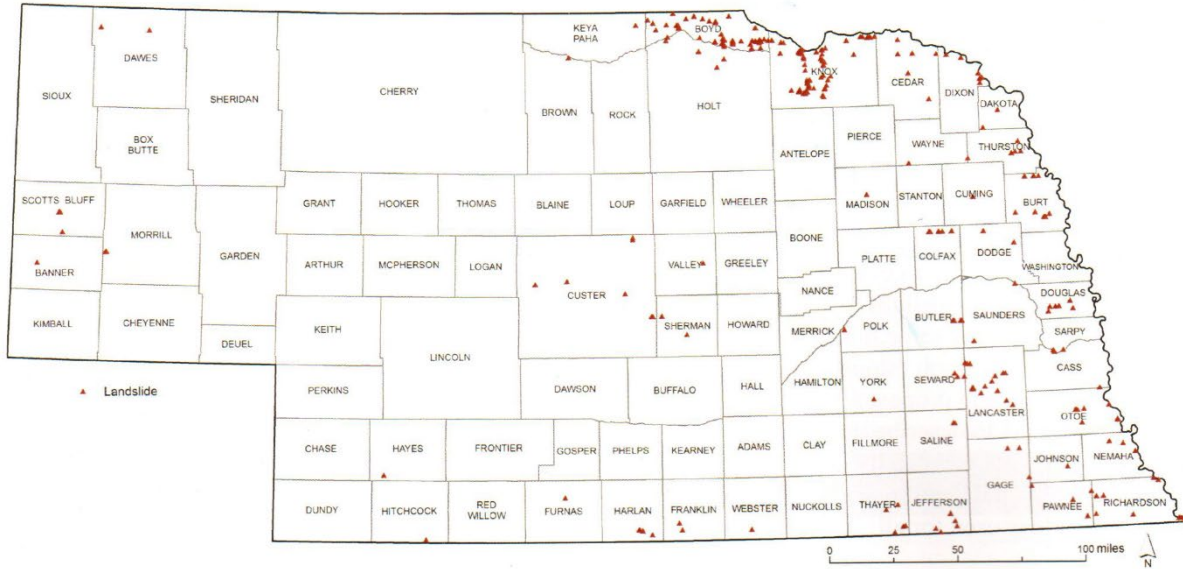
Figure 1.7 Reported landslides in Nebraska (after Eversoll, 2013). Red triangular dots represent location of landslide.

Therefore, it is obvious that detailed strength characteristics of soils in Nebraska need to be clarified and subsequent slope retrofitting and design techniques need to be developed. To achieve these goals the following researches were conducted:

- Characterization of shear strength parameters of overconsolidated soils in undrained and drained condition at low confining effective stress mimicking shallow depth condition.

- Characterization of swelling behavior of soils.

- Developing slope failure mechanism in Nebraska

- Developing suiTable shear strength for designing stable slopes in Nebraska

- Developing Nebraska specific slope retrofitting technique for existing slopes

Chapter 2 Literature Review

2.1 Slope stability analysis in overconsolidated soils

The behavior of overconsolidated soils is different from that of normally consolidated soils. For undrained conditions, overconsolidated soils tend to develop negative excess pore pressure and result in high shear strength, while the behavior of normally consolidated soils is opposite and results in lower shear strength as depicted in Figure 2.1.
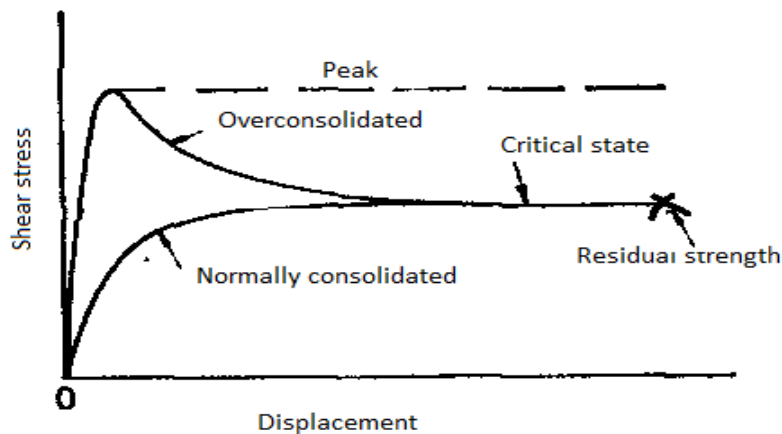
Figure 2.1 Shear test result on clayey soils under drained condition (Skempton 1970)

In designing slopes, the peak strength is typically used due to the fact that the soils in a slope will not experience the residual condition as far as the driving stress in the field does not exceed the peak strength. In particular soils such as overconsolidated swelling soils, however, the peak strength of the soil itself may be substantially reduced due to the stress release and swelling. For Loess, it may lose strength upon becoming wet. For layered soils, the strength reduction in localized layers may be accumulated as weathering cycles continue, and it may cause localized failure in weaker layers at some point. Once this localized failure and strength reduction happen in a critical layer, the next layer needs to provide additional resisting force which used to be provided by the failed layer, then this next layer may experience the failure and strength reduction

9

as time goes on. Therefore, the residual strength may be a better soil strength parameter in analyzing progressive failures in slopes. The similar concepts of progressive failure are reported by many researchers such as Terzaghi (1936), Henkel and Skempton (1956), Peterson et al. (1960), Skempton (1964), Bjerrum (1966), Chandler (1984), and Burland (1990).

For a slope called I-180/Superior St. located within the boundary of Lincoln, Nebraska, field measurement was conducted to confirm the progressive nature of slope failure in overconsolidated soils. Three different measurement techniques, total station based surveying, UAS (Unmanned Aerial System, a.k.a. Drone), and DSS (Distributed Strain Sensing), were applied to obtain deformation data even under harsh weather condition.

Total station based deformation measurement results for I-180/Superior St. plotted in Figure 2.2 shows that there are slow (0 to 0.02 ft/month) but progressive movement of slopes. It also indicates that surveyors observed a newly developed failure cracks on the upstream side of the slope, but the deformation could not be measured due to the damage in surveying pegs.

In addition, UAS based deformation surveying system showed comparable deformation profile to that from total station based surveying result. UAS, however, Figure 2.3 shows the deformation around the newly developed cracks, which is in the range of 0.02 ft/month.

Fiber optic cable based DSS system showed relative movement between anchoring points installed in the slope as a grid pattern. This DSS results were expected to show sections that initiate the movement and other sections that follow the failed sections. Figure 2.4.a shows the deflection between Sept. 21st, 2018 and Nov. 9th, 2018. Each section showed a negative deflection, which represents a lowering of strain, convergence of posts, and shortening of cable sections. During this time period, the deflection of each section was close to 0.7mm/month (0.02 ft/month), with the greatest magnitude of deflection shown in section 1.0 mm/month (0.03 ft/month). It agreed with

surveying and UAS results. Figure 2.4.b shows the deflection between Jan. 17th, 2019 and Apr. 17th, 2019. Notice the area outlined in green, which is the area of slope that had visibly failed prior to beginning data readings. During this time period, the deflections of most of the sections were around 17 mm/month (0.6 ft/month), except for the vertical sections on the area of visibly failed slope: Sections 6, 7, 9, and 10. These sections had deflections of around 33 mm/month (0.11 ft/month) which is about twice the magnitude of deflection as the other sections. This may indicate that the bottom of the hill (sections 6, 7, 9, and 10) is the critical section that initiated the progressive slope failure. Comparable surveying and UAS based deformation measurement could not be conducted due either to the damage to the surveying pegs or unfavorable weather condition.
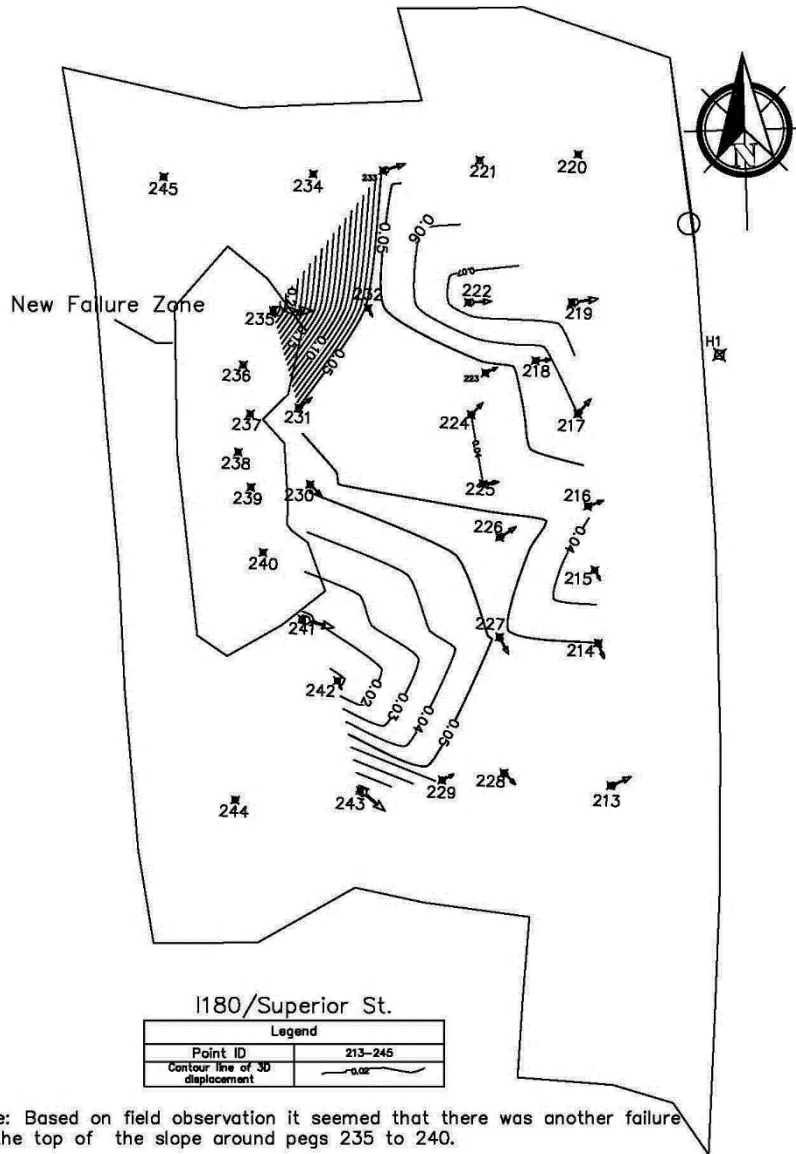
Figure 2.2 Slope movement contour during nine months for slope at I-180/Superior St. (Note: 1: Numbers for contours are in feet. 2: Length and direction of arrows indicate the magnitude and direction of surface movement. 3: Deformation along pegs 236 to 240 seemed high, but pegs were damaged due to severe ground subsidence/movement.)

12
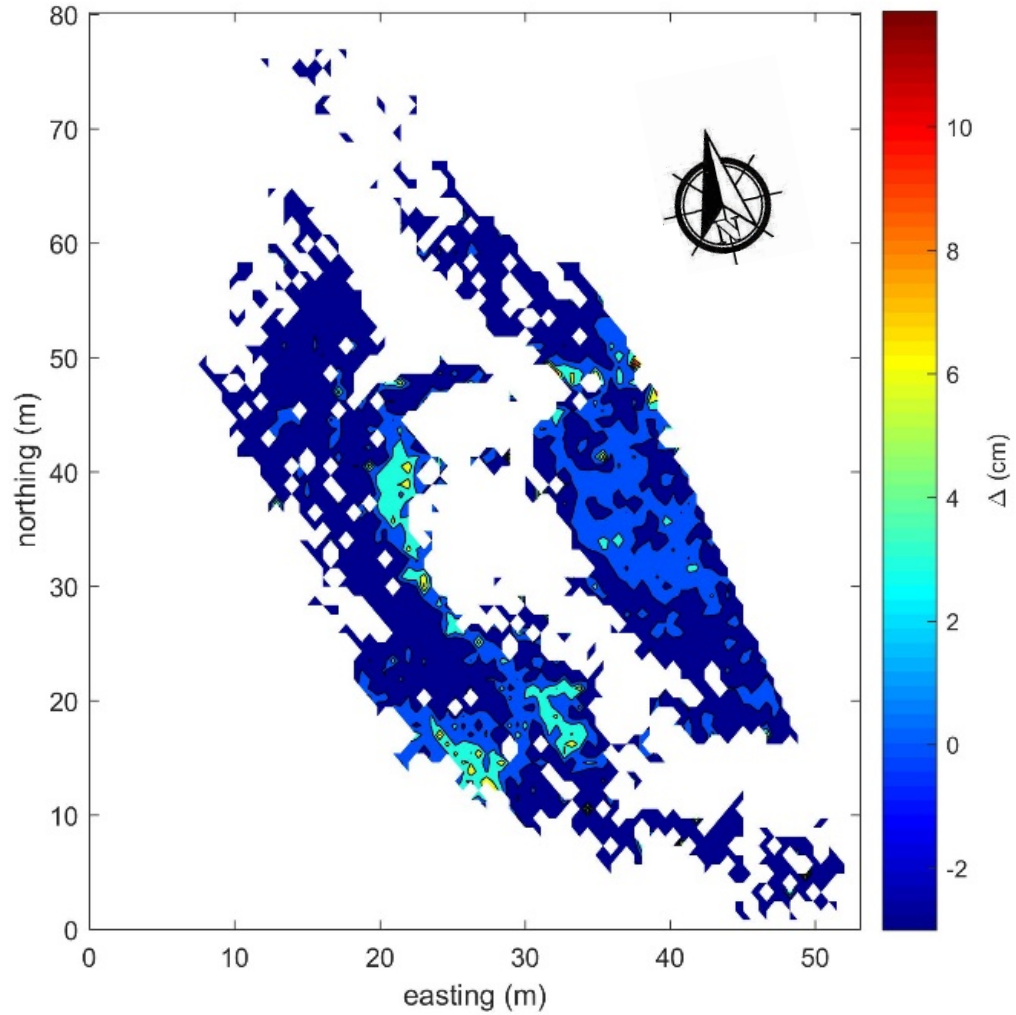
Figure 2.3 UAS (Unmanned Aerial System; a.k.a. Drone) based deformation profile for slope at I-180/Superior St. (Note: High deformation along the newly formed crack is pronounced with bright green color, Courtesy of Dr. Richard Wood.)
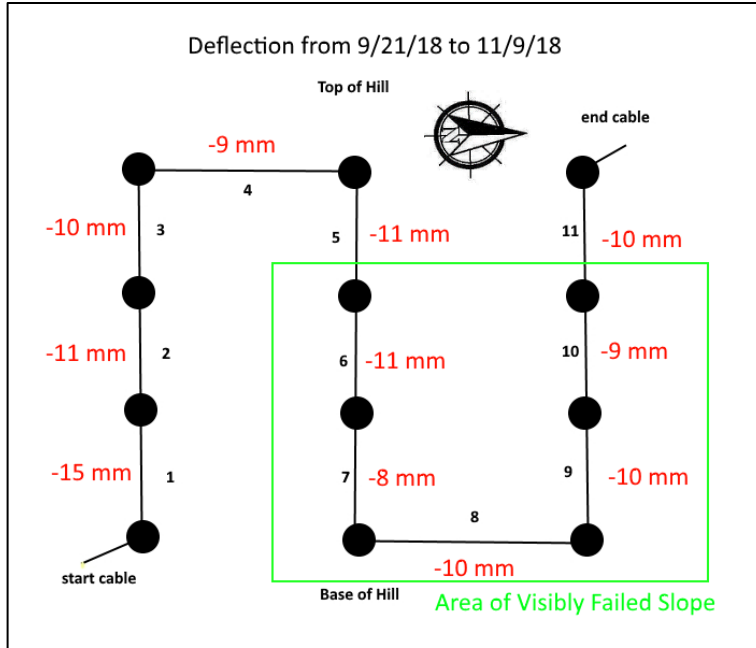
Figure 2.4.a Fiber optic based DSS (Distributed Strain Sensing) result for slope at I-180/Superior St. (Note: Left is South side.)
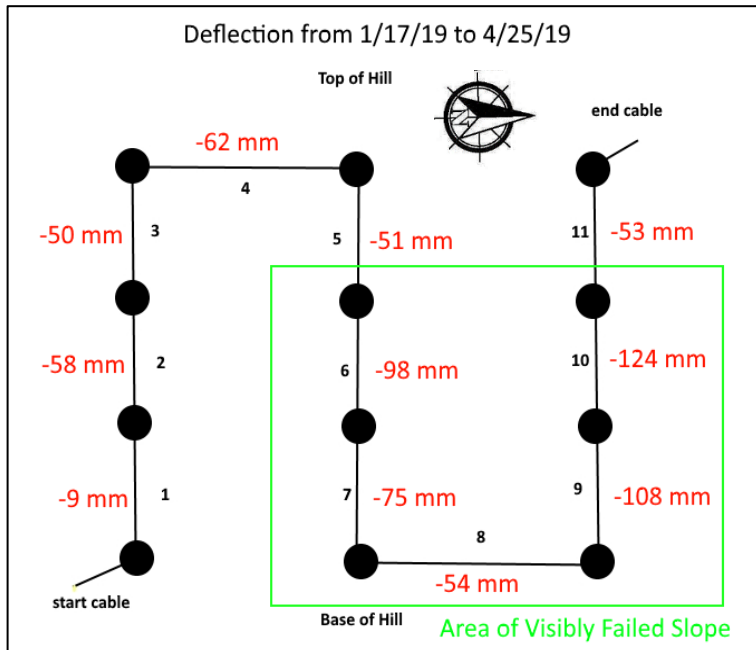
Figure 2.5.b Fiber optic based DSS (Distributed Strain Sensing) result for slope at I-180/Superior St. (Note: Left is South side.)

2.2 Quantification of strength reduction

Skempton (1964) introduced the term "residual factor" which is defined in equation 2.1:

$$R = \frac{S_f - S}{S_f - S_r} \qquad (2.1)$$

Where S_f is the peak strength, S_r residual strength, and S is the average shear stress acting on the slip surface. $R=1$ was assigned to the slopes that have previously experienced failure and their shear strength is in the residual strength condition. $R=0$ or the value close to zero was assigned to the slopes that showed the mobilized shear strength the same as the peak shear strength. Skempton (1964) reported that the typical residual factor of the slopes in overconsolidated fissured clays to be 0.5 to 0.8.

Chandler (1984) categorized the landslides that occurred in clayey soils based on the plasticity index of clays, concluding that low plasticity clays with a plasticity index PI lower than 25% had shear resistance close to the peak strength, and the clays with plasticity index PI higher than 25% had a shear strength around fully softened shear strength for first time slides.

Mesri and Abdel-Ghaffar (1993) also compared the shear strength of soft and stiff clays. They analyzed 35 different slopes in both soft and stiff clays. In this study, the back analysis was conducted to investigate the shear strength parameters for the first time failure. A reduction factor (η) as shown in equation 2.2 was calculated based on back analysis to compute the ratio between mobilized shear strength and peak shear strength. The research found that the clays with low plasticity can show the mobilized shear resistance close to peak strength. In overconsolidated clays with a plasticity index equal to 20% or higher, they reported that the shear strength might be

15

slightly higher than fully softened shear resistance. These results seemed in agreement with Chandler (1984).

$$\eta = \frac{Mobilized\ shear\ strength}{Peak\ shear\ strength} \qquad (2.2)$$

Stark and Duncan (1991) reported that the mechanism of strength loss in stiff fissured clays from peak to fully softened strength is a time dependent behavior, but they also reported that an intensive rainfall may cause a rapid dramatic reduction in strength from peak to fully softened strength. This finding may be particularly true for swelling clays in Nebraska, because swelling clays may actively absorb water and lose strength when subjected to extended precipitation.

2.3 Effect of expansive clay minerals on shear strength parameters of soils

The structure of clay minerals is consisted of two basic units, which are silica tetrahedron or silica sheet and alumina octahedron or alumina sheet (Das 2010). Among clay minerals, smectite group such as montmorillonite, beidellite, nontronite, and saponite usually shows higher swell behavior more than other clay minerals (Mitchell and Soga, 2005). Montmorillonite has a 2:1 structure. In this structure, one alumina sheet is sandwiched by two silica sheets. This mineral has an expandable interlayer structure and a large specific surface area, which can absorb a high volume of water. Swelled clay minerals by absorbing water, will have weak bonding force due to the increased distances between plates, resulting in low strength. In soils of high content of expansive clay minerals, the soils may expand until all clay particles may disperse in water, eventually resulting in zero strength condition.

Many researchers have studied the effect of expansive clay minerals on shear strength of soils, showing that the soils consisted of expansive minerals show saturated drained shear strength

lower than the soils which do not contain expansive minerals. Warkentin and Yong (1962) studied the drained shear strength behavior of clayey soils consisted of two types of montmorillonite and kaolinite. The sodium (Na) montmorillonite has a higher shear strength than calcium (Ca) montmorillonite at the same void ratio. According to Warkentin and Yong (1962), this behavior is because of the lower surface area of Ca-montmorillonite. Kaolinite clayey samples had a lower void ratio and showed lower swelling in comparison with montmorillonite clay.

Chapter 3 Evaluation of Strength of Soils Based on Back Analysis

3.1 Introduction

Back analysis of slope stability is a technique to estimate the mobilized shear strength of soils at failure. Typically, an engineer relies on trial and error technique and reduce the strength of soils gradually until the computed factor of safety of a failed slope is close to 1.0. During the process, the most probable field conditions such as ground water condition and layering system are used. However, it is noted that there is more than one variable (e.g. the case of multi-layered system) that may effect on the factor of the slopes, and therefore, the computed strength of soils should be regarded as an approximate estimation.

In this study, GeoStudio Standard 2016 is used for slope stability analysis. This software is based on several limit equilibrium methods (such as Morgenstern-Price, Bishop, Janbu, Spencer, etc.). Additionally, Autodesk AutoCAD 2017 was incorporated to define an accurate slope geometry model, which is then exported to GeoStudio to compute shear strength parameters corresponding to FS=1. Of the limit equilibrium analysis techniques available in GeoStudio, the Spencer method is chosen in order to consider both force and moment equilibrium without neglecting inter-slice forces. In the back analysis, the water Table was assumed to be at the slope surface and the tension crack was assumed to present at the top of any un-covered slopes.

Back calculations are performed on five documented slopes in Nebraska that are chosen based on consultation with NDOR engineers. The selected slopes are:

1. US-75, Mudslide, North of Plattsmouth

2. Verdigre East and South Slides, Knox County

3. Spencer Southeast, Boyd County

4. Santee Spur, Knox County

5. Bristow East, Boyd County

In subsequent sections, the above slopes are each modeled and back calculated parameters are computed, based on available documents and engineering judgment

3.2 US-75, Mudslide

3.2.1 Location, Geometry and Material Properties

The slope is located on Highway 75, 1.7 miles southwest of Plattsmouth, 2.5 miles west of the Missouri River, and 1.2 miles south of the Platte River. The slope failure occurred in the southeastern area of the flyover shown in Figures 3.1 and 3.2.
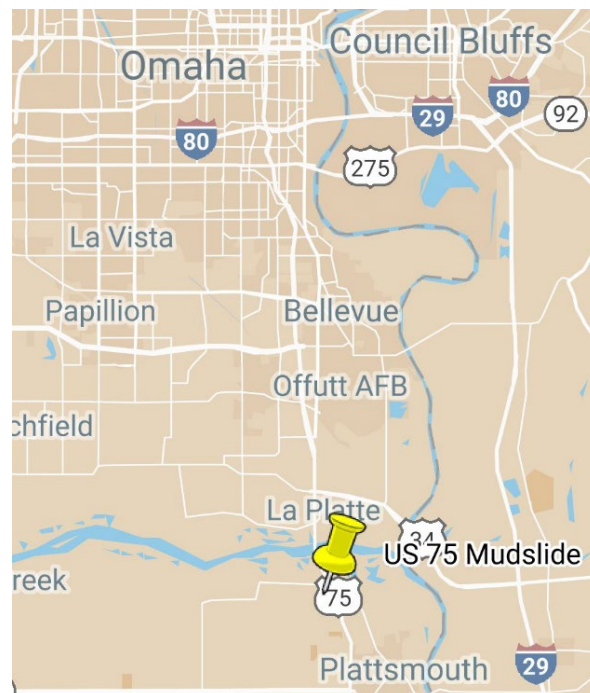
Figure 3.1 US-75, Mudslide location

The slope contains a thick layer of fill material that is mainly composed of Peoria. This layer resides on the top layer of slightly clayey silt that possesses low strength. The silt overlays a

19

layer of fine silty sand that is subject to fail during rainy seasons. The height of the selected slope cross section is at 39.56 ft with a slope angle of approximately 23 degrees. Scene of failure is shown in Figure 3.2.

Figure 3.2 US-75, Mudslide (NDOR, 2015)

3.2.2 Model and Results

Figure 3.3 shows the modeled slope based on design soil parameters, from which a factor of safety of 1.603 was obtained. This is an accepTable factor of safety, indicating a stable slope. In this case, the potential slip surface with the lowest factor of safety started at nearly the top edge of the slope, and after passing through the silt layer, it ended at approximately the toe of the slope.
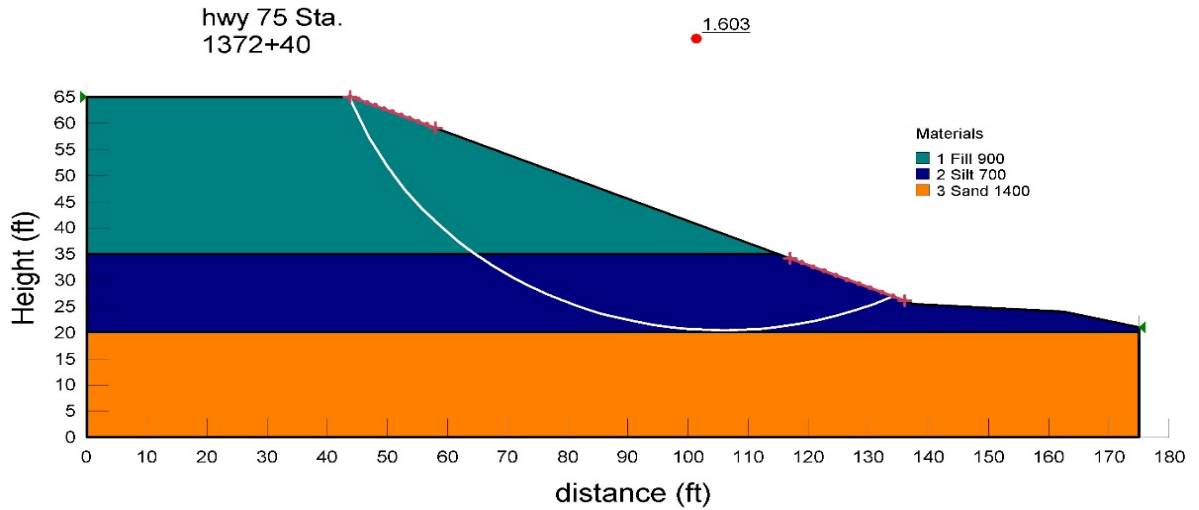
Figure 3.3 US-75, Mudslide

For back analysis, the internal friction angle of the soil at failure was assumed to be equal to zero considering that the soils are mostly cohesive. Using a trial and error method, the shear strength of the soil was evaluated to reach FS=1. Figure 3.4 depicts the back calculated slip surface and factor of safety. The slip surface location remained unchanged in comparison to Figure 3.3, but resulted in a factor of safety of unity.
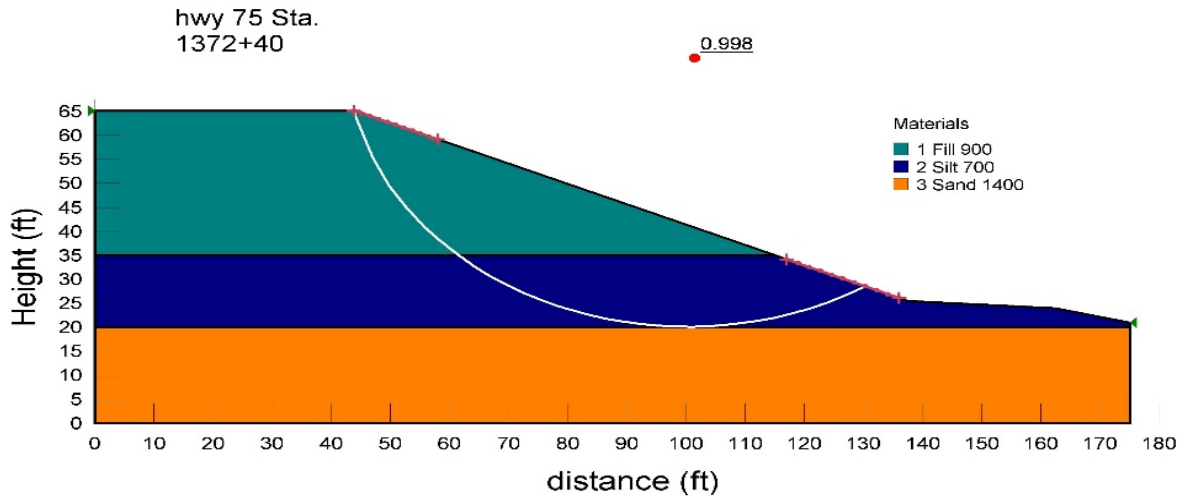
Figure 3.4 US-75, Mudslide, back calculated result

Table 3.1 shows that the strength parameters of the fill and silt were reduced by up to approximately 40% of their original values.

Table 3.1 Strength parameters before and after back analysis (US-75)

No.	Layer Description	Original parameters		Back calculated parameters	
		Cohesion(psf)	FS	Cohesion(psf)	FS
1	Fill (Peoria)	900		545	
2	Silt; Slightly Clayey	700	1.603	450	0.998
3	Sand, Fine Silty	1400		1400	

3.3 Verdigre East and South Slides, Knox County

3.3.1 Location, Geometry and Material Properties

The slope failures occurred to the south and southeast of Verdigre. The slope is located approximately 1.5 to 2 miles from the Verdigre Creek River—between its tributaries. The slide on Highway 14 was approximately 350 feet long, and the slides on Highway 84 were approximately

100 feet and 250 feet long respectively (Lindemann, 2011). Figure 3.5 illustrates the approximate locations of the slides. The slopes were designed using Nebraska's road construction standard (V:H=1:3).

A boring log shows that these two slopes have mostly reworked shales. In addition, the ground water Table is near the surface, which is possible during rainy seasons. Because of the location of the groundwater Table, most layers might have high water content, and the soils might be prone to failure.
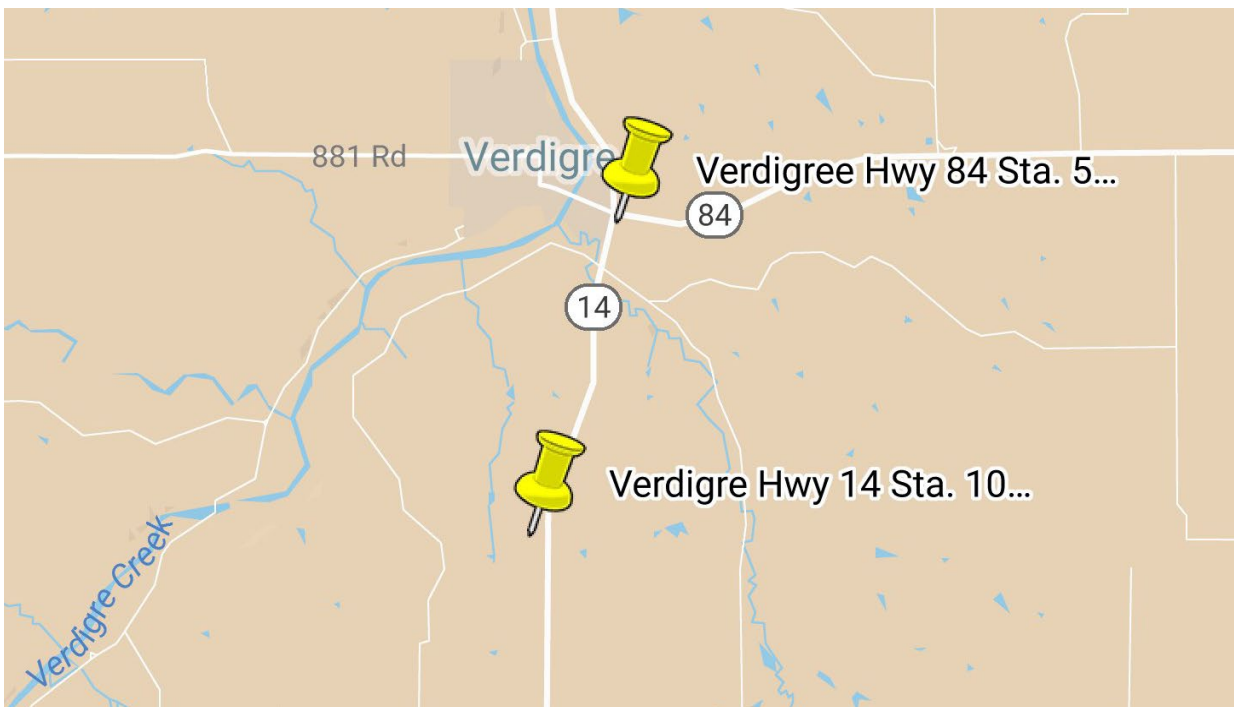
Figure 3.5 Verdigre East and South Slides location

3.3.2 Model and Results

Figure 3.6 shows the modeled slope on Highway 14. The modeled slope yields a factor of safety of 1.368. The slope contains twelve shale layers, which have variable strength. A succession

of weak layers with slightly different shear strength in a slope might cause progressive failure. Because the slope contains many adjacent weak layers, the potential slip surface passes through all of them. Figure 3.7 illustrates the back calculated slip surface which has FS=1. From comparison of original and back calculated strength parameters shown in Table 3.2, the strength parameters appeared to be decreased by around 25% of their original value in order to reach FS=1.
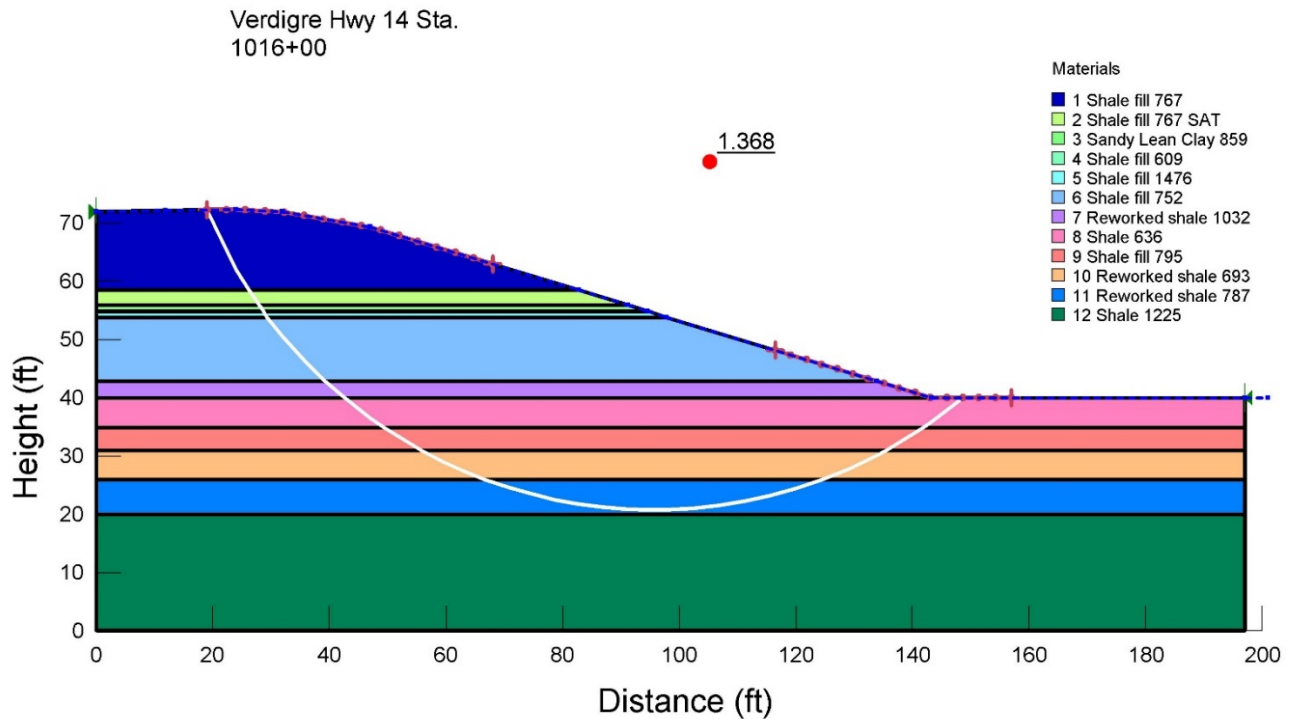
Figure 3.6 Factor of safety calculated for Verdigre slope (Highway 14)
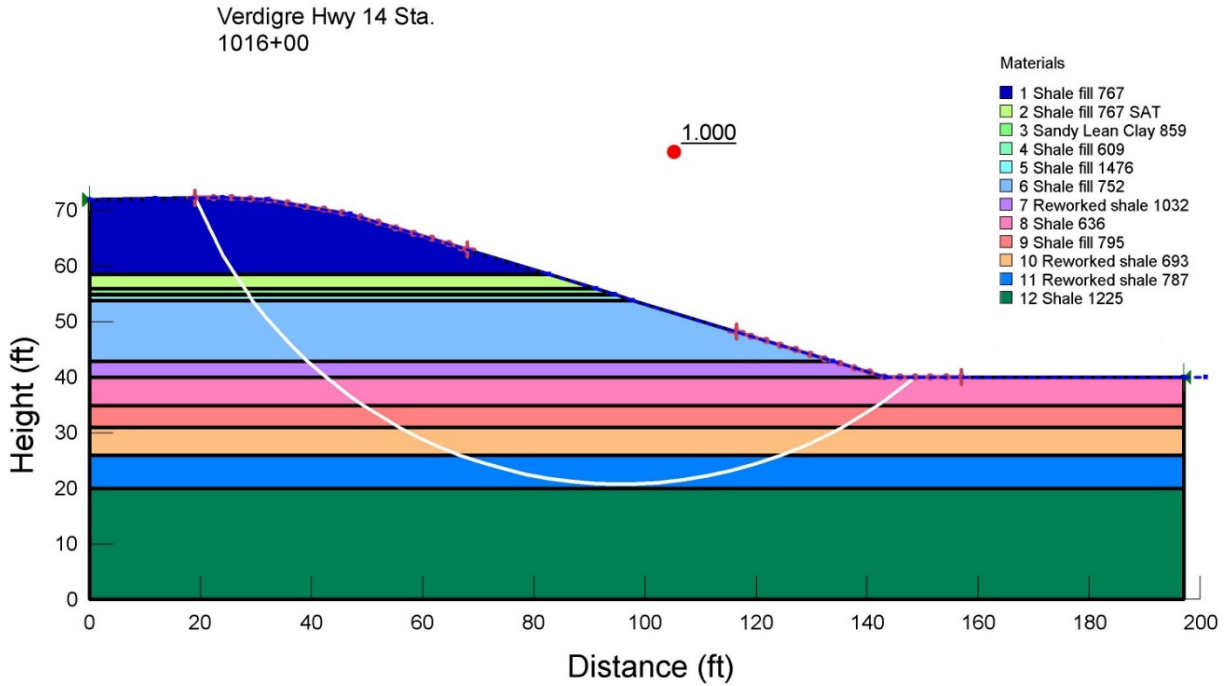
Figure 3.7 Factor of safety from back analysis for Verdigre slope (Highway 14)

The other slope failure near Verdigre occurred along Highway 84. As illustrated in Figure 3.8, the modeled slope already failed, because the factor of safety was less than one. This slope had a number of fill and reworked shale layers with a maximum thickness of 10 feet. Because the factor of safety was below unity, the actual strength parameters of the slope seemed lower than the strength parameters determined through bore log results. To correct this for the back calculated analysis, the strength parameters were increased to evaluate the minimum required strength of soils.

In this slope, there are two boring logs for designing the retrofitting technique. One is located around 50 ft east of the road centerline and the other is located around 150 ft east of the road centerline. Comparison of the two boring logs shows a reduced strength in the shale due to saturation - for the same shale layer at the same depth, the sample below the ground water Table shows lower strength parameters than the one above the ground water Table. The soil strength

25

below ground water Table is 740 psf while the soil strength above the ground water Table is 1497 psf. Back calculation of the slope (Figure. 3.9) results in an increase of the strength parameters of the material by around 22% (Table 3.3) in order to reach FS=1.

Table 3.2 Verdigre slide (Highway 14) back calculation results

No.	Layer description	Original parameters		Back calculated parameters	
		Cohesion(psf)	FS	Cohesion(psf)	FS
1	Fat clay (shale fill)	767		562	
2	Fat clay (shale fill), Saturated	767		565	
3	Sandy lean clay	859		660	
4	Fat clay (shale fill)	609		470	
5	Fat clay (shale fill)	1476		1100	
6	Fat clay (shale fill)	752	1.368	560	1
7	Fat clay (Reworked shale)	1032		750	
8	Fat clay (shale)	636		510	
9	Fat clay (shale fill)	795		562	
10	Fat clay (Reworked shale)	693		500	
11	Fat clay (Reworked shale)	787		565	
12	Fat clay (shale)	1225		1100	
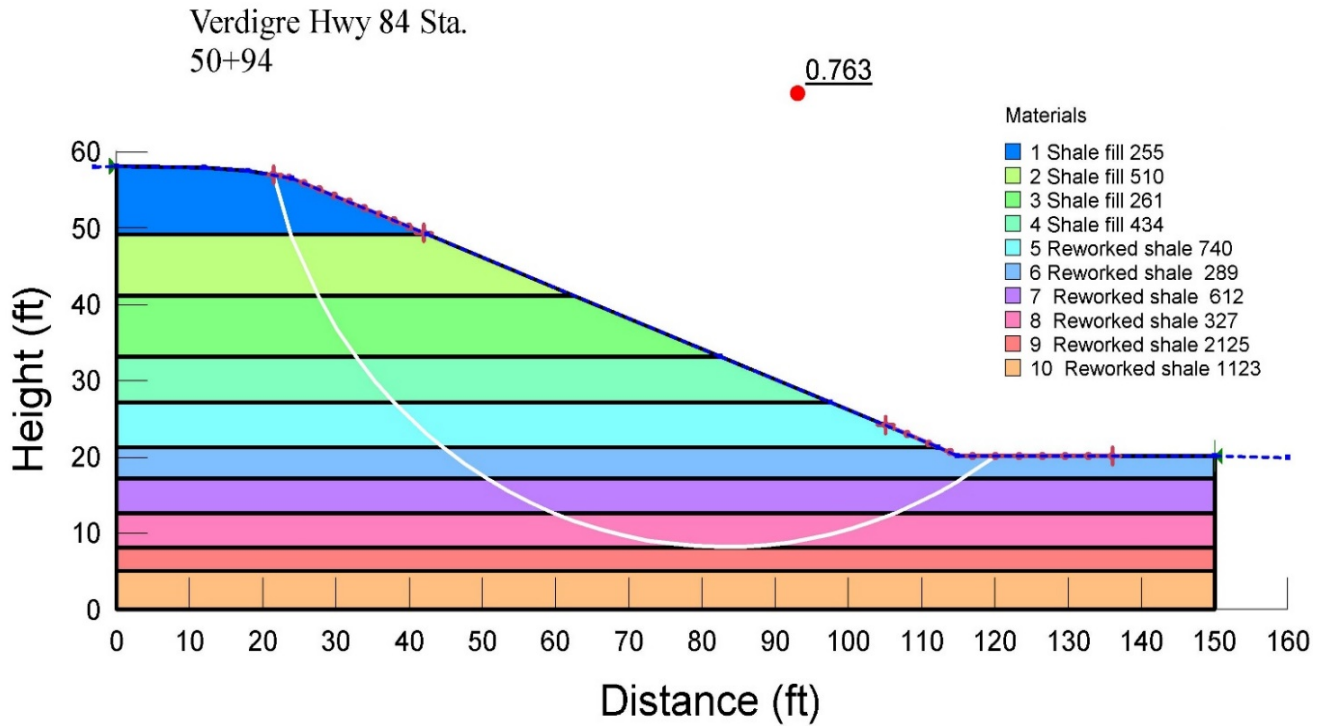
Figure 3.8 Factor of safety calculated for Verdigre slope (Highway 84)
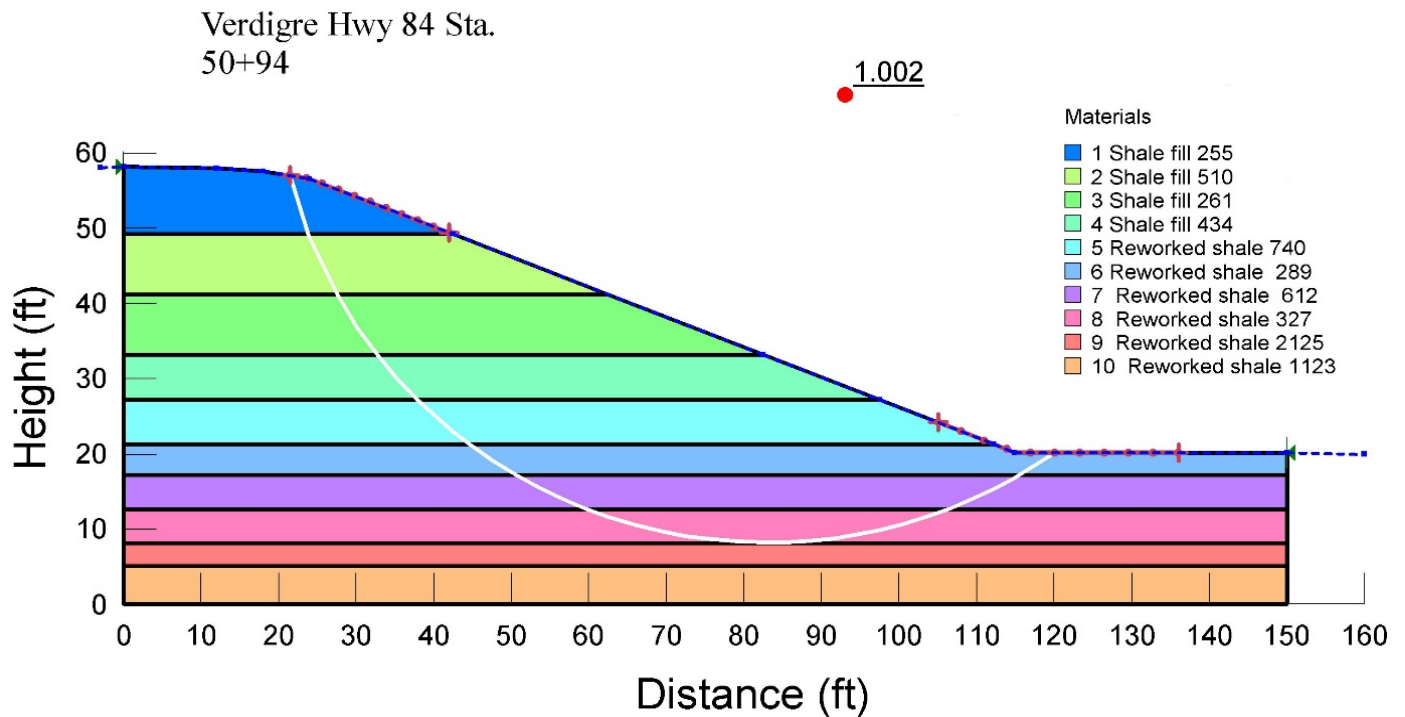
Figure 3.9 Factor of safety from back analysis for Verdigre slope (Highway 84)

Table 3.3 Back calculation result from Verdigre slide (Highway 84)

No.	Layer description	Original parameters		Back calculated parameters	
		Cohesion(psf)	FS	Cohesion(psf)	FS
1	Fat clay (shale fill)	255		350	
2	Fat clay (shale fill)	510		640	
3	Fat clay (shale fill)	261		310	
4	Fat clay (shale fill)	434		500	
5	Fat clay (Reworked shale)	740		850	
6	Fat clay (Reworked shale)	289	0.763	390	1.002
7	Fat clay (Reworked shale)	612		870	
8	Fat clay (Reworked shale)	327		440	
9	Fat clay (Reworked shale)	2125		2125	
10	Fat clay (Reworked shale)	1123		1123	

3.4 Spencer Southeast Slide

3.4.1 Location, Geometry and Material Properties

The slope is located in the northeastern part of the state between the Missouri River and the Niobrara River, approximately 0.2-miles south of where the Missouri River branches. Figure 3.10 shows the location of failed slope.
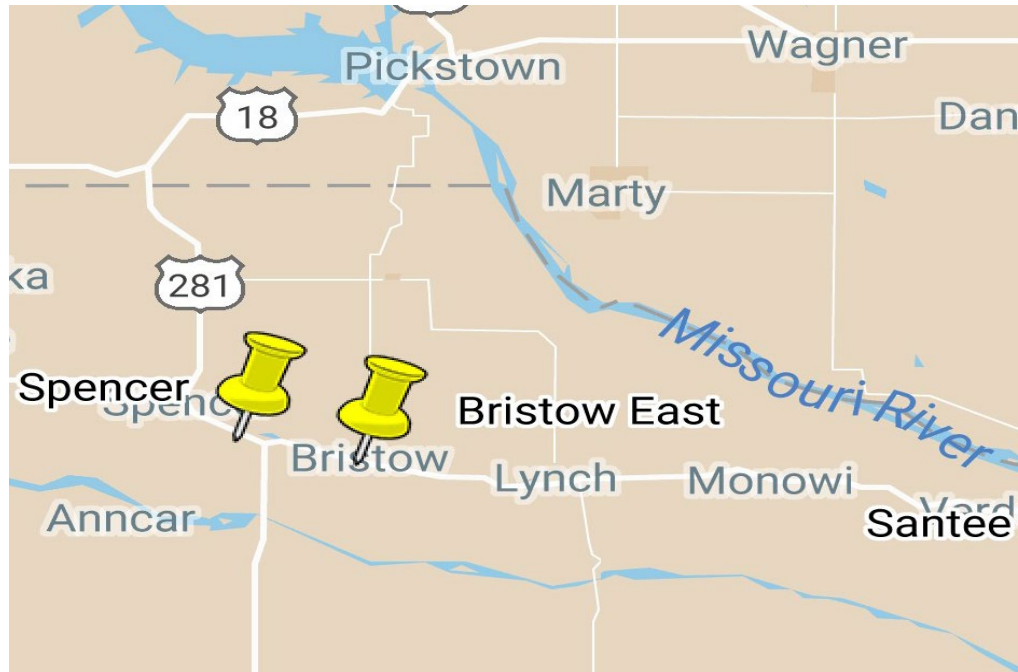
Figure 3.10 Spencer slope location

As shown in Figure 3.11, the failure of the slide is indicated by two large longitudinal cracks near the top of the slope. This area contains both shale and loess, both of which are easy to fail in the presence of water. The bore log data showed two weathered and two un-weathered layers of stiff shales. Undisturbed samples were tested in the laboratory using direct shear tests. The shear tests of the samples did not show a well-defined shear surface. They rather showed intrusion of different colored materials into the sample and occasional cracks.

Figure 3.11 Cracks on the top of the Spencer slope, (NDOR 2015).

3.4.2 Model and Results

Figure 3.12 shows the Spencer slope model which yields a factor of safety equals to 2.935 based on design soil parameters. Figure 3.13 shows a back calculated slip surface, which is somewhat different from the original one.
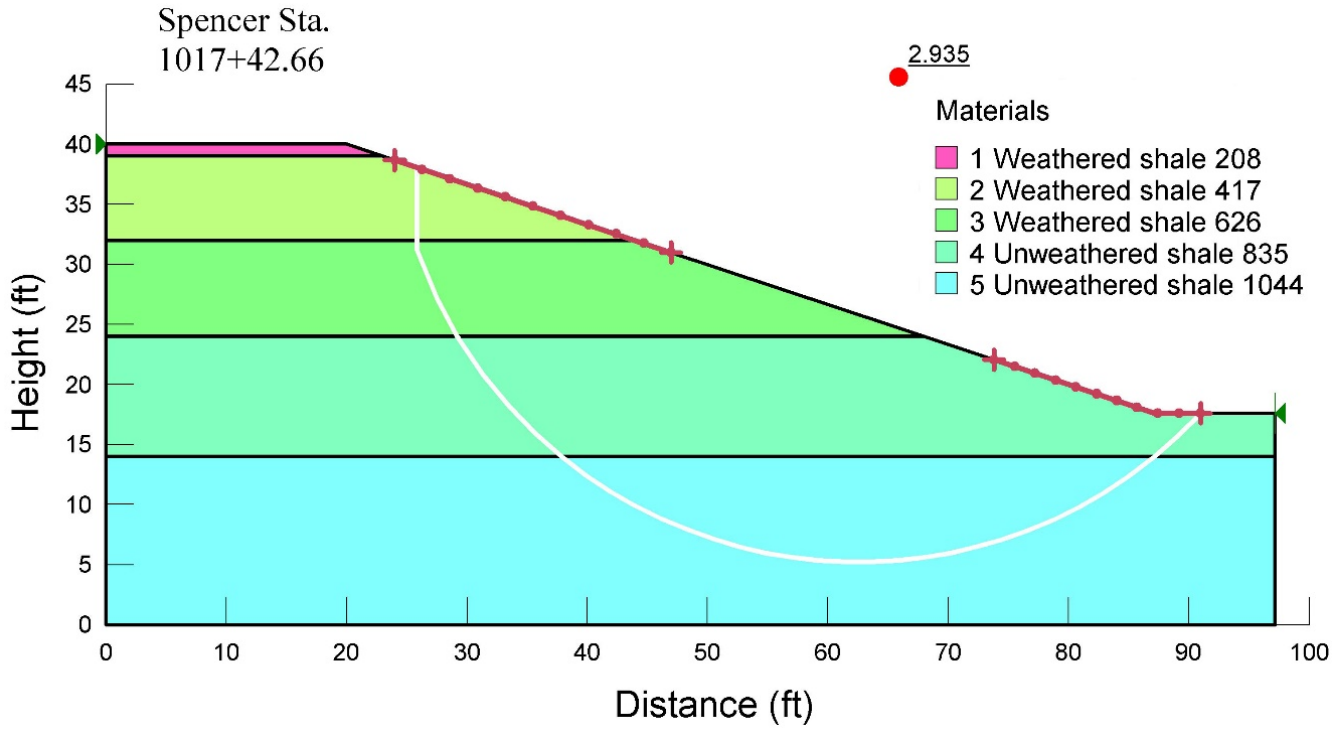
Figure 3.12 Factor of safety calculated for Spencer slide
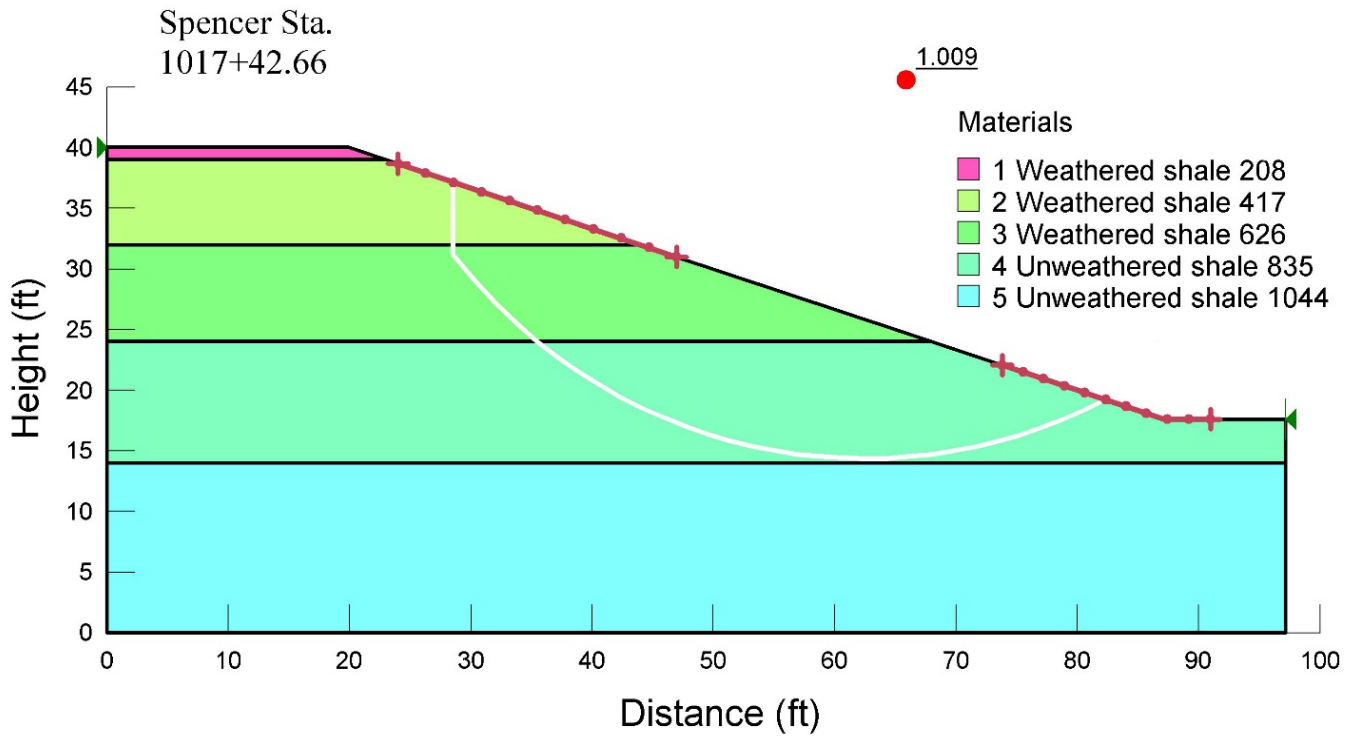
Figure 3.13 Factor of safety from back analysis for Spencer slide

31

The Figure shows that a decrement of the strength parameters of weathered shales changes the slip surface location. When the factor of safety equals one, the slip surface exists completely outside of the hard shale layer, which is reasonable. Table 3.4 shows that the back calculated strength parameters are approximately 65% of their original values. This strength reduction is likely due to the development of cracks and associated strength weathering/reduction along the weak interface between shale layers.

Table 3.4 Back calculation result from Spencer slide

No.	Layer discreption	Original parameters		Back calculated parameters	
		Cohesion(psf)	FS	Cohesion(psf)	FS
1	Weathered shale	208		150	
2	Weathered shale	417		180	
3	Weathered shale	626	2.935	220	1.009
4	Unweathered shale	835		275	
5	Unweathered shale	1044		1044	

3.5 Santee Spur

3.5.1 Location, Geometry and Material Properties

This slope failure occurred in northeastern Nebraska close to the Missouri River. The slope is approximately 1.2 miles from the Missouri River as shown in Figure 3.14. This slide was approximately 125 feet long and developed a longitudinal crack on the centerline of the roadway (Lindemann, 2010). The boring logs from the site showed that the soil layers consisted of asphalt milling and several layers of weathered and unweathered shales with variable strength. The thicknesses of the weathered shale layers were almost as high as the total height of the slope. The slope angle was designed based on the Nebraska road construction standard (1:3 slope).
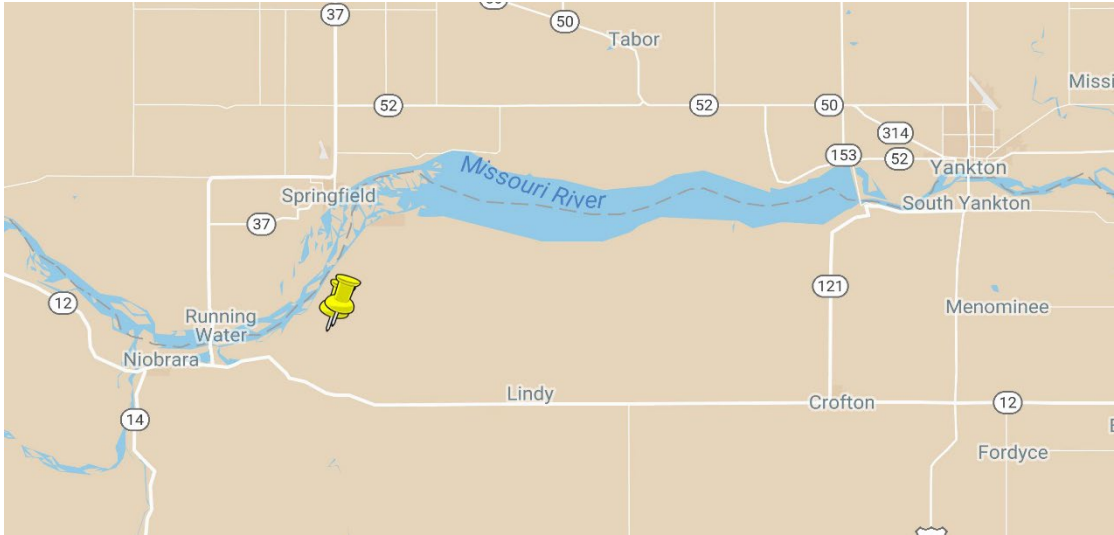
Figure 3.14 Santee slope location

3.5.2 Model and Results

As illustrated in Figure 3.15, the initial factor of safety (9.267) for this project turned out to be quite high. The failure occurred along a slip surface that passed through weathered shales.
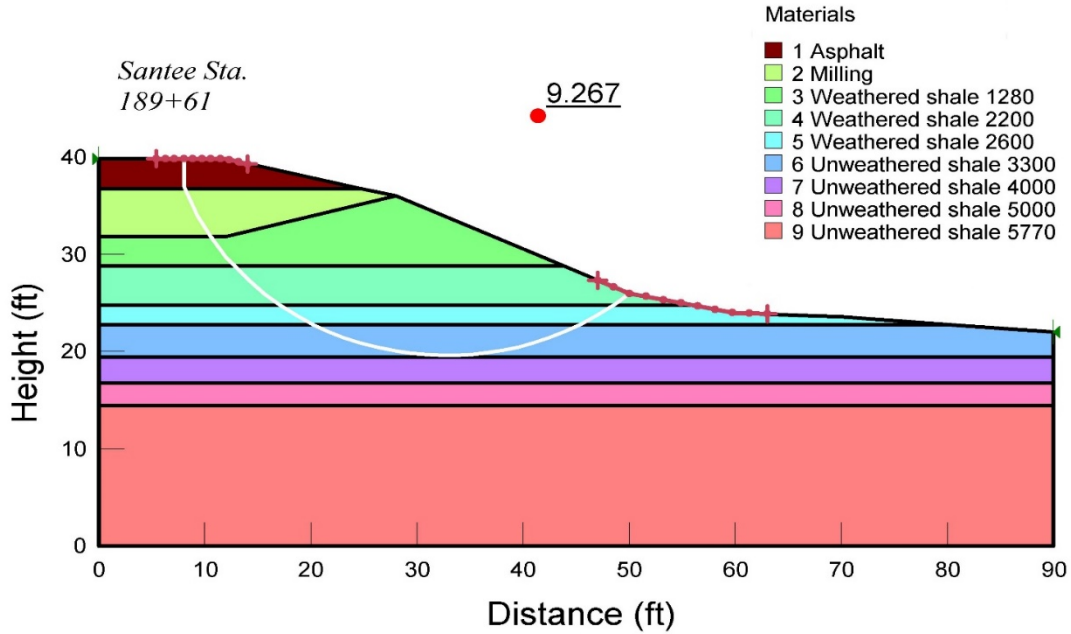
Figure 3.15 Factor of safety calculated for Santee slide
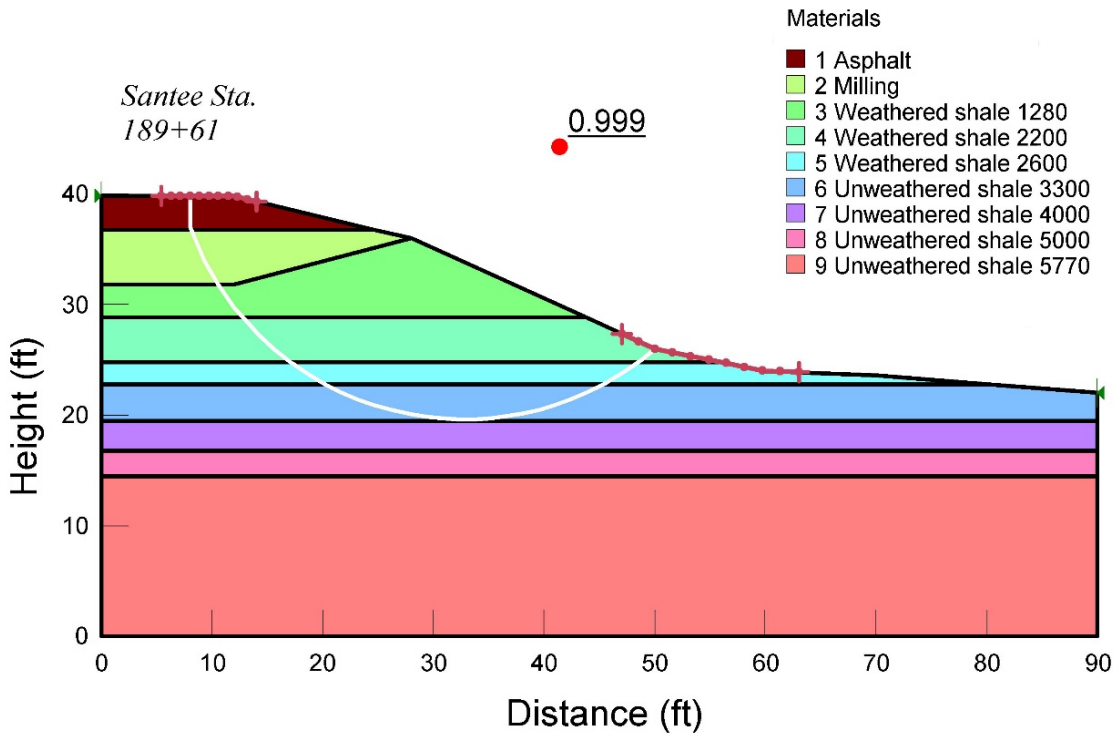
Figure 3.16 Factor of safety from back analysis for Santee slide

Figure 3.16 shows that the back calculated slip surface for the Santee slope failure is similar to the initial slip surface shown in Figure 3.15. Table 3.5 shows that the strength of weathered shales was reduced by nearly 85% of the original values in order to obtain a factor of safety of unity. Because this drastic strength change is not common, further investigation is needed.

Table 3.5 Back calculation result from Santee slide

No.	Layer description	Original parameters		Back calculated parameters	
		Cohesion(psf)	FS	Cohesion(psf)	FS
1	Asphalt	10000		10000	
2	Milling	-		-	
3	Weathered shale	1280		110	
4	Weathered shale	2200		180	
5	Weathered shale	2600	9.267	300	0.999
6	Unweathered shale	3300		350	
7	Unweathered shale	4000		4000	
8	Unweathered shale	5000		5000	
9	Unweathered shale	5700		5700	

3.6 Bristow

3.6.1 Location, Geometry and Material Properties

This slope is located along Highway 12, approximately four miles east of the Spencer slope site (Figure. 3.17). According to boring log, the slope contains a combination of fill materials (fill shale) that overlay undisturbed layers of shale with a total depth of 25 feet. The natural shale is located at a depth of 16 to 20 feet. Again, similar to previous slope, the location of this slope is in an area with relatively high precipitation with a combination of both shale and loess layers exist.
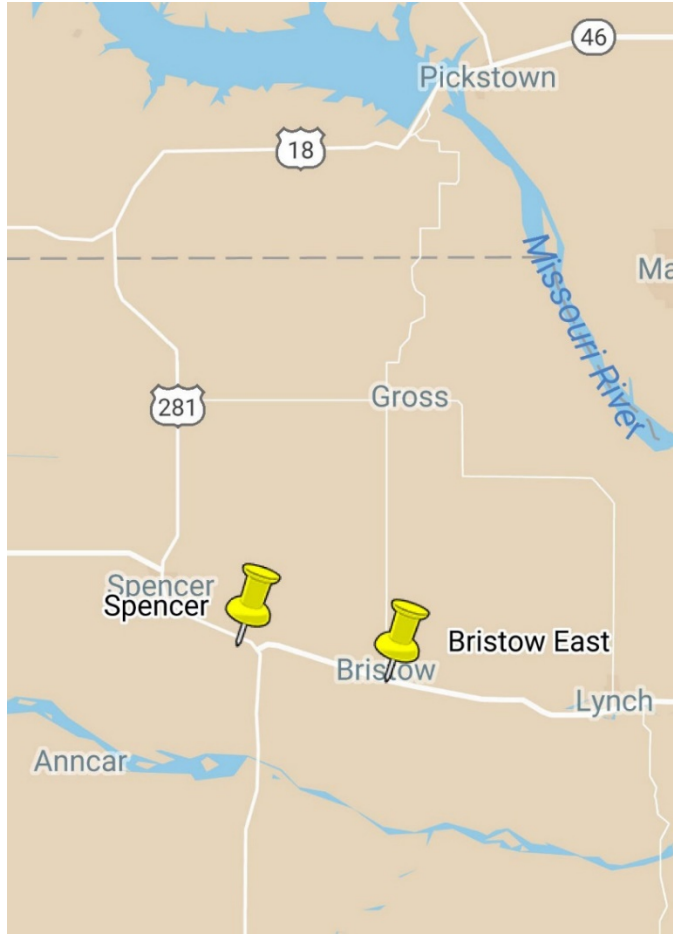
Figure 3.17 Bristow slope location

3.6.2 Model and Results

As illustrated in Figure 3.18, the calculated factor of safety with the initial design parameters is 3.573, which appears to be quite conservative. The figure shows that the slip surface occurs in the fill materials. The failure surface starts at the top—close to the boundary of the asphalt along and fill materials—and continues to the toe of the slope. Figure 3.19 shows the back calculated slip surface with FS=1. The failure line of the calculated slip surface is similar to the initial slip surface. A comparison between the strength parameters in Table 3.6 shows that they

were reduced by an average of 68% of their original values. This reduction is most likely due to the reduced strength of shale layers during wet seasons.
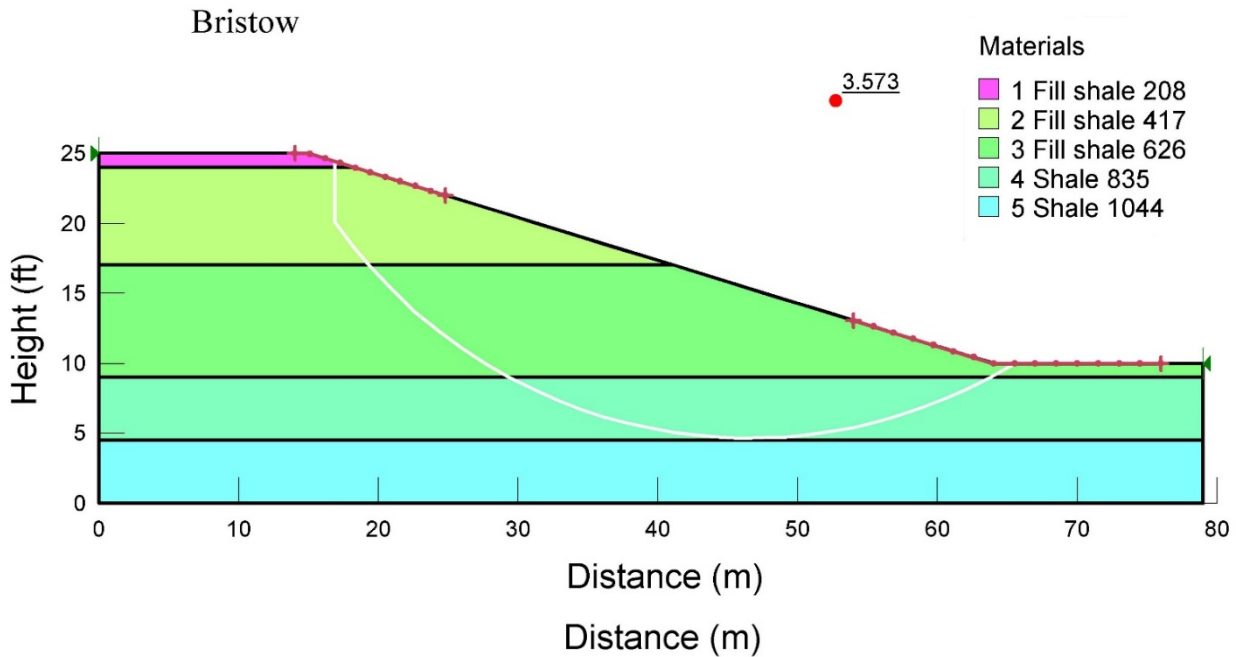
Figure 3.18 Factor of safety calculated for Bristow Slide
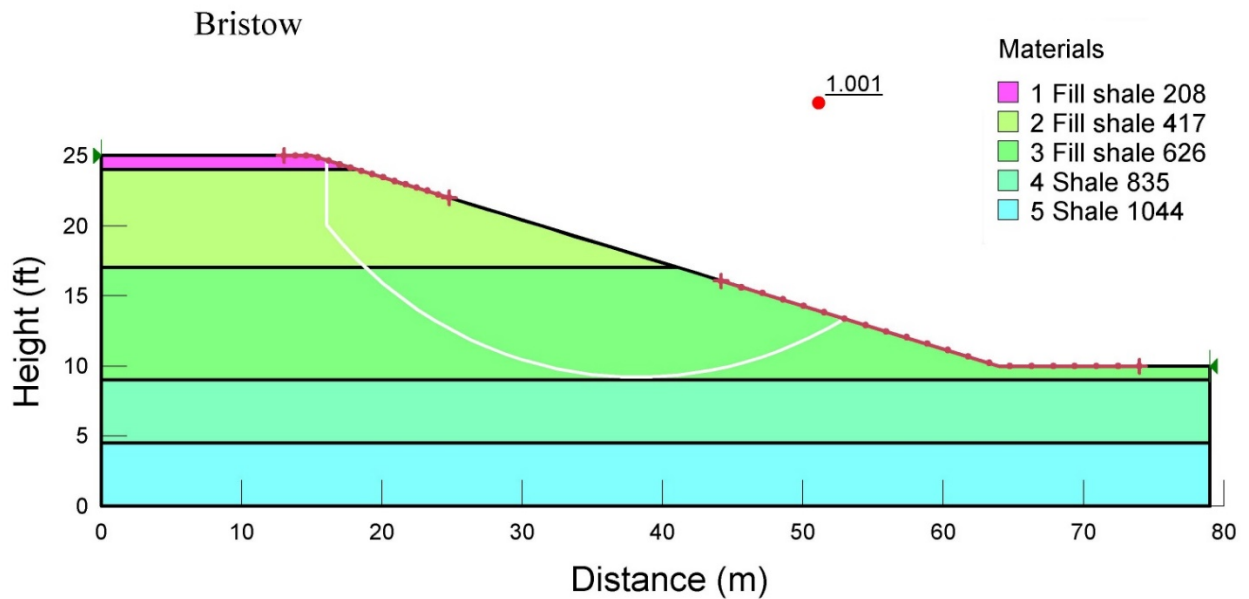
Figure 3.19 Factor of safety from back analysis for Bristow slide

Table 3.6 Back calculation result from Bristow slide

No.	Layer discerption	Original parameters		Back calculated parameters	
		Cohesion(psf)	FS	Cohesion(psf)	FS
1	Fill shale	208		80	
2	Fill shale	417		115	
3	Fill shale	626	3.573	177	1.001
4	Shale	835		835	
5	Shale	1044		1044	

3.7 Discussion and Conclusion

As shown in Figure 3.20, all selected slopes were located in northeastern and eastern Nebraska.

These areas have a combination of several factors—glacial deposits, presence of Loess, steeper

than average surface topography, high precipitation, and variable extreme temperature—
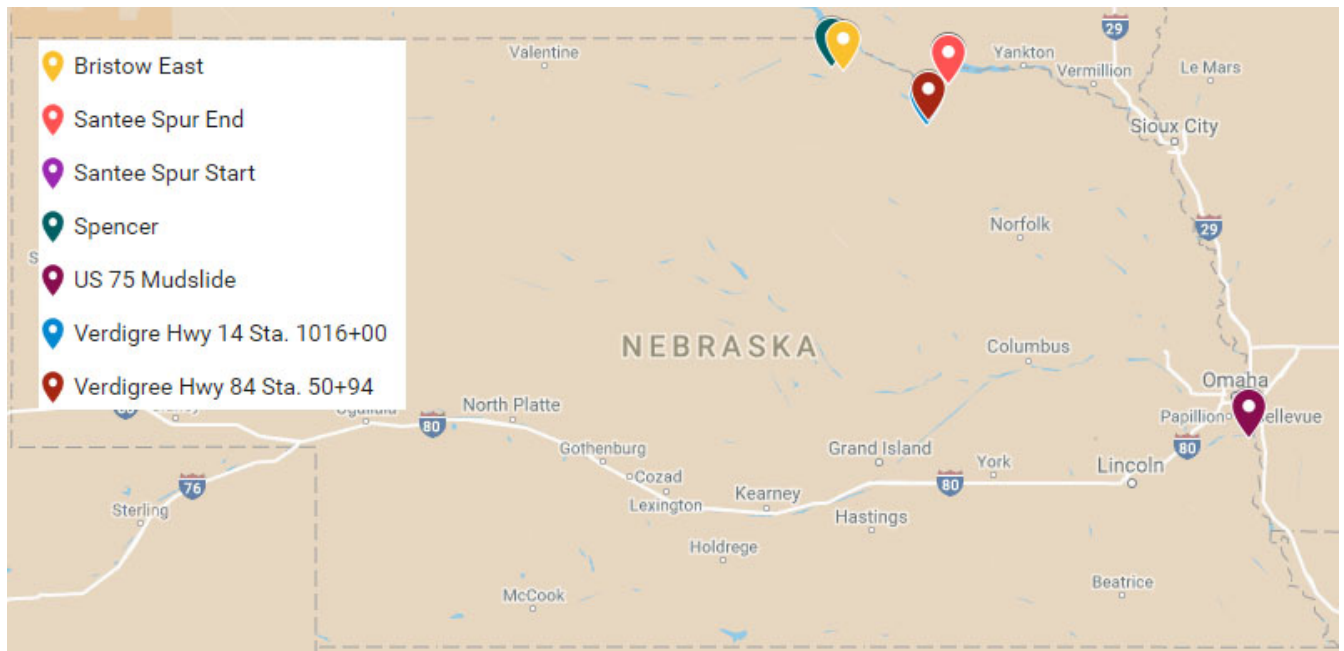
Figure 3.20 Selected slopes locations

that make slopes more unstable. However, the Santee slope failure will require an additional field visit when weather conditions allow, because this slope showed drastic strength reduction crediting it solely due to weathering.

In overall, the shear strength reduction of above five failed slopes seemed to be in the range of 22% to 90% of their initial strength (also meaning that 78% to 10% of their initial strength was maintained) as shown in Table 3.7. The results generally agree with findings from previous researches by Skempton (1964) and Mesri and Abdel-Ghaffar (1993).

Table 3.7 Summary of strength reduction from back analysis

Location	Strength Reduction Ratio Based on Back Analysis
US-75	40%
Verdigree East and South	24%
Highway 84	22%
Spencer	40 to 30%
Santee Spur	90%
Bristo	68%

Chapter 4 Description of Materials and Testing Procedure

4.1 Description of Soil Condition

The objective of this research is to investigate the detailed shear strength characteristics of overconsolidated soils in Nebraska, particularly the factors affecting the reduction of shear strength in these soils. The experimental work of this research involved the measurement of the shear strength for the soils in different conditions of triaxial tests such as confined and unconfined conditions, or drained and undrained conditions. Through the thoughtful evaluation of the shear strength considering these factors, a better understanding of failure mechanisms in overconsolidated soils associated with the strength reduction of the soils was obtained. This chapter describes the materials used for the experimental component of the study, the experimental apparatus, and procedures adopted for laboratory experiments.

4.2 Site location and investigation

Three different sites were selected for sampling. The first boring log was drilled in a failed slope located at I-180 and Superior St. in Lincoln, NE. The slope was a cut slope on highway I-180. Site visitation was conducted on the slope to have a better understanding of the geometry of the slope (Figure 4.1). It seemed that there was a rotational movement in this slope, which started from the top and ended at the toe. Furthermore, several longitudinal cracks were observed around the top of the slope. The samples were taken from the top of the slide to have a close enough soil stratigraphy similar to that of the failed slope. The dominant formation of this area is usually a layer of Peoria loess overlaid on the glacial till formation. Information regarding the slope's material is discussed in the next sections.

Figure 4.1 Failed slope at I-180 and Superior Street (2017)

The second site was a failed slope near North-Loup, NE. This site was also a cut slope. In this area usually the loess formation overlaid on top of the glacial till formation. The third site was Spencer slope, located in the northeastern part of the state approximately 0.2 miles north of Spencer dam. This area consisted of shale materials. The slope was under repairs during the research.

4.3 Drilling and sampling program

Drilling and sampling were performed by the Nebraska Department of Transportation using hollow steam augurs and Shelby tubes (Figure 4.2). After reaching the desired depth, the Shelby tubes were used for taking undisturbed samples.

Figure 4.2 Drilling equipment (I-180 and Superior St.)

For the I-180 and Superior St. failed slope, one boring log was considered at the top of the slope and six Shelby tube samples were taken from different depths on a range of 2.5 ft to 26.5 ft depths as shown in Table 4.1. In this research, the symbol "IS" represent the samples from I-180 and Superior St.

Table 4.1 Samples depth from boring log on failed slope at I-180 and Superior St.

Sample ID	Depth (ft)	Formation
IS-2.5	2.5-4	Peoria Loess
IS-4.5	4.5-6	Peoria Loess
IS-9.5	9.5-11.5	Peoria Loess
IS-14.5	14.5-16.5	Glacial till
IS-19.5	19.5-21.5	Glacial till
IS-24.5	24.5-26.5	Glacial till

There were two boring logs for the North-Loup project. As the boring logs were close to each other (about 3 ft distance), only one of them was selected for this study. Table 4.2 shows the depth of the samples and the formation of the soils. In this research, letters "NL" represent the samples from North Loup.

Table 4.2 Samples depth from boring log on failed slope at North-Loup

Sample ID	Depth (ft)	Formation
NL-4.5	4.5-6.0	Peoria Loess
NL-14.5	14.5-16.5	Glacial till
NL-19.5	19.5-21.5	Glacial till

4.4 Description of field soils

4.4.1 I-180 undisturbed samples

The main stratigraphy of the soils from the I-180 and Superior bore logs showed the similar trend of Nebraskan glacial till deposits. Glacial tills usually consist of a high amount of overconsolidated clay (because of high overburden pressure due to the weight of the ice sheets)

43

mixed with silt, sand, gravel, and boulders. Tills varied in color because the percentage of sand and silts are not constant. However, unweathered tills are usually dark gray in color. Glacial till deposits in Nebraska are covered by loess formations. Loess deposits cover approximately one-half of the state, that half being the eastern one.

In the shallow depth, there was a layer of Peorian loess with a thickness of around 9 ft (IS-2.5 and IS-4.5). The soil consisted of mostly silt material with a mixture of clay and very fine sand. The trace of roots of plants and bushes was observed, especially in shallow depths in IS-2.5 (2.5-4ft). As shown in Figure 4.3, there were several cracks and fissures inside the sample, of which one was more significant and spanned the majority of the length of the Shelby tube. From the depth of around 9 to 12 ft, a layer of fine sand was observed (IS-9.5) along with some silty material. It was not possible to extrude the sample from the Shelby tube without crumbling. The sample from a depth of 14.5-16.5 ft had a large amount of sand particles in it. The soil consisted of clay, silt, and sand materials. The size of the sand particles was bigger than those in the upper layers (IS-2.5 & IS-4.5), and it was distributed all around the sample. Random gravel particles with the size of about 8 mm to 12 mm were also seen. In this sample, some roots of plant and twigs were observed (Figure 4.4). Natural fissures and cracks were seen during the sample trimming. It made sample trimming process difficult. In some parts of the sample, a brittle clump of sand particles that easily crumbled was observed.

Figure 4.3 Cracks and fissures inside the Shelby tube (IS-2.5) form shallow depth (I-180 and Superior St.)

Figure 4.4 Non-uniformity and cracks in Sample IS-14.5 (I-180 and Superior St.)

4.4.2 North-Loup undisturbed samples

For this project, based on the available samples and the CPT test results in the field, three Shelby tubes from different depths were selected for testing. The first sample was chosen from shallow depth (4.5 ft to 6.5 ft) and named NL-4.5. It was a clayey sand (SC) with very fine sand particles. The sample was a very delicate material in terms of difficulty in sample preparation procedure. The soil was moist with initial water content at 23.5%. The sample from a deeper depth was NL-14.5 from 14.5 to16.5 ft. The soil was sandy silty clay (CL-ML) with an initial moisture content of 19.9%. As shown in Figure 4.5, there were some openings and cracks on the sample. The tube was cut to a smaller length to facilitate the sample extrusion due to difficulties in extruding it using a hydraulic sample extruder. Pieces of chalk were observed inside the sample.

Figure 4.5 Cracks on sample NL-14.5

The next sample from 19.5 ft to 21.5 ft depth was named NL-19.5. The soil was lean clay with a good amount of very fine sand. However, the soil consisted of some silt material as well. Random gravel particles with a size of around 4 mm were also seen. The initial moisture content varied from 25.8% to 31.2%. At the deeper depth, the initial water content increased. In the middle of the layer, the color of the soil became darker.

4.4.3 Spencer samples

The samples from this failed slope consisted of shale and highly overconsolidated clayey materials. Generally, the soil was weathered, and cracks and fissures were seen on it. The material was dark and very hard to trim. Due to many cracks and openings, it was challenging to prepare a specimen from these materials, especially in shallow depth that was more weathered (Figure 4.6). Therefore, in this study, the samples in the site were not used for strength tests such as the triaxial and the unconfined compression test, but for only swelling tests.
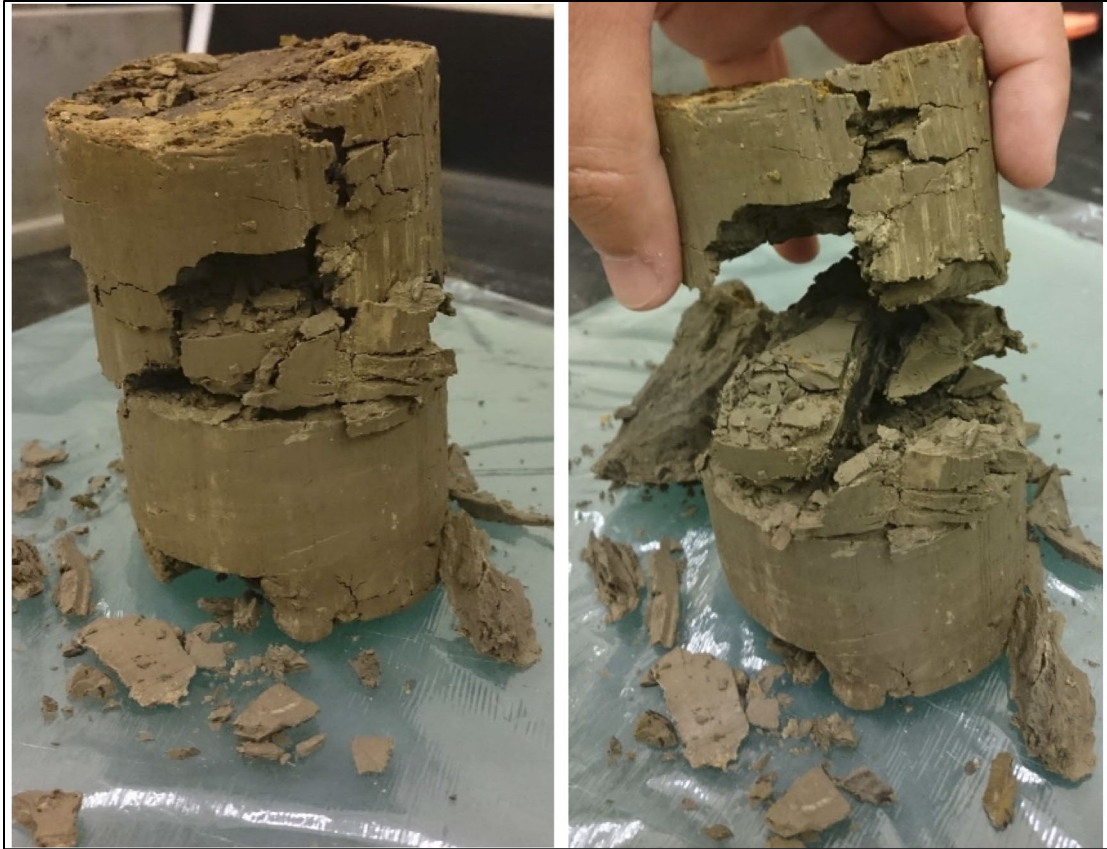
Figure 4.6 Cracks and fissures on samples from Spencer slope

4.5 Testing procedure

4.5.1 Water contents

The natural water content of each sample was determined based on ASTM-D2216. In addition, the water content of samples was measured after the triaxial tests.

4.5.2 Atterberg limits

The liquid limit, plastic limit, and plasticity index of samples from each Shelby were determined based on ASTM-D4318.

4.5.3 Unconfined compression tests

Unconfined compression tests were conducted based on ASTM-D2166. This test provides shear strength parameters of soils with rapid loading and without pore pressure dissipation.

4.5.3.1 Apparatus

An automated test apparatus from the GeoJac (Sigma-1 5K) system was used to conduct the unconfined compression test. The machine consisted of a load frame (Servo3613), computer (HP Desktop Tower 251-a244), power supply (GeoTac-110Vac), and network module (NMC-285). The load frame had a capacity of 2000 pounds and a 1.5-inch stroke. A vertical load cell with a capacity of 500 pounds was connected to the piston. There was a vertical deformation sensor (LVDT) inside the machine, which could measure the vertical movement with the accuracy of 1×10^{-4} in.

4.5.4 Swell pressure tests

To investigate the swell pressure of undisturbed samples, the swell pressure test based on ASTM-D4546 was conducted on samples. In this test method, an intact sample was prepared in the consolidation ring with the dimension of (H×D=1 × 2.5 inches. Then the sample and ring were placed inside the consolidation cell with porous stones on the top and bottom. The sample was inundated with distilled water, and the test was performed. The load cell piston did not allow the sample to swell by increasing the load corresponding to the swell pressure of the sample. For this purpose, a servo- controlled consolidation apparatus from GeoTac (Sigma-1 5K) was used. The configuration of this machine was similar to the one, which was used for unconfined compressive tests.

4.5.5 Triaxial compression tests

Drained and undrained triaxial compression tests were performed according to ASTM D7181 and D4767, respectively. The tests were conducted with an automatic stress path triaxial apparatus form GeoTac (TruePath system) shown in Figure 4.7. Two electromechanical pumps drive the water into the specimen and triaxial cell. The cell pressure actuator had a capacity of 170 ml and 300 psi pressure. The pore pressure actuator had a capacity of 75 ml and 300 psi. Each pump was connected to a water container, which provided the needs of the pumps. The volume and fluid pressure could be measured in both pumps with resolutions of 1 mm^3 and 0.1 kPa, respectively. During the test, those pumps controlled the back pressure and cell pressure automatically according to pre-set condition.

Before starting the test, each of the sensors needed a calibration. Depending on the type of triaxial test (drained or undrained), after the consolidation stage, the drainage valves were kept open (drained condition) or closed (undrained condition). In the undrained condition, the excess pore water pressure during the shear stage was measured with a pore pressure transducer connected to the sample. In this stage, the cell pressure kept constant and the axial load was applied to the sample with a constant strain rate. According to ASTM, the rate of shearing is dependent on the time of 90% consolidation. In this standard, it is assumed that the failure occurred after 4% axial strain.
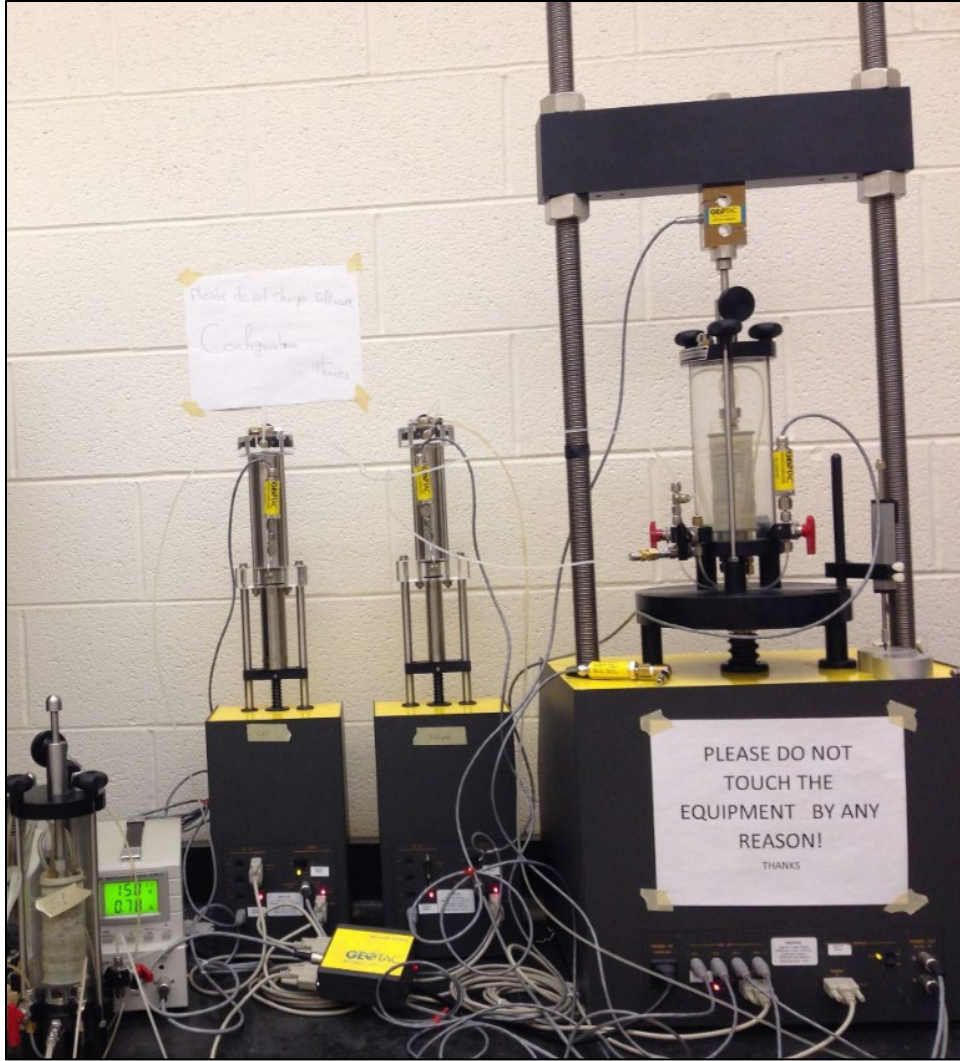
Figure 4.7 GeoTac automated triaxial apparatus

Therefore, the suiTable strain rate in the drained condition with the side drain (filter paper strip) was determined by the following equation:

$$\dot{\varepsilon} = \frac{4\%}{16t_{90}}$$

(4.1)

where t_{90} is the time of 90% consolidation.

In the undrained condition, equation 4.1 changes to the following equation:

$$\dot{\varepsilon} = \frac{4\%}{10t_{50}}$$

(4.2)

where t_{50} is the time of 50% consolidation.

The test continued until the maximum desired strain or maximum desired axial load were reached. The advantage of this software was that it allowed the user to adjust the test setting before each stage.

4.5.6 XRD test

X-ray diffraction (XRD) analyses were conducted by Dr. Shah Vallopilly at the Nebraska Center for Material and Nanoscience using the PANalytical Empyrean diffractometer (PANalytical Inc., Westborough, MA, USA) with Cu-Kα radiation (1.5418 Å) at the 40 kV, 45 mA setting. A mask of 20 mm and a divergence slit of 1/2° were used on the incident beam path. The powder samples with 25 mm × 25 mm area were prepared on the low background quartz plate sample holder, and the powder X-ray diffraction data was collected by continuously scanning a solid state PIXcel3D detector at the rate of 0.027°/s. A Nickel foil filter was used to eliminate the diffraction peaks due to a possible Kβ wavelength.

Profile analysis of the powder diffractograms by the Rietveld method was carried out using TOPAS v5 (Bruker, AXS) software. Bragg intensities based on the crystallographic information of different mineral phases of interest such as Montmorillonite, Illite, Kaolinite, together with common soil materials such as quartz and calcite were generated, and the profile convolution based on a Fundamental Parameter Approach (FP) was implemented to simulate the diffraction profile. Various crystallographic and microstructural parameters were obtained by least-square refinement.

Relative weight percentages of different phases are calculated based on the scale factors obtained from the refinement process.

4.5.7 Sample preparation

The samples are transferred from the field to the laboratory with Shelby tubes. A sample extruder from Material Testing Products was used to extrude the intact samples from the Shelby tubes. After extruding the samples, the sample was trimmed and carved in a sample trimer frame. Depending on sample stiffness, several different trimers and knives were used to carve the samples.

The size of the samples was in the standard range (D×H= 1.4 in × 3.2 in), and the H/D ratio was approximately 2.3. All samples were prepared at the same size to eliminate the size effect on the strength of the samples. The procedure of sample preparation for the swell pressure test was the same as the sample preparation procedure for the consolidation test according to the ASTM standard, except that the sample was not saturated initially. The number of prepared samples for swelling pressure tests, unconfined compression tests, and triaxial tests are summarized in Table 4.3. The samples were classified by each Shelby tube obtained from three different locations such as I-180 & Superior St., North- Loup and Spencer.

Table 4.3 Number of prepared samples for swelling pressure test, unconfined compression test, and triaxial tests

Location	Sample Name	Depth (ft)	Number of samples			
			Swell test	Unconfined compression test	Consolidated drained triaxial test	Consolidated undrained triaxial test
I-180 & Superior St.	IS-2.5	2.5-4	1	2	2	-
	IS-4.5	4.5-6	-	2	2	1
	IS-14.5	14.5-16.5	1	2	2	-
	IS-19.5	19.5-21.5	1	2	-	-
	IS-24.5	24.5-26.5	1	2	-	-
North- Loup	NL-4.5	4.5-6	1	2	2	-
	NL-14.5	14.5-16.5	1	2	1	-
	NL-19.5	19.5-21.5	1	2	-	-
Spencer	-	3.5-4	1	Not good for testing	Not good for testing	Not good for testing
	-	4.5-7	1	Not good for testing	Not good for testing	Not good for testing
	-	7.5-8	1	Not good for testing	Not good for testing	Not good for testing
	-	8-8.5	1	Not good for testing	Not good for testing	Not good for testing

Chapter 5 Test Results and Discussion

<u>5.1 Gradation</u>

A set of gradation tests including sieve analysis and hydrometer tests were conducted on specimens from each Shelby tube obtained from I-180 and Superior St. and North-Loup. Only IS-2.5, IS-4.5, and IS-14.5 samples were selected among five Shelby tubes obtained from I-180 and Superior St., and only NL-4.5 and NL-14.5 were selected among three Shelby tubes obtained from North-Loup for gradation tests. For each Shelby tube, two samples were taken to conduct gradation tests except IS-4.5 and NL-14.5. The gradation test for IS-4.5 was conducted three times, and the test of NL-14.5 was conducted one time. Figure 5.1 shows the results of the gradation tests on the samples. Particle size distribution parameters and soil classification from each test based on the unified soil classification system are shown in Table 5.1. According to the unified soil classification system, the samples belonged to CL (Low compressibility clay, sandy lean clay) and SC (clayey sand). Although IS-2.5, IS-4.5, and NL-4.5 were categorized as SC (clayey sand), the percentage of finer material was very close to clayey soils, and it was difficult to clearly distinguish them from clayey soils (Table 5.1). Additional noTable information is that the uniformity coefficient is extremely high due to the wide variation of particle sizes.
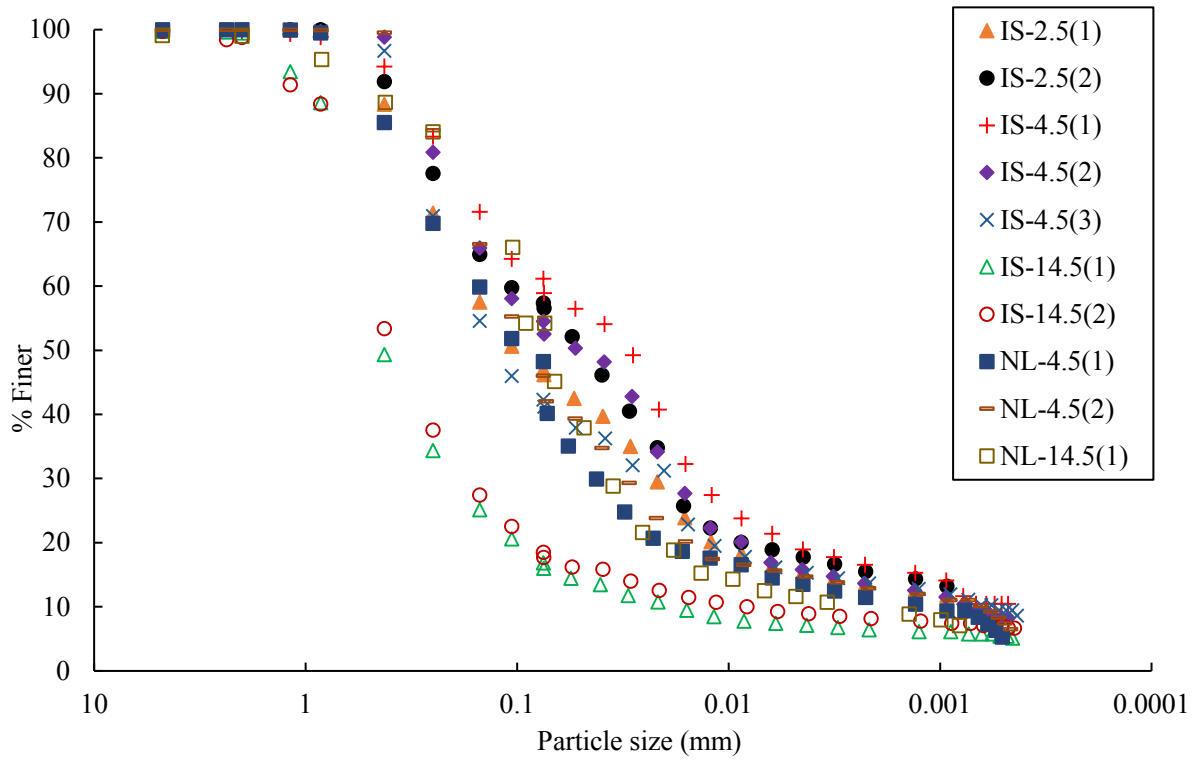
Figure 5.1 Gradation of samples from I-180 and Superior St., and North-Loup failed slopes

Table 5.1 Soil classification according to unified classification system

Location	Sample name	F_{200} (%)	F_4 (%)	Uniformity coefficient (C_u)	Coefficient of gradation (C_c)	Classification	Group
I-180 and Superior St.	IS 2.5(1)	47.0	100	228.6	3.9	SC	Clayey sand
	IS-2.5(2)	57.3	100	265.0	7.6	CL	Sandy lean clay
	IS-4.5(1)	61.2	99.7	114.3	5.2	CL	Sandy lean clay
	IS-4.5(2)	54.5	100	184.6	4.6	CL	Sandy lean clay
	IS-4.5(3)	42.3	100	10.0	12.3	SC	Clayey sand
	IS-14.5(1)	16.8	99.7	28.9	4.3	SC	Clayey sand
	IS-14.5(2)	18.5	99.7	61.3	7.4	SC	Clayey sand
North-Loup	NL-4.5(1)	48.2	100	125	9.8	SC	Clayey sand
	NL-4.5(2)	46.0	100	184.6	12.3	SC	Clayey sand
	NL-14.5(1)	55.6	99.8	90	10.6	CL-ML	Sandy silty clay

5.2 Atterberg limits

Atterberg limit tests that were conducted on samples from each Shelby tube were selected for triaxial testing, and the results are presented in Table 5.2. The test symbols are the same as that of the gradation test. As shown in Table 5.2 and Figure 5.2, the samples belonged to medium plasticity soils. The range of liquid limits was 37% to 51% with the plasticity index about 16% to 27%. However, the sample from the Shelby tube NL-14.5 showed a low plasticity index (6.3%) due to the presence of sand particles.

Table 5.2 Atterberg limits of the samples.

Shelby	Sample name	LL (%)	PL (%)	PI (%)	Average PI (%)
IS-2.5	IS-2.5(1)	41.7	21.6	20.1	21.2
	IS-2.5(2)	45.5	23.2	22.3	
IS-4.5	IS-4.5(1)	39.5	23.4	16.1	18.5
	IS-4.5(2)	42.2	23.4	18.8	
	IS-4.5(3)	42.5	21.8	20.7	
IS-14.5	IS-14.5(1)	46.2	25.1	21.1	23.8
	IS-14.5(2)	51.5	25	26.5	
NL-4.5	NL-4.5(1)	38	17.3	20.7	20.0
	NL-4.5(2)	33	13.6	19.4	
NL-14.5	NL-14.5(1)	29.1	22.8	6.3	-
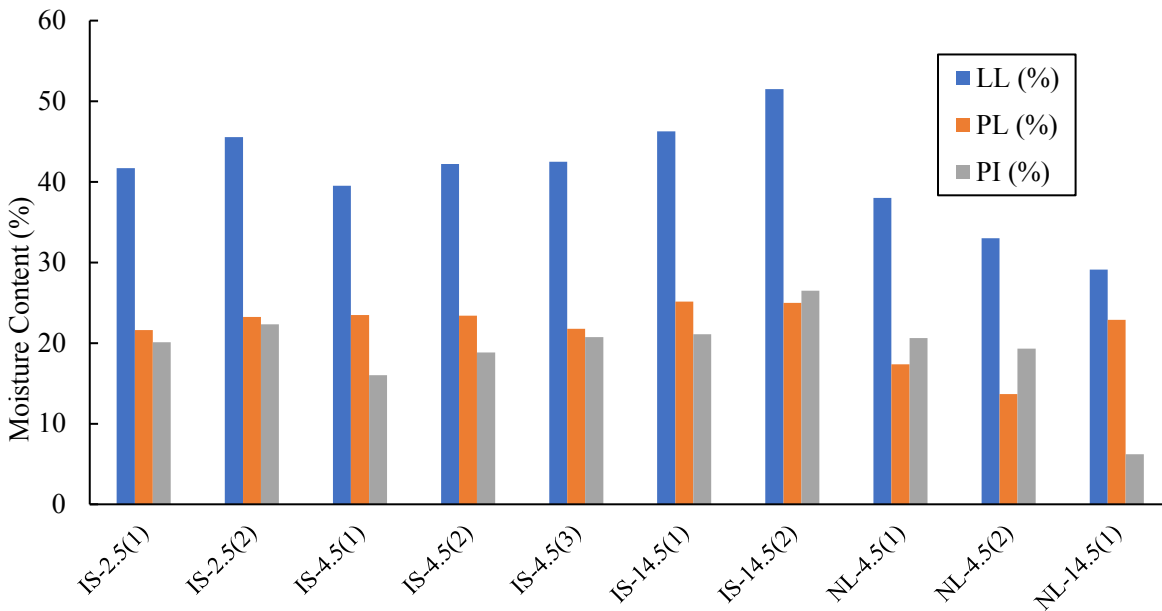
Figure 5.2 Comparison of Atterberg limits

5.3 Unconfined compression strength

The standard test method for an unconfined compression test (ASTM-D2166) was used to measure the unconfined compressive strength of the specimens. For each Shelby tube, two samples were prepared, and the test was conducted on samples at a constant strain rate of one percent per minute.

5.3.1 Unconfined compression strength of samples from I-180 and Superior St.

The unconfined compression test was conducted on the samples from this failed slope, and the unconfined peak strength and the unconfined residual strength are shown in Table 5.3. The first three samples (IS-2.5, IS-4.5, and IS-9.5) belonged to loess formation, and the rest of samples (IS-14.5, IS-19.5, and IS-21.5) belonged to glacial till formation. The tests were conducted for the specimen of IS-2.5 to IS-24.5 (loess material) obtained from Shelby tubes except IS-9.5. For the sample (IS-2.5) at the shallowest depth (2.5 ft- 4 ft), the unconfined shear strength of this depth was high (1880 psf) compared to other samples from this failed slope. The undisturbed sample extruded from the Shelby tube had some natural longitudinal cracks (Figure 4.3), which did not appear in the prepared samples for unconfined compression tests. Moreover, the initial water content of the IS-2.5 was low (13.2% on average). The overconsolidated soils, which contain clay particles at low initial water content usually show higher shear strength (Zydron and Dqbrowska 2012, Bláhová et al. 2013, Daffala 2013). Therefore, the sample showed a high value of unconfined strength.

Table 5.3 Unconfined compression (UC) test at strain rate of 60 %/min on undisturbed samples from I-180 and Superior St.

Shelby	Sample name	Depth (ft)	Strain at failure (%)	Peak shear stress (psf)	Residual shear stress (psf)	Water content (%)	Type of test
IS-2.5	UC-IS-2.5(1)	2.5-4	2.7	1880	570	12.7	UC
	UC-IS-2.5(2)		1.17	1433	390	13.7	UC
IS-4.5	UC-IS-4.5(1)	4.5-6	2.2	1220	137	8.4	UC
	UC-IS-4.5(2)		1.8	764	72.45	N/A	UC
IS-14.5	UC-IS-14.5(1)	14.5-16.5	1.49	205	5	N/A	UC
	UC-IS-14.5(2)		1.76	263	30	17.9	UC
IS-19.5	UC-IS-19.5(1)	19.5-21.5	3.85	1540	344.5	29.9	UC
	UC-IS-19.5(2)		3.28	1444	293	37.0	UC
IS-24.5	UC-IS-24.5(1)	24.5-26.5	2.51	2249	389	31.3	UC
	UC-IS-24.5(2)		2.51	2755	1229	30.4	UC

As shown in Table 5.3, the average unconfined compressive strength of the samples from the IS-2.5 was about 1650 psf. However, it is noted that the unconfined compressive strength of the sample in the field contain many cracks, as shown in Figure 4.3. Therefore, it is believed that the unconfined shear strength of field soils in the location of IS-2.5 could be lower than that of the IS-4.5 specimens.

Usually, the peak shear strength of overconsolidated soils is high enough to show the factor of safety higher than one, which means a stable slope. However, in progressive failure, which is likely to occur in Nebraska, as discussed in chapter two, the average shear strength of soils or a massive portion of it is on residual condition. Therefore, the magnitude of the shear strength reduction from peak strength to residual strength is important in long-term stability analysis. Thus, the residual factor (equation 2.1) as presented by Skempton (1964), was computed as shown in Table 5.4. Moreover, the reduction factor (equation 2.2) which was proposed by Mesri and Abdel-

Ghaffar (1993) was computed, as shown in Table 5.4. From the reduction factor (η) for sample IS-2.5, which was about 0.7, there was about 70% reduction in the shear strength of the soil. Therefore, if a slope is designed based on unconfined peak shear strength, the factor of safety may reduce by 70%, which may be decreased to unity or less, and the slope will fail. The R and η agreed well with existing research (Skempton 1964 and Mesri and Abdel-Ghaffar 1993).

Table 5.4 Reduction factor (Mesri and Abdel-Ghaffar 1993) and residual factor (Skempton (1964) on undisturbed samples from I-180 and Superior St.

Shelby tube No.	Sample name	Peak shear stress (psf)	Residual Strength (psf)	Residual factor (R)	Reduction factor (η)
IS-2.5	UC-IS-2.5(1)	1880	570	1.0	0.27
	UC-IS-2.5(2)	1433	390	0.85	0.35
IS-4.5	UC-IS-4.5(1)	1220	137	0.97	0.13
	UC-IS-4.5(2)	764	72.45	0.85	0.12
IS-14.5	UC-IS-14.5(1)	205	5	0.87	0.15
	UC-IS-14.5(2)	263	30	0.95	0.12
IS-19.5	UC-IS-19.5(1)	1540	344.5	0.97	0.24
	UC-IS-19.5(2)	1444	293	0.92	0.26
IS-24.5	UC-IS-24.5(1)	2249	389	0.98	0.28
	UC-IS-24.5(2)	2755	1229	1.0	0.22

A reason for the sharp shear strength reduction from peak to residual strength may be due to the weak inter-particle bonds of the soil material (Skempton 1970). These inter-particles bonds may contribute as a glue to connect the particles to each other. The quality of the inter-particle bonds may be dependent on the clay mineralogy and stress history of the soil (Li et al. 2016). This noTable shear strength reduction was also seen in the samples from IS-4.5, IS-14.5, IS-19.5, and IS-21.5. As shown in Figure 5.3, there is a sharp reduction from peak strength to residual strength on samples from IS-4.5. The average reduction factor for samples from IS-4.5 was about 0.13, which means that there was about 87% reduction of the shear strength of the soil.
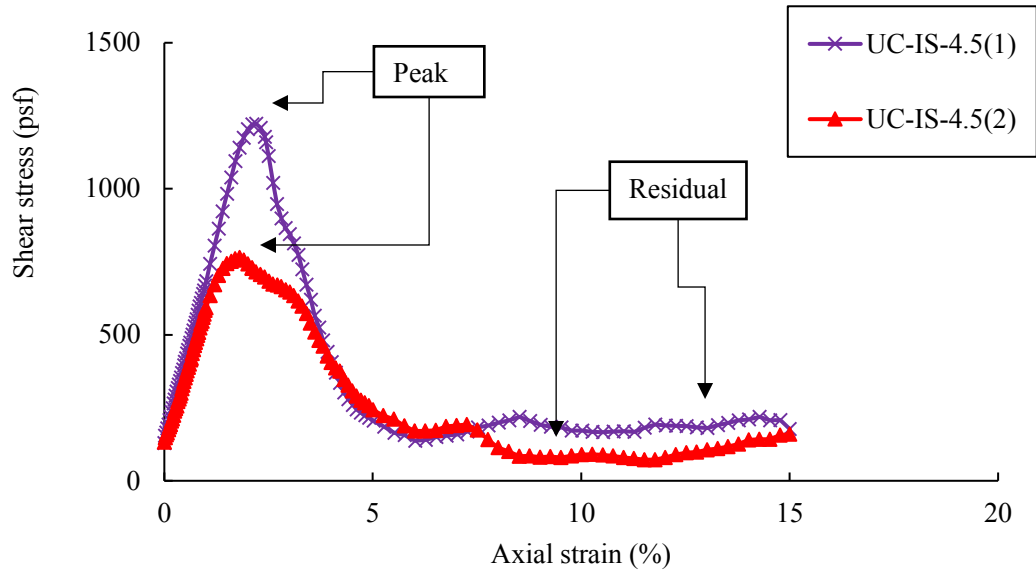
Figure 5.3 Peak and residual shear strength from unconfined compression test on IS-4.5 (I-180 and Superior St.)

Significant shear strength reduction from peak to residual strength for other soils was reported by Skempton (1964), Chandler and Skempton (1974), and Mesri and Abdel-Ghaffar (1993), as shown in Table 5.5.

The average initial water content (11.4%) of samples from Shelby tubes IS-2.5 and IS-4.5 was about one-half of the average plasticity index (21.2%) of the samples, and the samples were almost in dry condition. When the initial water content was higher, the sample showed lower shear strength than the presented condition from unconfined compression tests in Table 5.3.

Table 5.5 Shear strength reduction in slope stability from previous literatures

Literature	Type of soil	Residual factor (R)	Reduction factor (η)	Location
Skempton (1964)	London clay	1.0	-	Jackfield slide
	London clay	0.61	-	Kensal Green slide
	London clay	0.6	-	Northolt slide
	London clay	0.8	-	Sudbury Hill slide
	London clay	0.92	-	-
Chandler and Skempton (1974)	Lias clay	0.65	-	-
Mesri and Abdel-Ghaffar (1993)	London clay	-	0.45	-
	-	-	0.67	River Albedosa slide
	-	-	0.6	Failure at Wettern
	Lias clay	-	0.57	Brecciated failure
	London clay	-	0.65	-

The sample from the 9.5 ft to 11.5 ft depth (IS-9.5) was from a layer of clean sand, on which it was not possible to conduct the unconfined compression test. The initial water content of this specimen was 3.8%, making it practically a dry soil. A rough estimation of the undrained shear strength of this layer was measured using a vane shear test on the sample inside the Shelby tube, and it was 2000 psf. However, it is noted that the result of vane shear test should be used as a reference number because this test is appropriate to estimate the undrained shear strength of cohesive soils.

As shown in the Figure 5.4, the samples from IS-14.5 at the depth of 14.5 ft-16.5 ft had lots of fissures and cracks inside the sample, which might be the reason why these samples showed the lowest unconfined shear strength. In addition, the sample from this Shelby tube contained a high amount of fine sand (83%) mixed with silt and clay particles (17%). Moreover, the samples obtained from IS-14.5 had a relatively low density equal to 88.5 pcf similar to the loess layers that

overlaid it. The maximum reduction factor of unconfined shear strength for IS-14.5 was as high as (95%). The presence of the weak layers such as IS-14.5 might be a serious trigger for global shear strength reduction of a slope and cause a progressive failure.

Figure 5.4 Cracks and fissures inside of the sample from IS-14.5 (I-180 and Superior St.)

The glacial till deposits from 19.5 ft- 21.5 ft (IS-19.5) and 24.5 ft- 26.5 ft (IS-24.5) depths showed the highest unconfined shear strength and residual strength from this failed slope as shown in Figure 5.7.

This significant shear strength reduction from peak to residual strength was reported by Skempton (1964), Chandler and Skempton (1974), and Mesri and Abdel-Ghaffar (1993), as shown in These highly plastic stiff clays from IS-19.5 had an unconfined strength around six times greater than IS-14.5. The unconfined shear strength of IS-24.5 was about 1.5 times higher than IS-19.5. The existence of the other layers such as chalk (Figure 5.5) in the IS-19.5 sample, the presence of a thin layer of sand and gravel inside the sample (Figure 5.6), and its higher initial water content might have decreased the overall strength of this sample. From the reduction factor (η), the unconfined shear strength of the samples from I-180 and Superior St. was reduced on average 80%

from the peak strength. This considerable reduction can decrease the factor of safety and the stability of the slope dramatically. A summary comparison of peak and residual unconfined compression strength from I-180 and Superior St. is shown in Figure 5.7.

Figure 5.5 Layer of chalks (red arrow and boxes) in sample IS-19.5 (I-180 and Superior St.)

Figure 5.6 Sand particles inside of sample IS-19.5 (I-180 and Superior St.)
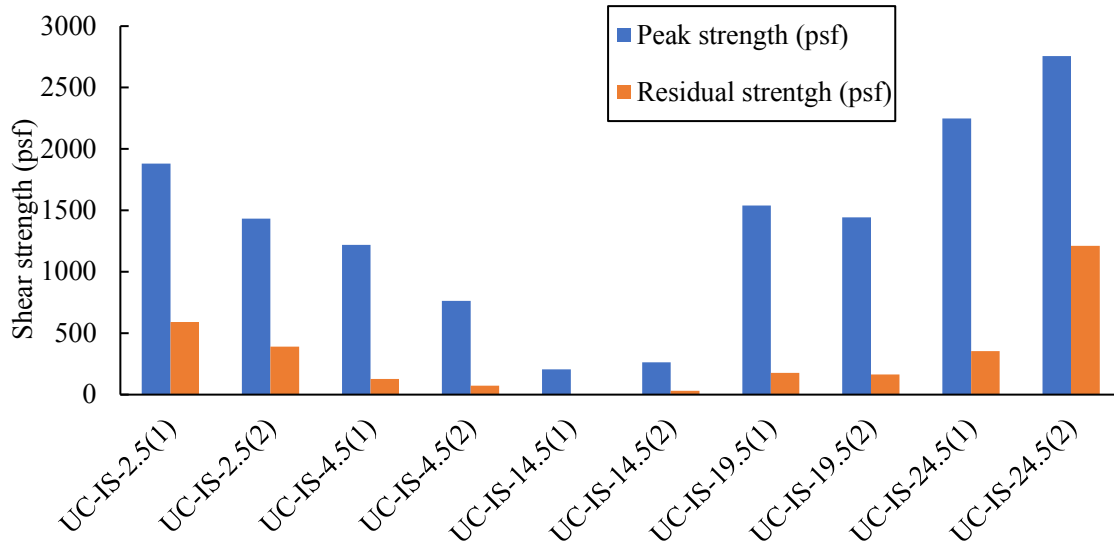
Figure 5.7 Comparison of peak and residual unconfined compression strength from different depth (I-180 and Superior St.)

5.3.2 Unconfined compression strength of samples from North-Loup

The samples obtained from the North-Loup belonged to Peoria loess. As shown in Table 5.6, the unconfined compressive strength of the samples was significantly lower than the samples consisting of glacial till formation in the I-180 and Superior St. slope. It is noted that the critical factor for showing low unconfined compression shear strength might be related to low inter-particle bonds of loess materials when the initial moisture content is high. With the presence of the water, the loessy soils lose their cementation between particles and present low strength. For example, a comparison between the samples from NL-14.5 and NL-19.5 showed that the unconfined compressive strength was decreased from 500 psf to 291 psf, respectively when the initial water content was increased from 19.9% to 25.8%. The NL-14.5 and NL-19.5 have very similar composition as of sandy silty clay. As shown in Figure 5.8, there is a sharp reduction from peak shear strength to the residual shear strength of samples from NL-14.5, which is a typical

67

behavior of collapsible soils. The stress-strain curves for unconfined compression test results for

other samples from this location are illustrated in Appendix A.

Table 5.6 Unconfined compression (UC) test on undisturbed samples from North-Loup

Sample	Sample No.	Depth (ft)	Strain at failure (%)	Strain Rate (%/min)	Peak shear stress (psf)	Residual shear strength (psf)	Water content (%)	Type of test
NL-4.5	UC-NL-4.5(1)	4.5-6	5.01	60	195.5	42	23.5	UC
	UC-NL-4.5(2)		5.4	60	437.96	164		UC
NL-14.5	UC-NL-14.5(1)	14.5-16.5	1.72	60	500	68	19.9	UC
	UC-NL-14.5(2)		1.39	60	412	13		UC
NL-19.5	UC-NL-19.5(1)	19.5-21.5	2.69	60	291	39	25.8	UC
	UC-NL-19.5(2)		2.51	60	338	133	31.2	UC
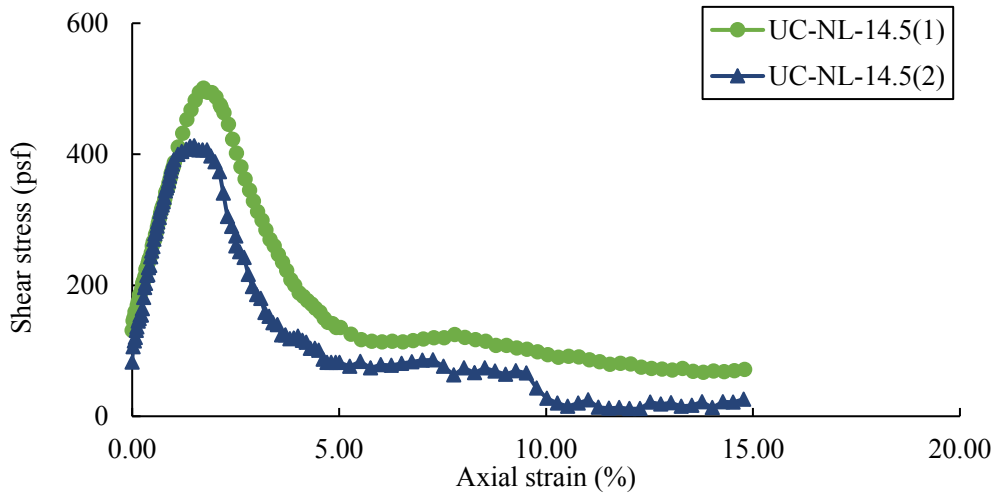
Figure 5.8 Peak and residual shear strength from unconfined compression test on NL-14.5 (North-Loup)

Table 5.7 shows the residual shear strength from North-Loup. The low residual shear strength supports the idea that the slope has a high potential for further movement after the first-time failure where the shear strength of the overconsolidated soils are at residual deformation condition, because the residual shear strength of the soils is almost negligible. This condition may be exacerbated during prolonged rainfall. Low residual shear strength at a shallow depth may be the main reasons for subsequent movements of slopes after the first-time failure. In case of heavy rainfall where the height of the phreatic surface increases, the pore water pressure may increase for a short period of time in shallow depth, and the effective stress and shear strength acting on this depth may be reduced significantly.

Table 5.7 Reduction factor (Mesri and Abdel-Ghaffar 1993) and residual factor (Skempton (1964) on undisturbed samples from North-Loup

Sample	Sample No.	Peak shear stress (psf)	Residual Strength (psf)	Residual factor (R)	Reduction factor (η)
NL-4.5	UC-NL-4.5(1)	195.5	42	0.45	0.64
	UC-NL-4.5(2)	437.96	164	1.0	0.28
NL-14.5	UC-NL-14.5(1)	500	68	0.77	0.34
	UC-NL-14.5(2)	412	13	0.62	0.40
NL-19.5	UC-NL-19.5(1)	291	39	0.32	0.72
	UC-NL-19.5(2)	338	133	0.63	0.60

Moreover, the presence of some weak layers with particularly low shear strength compared to the other layers are the additional reason for slope failure. For example, the unconfined shear strength of samples from IS-14.5 were about one seventh of the average unconfined shear strength of samples from the I-180 and Superior St. slope and it contained fine sand layers. Therefore, the shear strength of soils around the depth of IS-14.5 is reduced to the residual condition much faster than the other layers by rain water and initiated the failure. As shown in Figure 5.7, the residual

strength of this sample was almost negligible. Therefore, an additional stress is transferred to the adjacent layers and progressively reduces the shear strength of the entire slope and causes a failure. Moreover, fissures and cracks may become an additional source of stress concentration and increase the gap between the peak and the residual strength in overconsolidated soils (Skempton 1964).

5.4 Swell pressure tests

A series of swell pressure tests (ASTM- D4546) were conducted on undisturbed samples to investigate the swell pressure of the soils, which may have an effect on the shear strength reduction behavior of the samples.

Figure 5.9 shows the swell pressure test results on I-180 and Superior St. (noted as IS) and the North-Loup (noted as NL) undisturbed samples. According to XRD test results (Appendix C), swelling pressure might be increased due to a high percentage of montmorillonite found in XRD tests (Appendix C). For example, the IS-2.5, which had 0.01% montmorillonite and 20.52% illite, had a swell pressure about 100 psf. While, as shown in Figure 5.10, IS-24.5 consisted of about 10% montmorillonite, 15% illite, and 25% kaolinite with the swell pressure of about 500 psf, which was the highest swell pressure among the samples from the I-180 and Superior St. slope. As shown in Figure 5.9, the swell pressure of the soil layers from North-Loup was very low, where NL-4.5 and NL-19.5 showed approximately negligible pressure. It is believed that as the swell pressure of this material was insignificant, perhaps, they did not consist of expansive minerals and the swell pressure curve was approximately plateau.
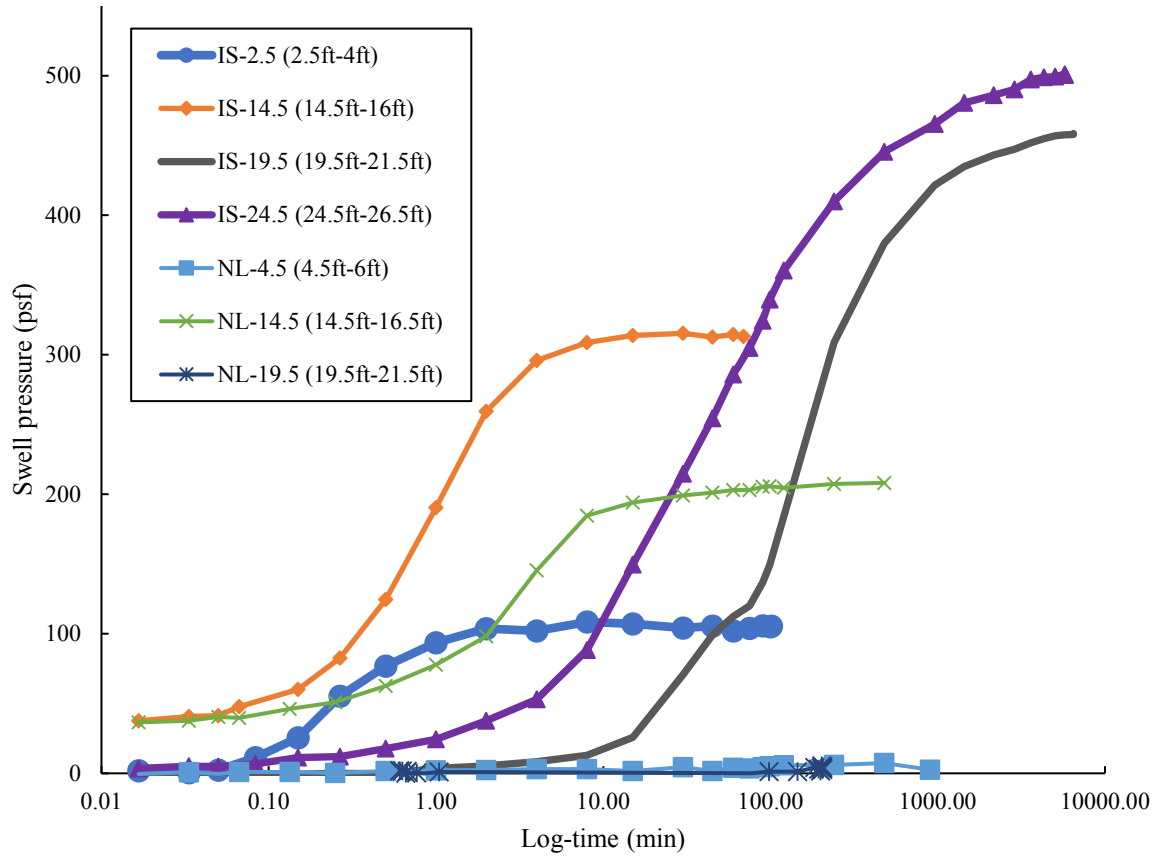
Figure 5.9 Swell pressure results for I-180 and Superior St. (IS) and North-Loup (NL)
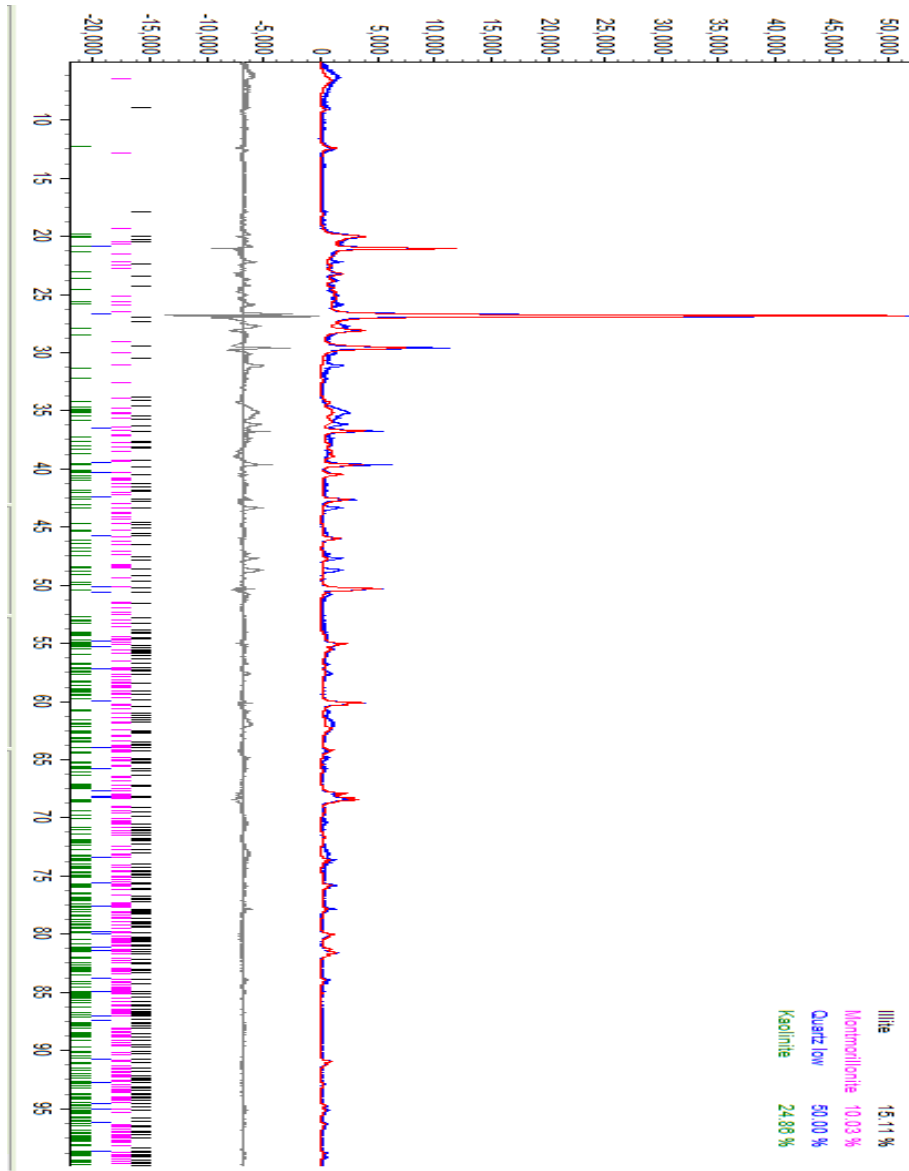
Figure 5.10 XRD analysis on sample from IS-24.5, I-180 and Superior St. slope (Glacial till, 24.5 ft-26.5 ft)

According to the swell pressure test results from undisturbed samples from I-180 and Superior St., and North-Loup, and a comparison with swell pressure results from Spencer slope (Figure 5.11), which consisted of Pierre shale material, the swelling phenomenon of the Pierre shale formation in Spencer may exert a significant effect on the stability of slopes due to considerably higher swell pressure. As shown in Figure 5.11, the swelling pressure was higher

than samples from I-180 and Superior St. and North-Loup, which might relate to the amount of expansive minerals in the samples. For example, as shown in Table 5.8, the percentages of montmorillonite at a shallow depth (3.5 ft – 4 ft) in Spencer was 6.64 %, while the percentages of montmorillonite at a similar depth (2.5 ft – 4.5 ft) in I-180 and Superior St. was 0.01%, in which the swelling pressure was 106 psf and 409 psf, respectively. Therefore, the water content of the soil could be increased due to swelling for the Spencer slope, and it might cause a significant reduction in shear strength of the soil (Calabresi and Scarpelli 1985, and Wong 1998). As shown in Figure 5.11, the highest swell pressure of samples from Spencer was 4000 psf at the depth of 8 ft to 8.5 ft. At this depth, the overburden pressure was about 5300 psf. Therefore, the soil did not swell. However, when these shales are exposed to zero or reduced pressure due to cutting, it may swell and act as a starting point of progressive failure.

Table 5.8 Clay mineralogy from XRD test

Sample ID	Quartz low (%)	Illite (%)	Kaolinite (%)	Montmorillonite (%)	Calcium carbonate (%)
IS-2.5	74.92	20.52	3.35	0.01	1.20
IS-4.5	72.73	19.27	6.81	0.01	1.19
IS-19.5	51.49	15.29	23.02	11.20	-
IS-24.5	50.00	15.11	24.86	10.03	-
Spencer (3.5ft-4ft)	43.44	5.02	5.9	6.64	38.99
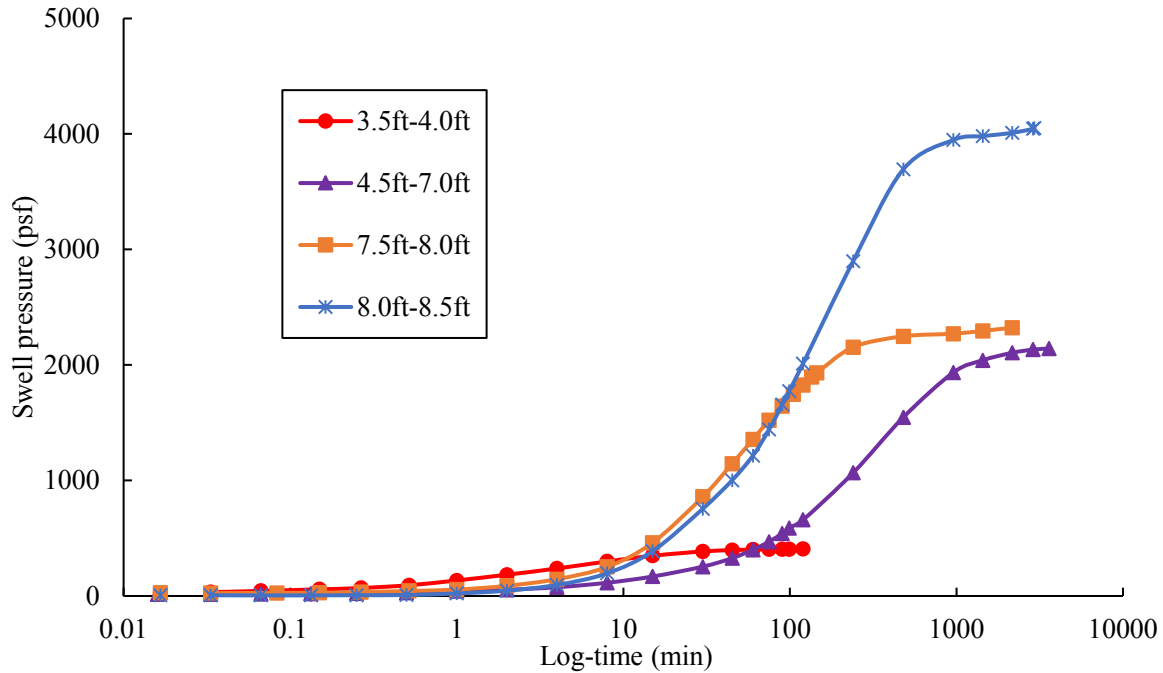
Figure 5.11 Swell pressure results from Spencer undisturbed samples

The rate of swelling pressure for samples was predicted similar to the method that coefficient of consolidation was predicted by Casagrande and Fadum (1940), and equation 5.1 was used to predict the coefficient of rate of swelling pressure (similar to the equation for predicting the coefficient of consolidation).

$$c_v = \frac{T_v \times H_{dr}^2}{t_{50}}$$ (5.1)

where c_v is the coefficient of the rate of swelling, T_v is the time factor, H_{dr} is average longest drainage path during the swell pressure test, and t_{50} represents the time corresponding to 50% swell pressure.

For each sample, t_{50} was calculated from the swell pressure versus time (Figure 5.9 and Figure 5.11) based on the method proposed by Casagrande and Fadum (1940). The time factor (T_{50}) was calculated based on the proposed number from Das (2010) for a 50% average degree of consolidation. As the samples were drained at both the top and bottom, H_{dr} was considered equal to one-half of the average height of the sample during the swell pressure test (equal to 0.5 in). Table 5.9 shows the calculated coefficient rate of the swelling based on equation 5.1.

Table 5.9 Coefficient of rate of swelling pressure

Location	Shelby tube	Depth (ft)	t_{50} (min)	Coefficient of rate of swelling (in^2/min)
I-180 & Superior St.	IS-2.5	2.5-4	0.34	0.1449
	IS-14.5	4.5-6	1.1	0.0448
	IS-19.5	19.5-21.5	190	0.0003
	IS-24.5	24.5 -26.5	46	0.0011
North-Loup	NL-4.5	4.5-6	13	0.0038
	NL-14.5	14.5-16.5	2.7	0.0182
Spencer	-	3.5-4	6	0.0082
	-	4.5-7	350	0.0001
	-	7.5-8	54	0.0009
	-	8-8.5	140	0.0004

5.5 Triaxial compression tests

A series of consolidated drained and consolidated undrained triaxial tests were conducted for undisturbed samples according to ASTM- D7181 and ASTM- D4767, respectively. Both drained and undrained shear tests were conducted to investigate the role of pore water pressure in the shear strength of overconsolidated soils. Table 5.10 shows the type of conducted test (drained or undrained), and the applied confining stress on each sample. It is noted that the first two letters

of the name of the samples show the type of triaxial test conducted on the samples (CD refers to
consolidated drained test and CU refers to consolidated undrained test).

Table 5.10 Type of triaxial test conducted on samples and applied confining stress

Location	Shelby tube	Depth (ft)	Sample name	Type of test	Confining stress (psf)
I180-Superior St.	IS-2.5	2.5-4	CD-IS-2.5(1)	Consolidated drained (CD)	288
			CD-IS-2.5(2)	Consolidated drained (CD)	72
	IS-4.5	4.5-6	CD-IS-4.5(1)	Consolidated drained (CD)	488
			CD-IS-4.5(2)	Consolidated drained (CD)	216
			CU'-IS-4.5(3)	Consolidated undrained (CU')	216
	IS-14.5	14.5-16.5	CD-IS-14.5(1)	Consolidated drained (CD)	1440
			CD-IS-14.5(2)	Consolidated drained (CD)	216
North-Loup	NL-4.5	4.5-6	CD-NL-4.5(1)	Consolidated drained (CD)	648
			CD-NL-4.5(2)	Consolidated drained (CD)	216
	NL-14.5	14.5-16.5	CD-NL-14.5(1)	Consolidated drained (CD)	216

5.5.1 Over-consolidation ratio

The over-consolidation ratio (OCR) of the soils is defined as the ratio of the maximum
stress that soil experienced in the past, divided by the current stress (equation 5.2). The
overconsolidated soils have an OCR greater than one.

$$OCR = \frac{\sigma_c}{\sigma_0} \tag{5.2}$$

where σ_c is pre-consolidation stress and σ_o is current stress. To predict the pre-consolidation stress of the soils, the relationship between effective stress and void ratio or axial strain from the consolidation test is needed. The results from the consolidation stage from triaxial tests are just volume change versus time at a certain effective confining stress, which is unlikely to be used for predicting the pre-consolidation stress of the samples. Therefore, in this research, the pre-consolidation stress of the samples was approximately calculated by using empirical correlation (equation 5.3) from Stas and Kulhawy (1984).

$$\sigma_c = 10^{(1.11-1.87LI)} \tag{5.3}$$

where LI is liquidity index of the samples (equation 5.4).

$$LI = \frac{\omega - PL}{PI} \tag{5.4}$$

where ω is water content, PL is plastic limit, and PI is plasticity index of the samples.

Table 5.11 shows the calculated LI for the samples. According to Das (2010), LI less than zero (negative value) represented the highly overconsolidated soils. As shown in Table 5.11, the OCR of the samples was predicted to be 4 to 15, except IS-2.5(2), IS-14.5(2), and NL-4.5(2) that had an over-consolidation ratio of 40, 51, and 44, respectively. These very high OCR could be because of the low effective confining stresses, which were applied on the samples. For example, the effective confining stress of IS-2.5(2) was 72 psf. According to Peck et al. (1973), highly overconsolidated soils had an OCR greater than 6. Therefore, it can be concluded that the samples from I-180 and Superior St. and North-Loup are categorized as highly overconsolidated soils.

Table 5.11 Estimated over-consolidation ratio of the samples

Sample ID	LI (%)	Average LI (%)	Predicted Preconsolidation stress (psf)	Confining Stress (psf)	OCR
IS-2.5(1)	-0.49	-0.52	2851.70	288	10
IS-2.5(2)	-0.54			72	40
IS-4.5(1)	-0.76	-0.58	2132.20	488	4
IS-4.5(2)	-0.55			216	10
IS-4.5(3)	-0.45			216	10
IS-14.5(1)	-0.24	-0.20	11069.09	1400	8
IS-14.5(2)	-0.17			216	51
NL-4.5(1)	-0.05	-0.24	9503.66	648	15
NL-4.5(2)	-0.42			216	44

5.5.2 Shear stress-strain behavior

Figure 5.12 shows the stress-strain behavior for the six consolidated drained tests conducted on specimens from I-180 and Superior St. slope. As shown in the Figure, with decreasing the effective confining stress on samples, there is a dramatic reduction on the shear strength of soils as expected. As an example, the shear strength of IS-2.5 at 288 psf effective confining stress was 2870 psf while the shear strength of soil at low effective confining stress (72 psf) was 475 psf. The reduction rate of the drained shear strength of IS-2.5 due to reduced confining stress is about 0.8. This value was calculated as a ratio between the drained shear strength reduction from high to low effective confining stress to the drained shear strength of the soil at high confining stress. In other words, the samples from IS-2.5 lost about 80% of their shear strength when low confining stress was reduced. If this high reduction of shear strength of the soil is considered in the stability of the slope, it can reduce the factor of safety by 80%.
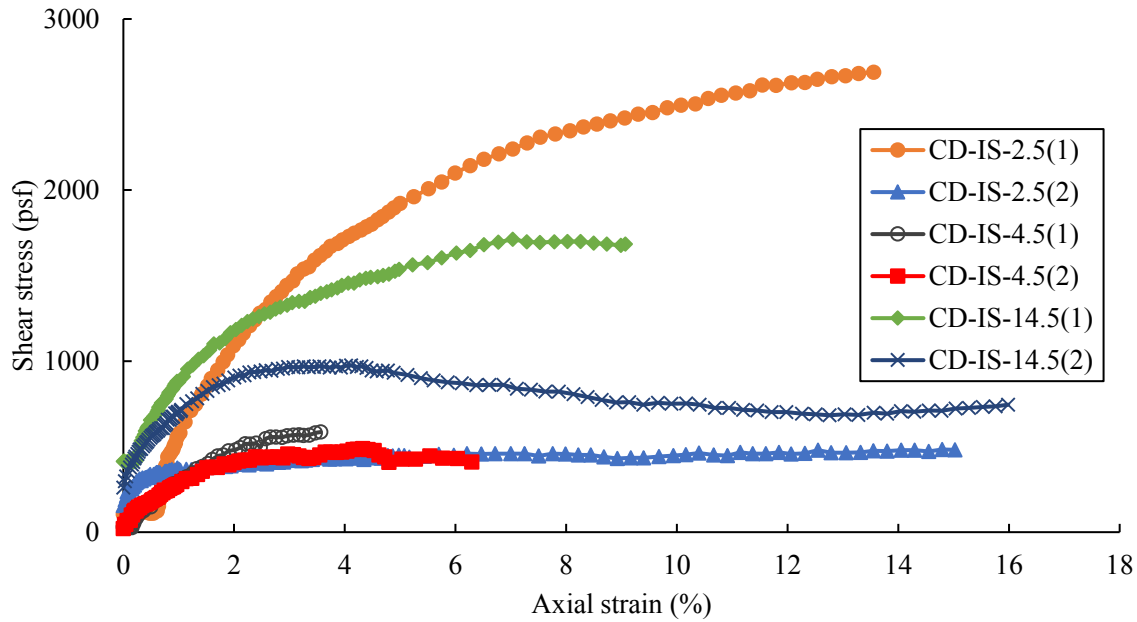
Figure 5.12 Consolidated drained stress-strain curves for I-180 and Superior St.

A significant portion of strength reduction in sample IS-2.5 (2.5 ft-4 ft) might be due to voids and cracks on the sample, as shown in Figure 4.3. However, this sharp shear strength reduction from high effective confining stress to low effective confining stress might be as a result of inhomogeneous material in both samples from IS-2.5. The effective stress based Mohr's circle from IS-2.5 is shown in Figure 5.13. The calculated effective internal friction angle of IS-2.5 was about 55°, which is impossible. A comparison of Mohr's circles of this sample shows that the Mohr's circle of CD-IS-2.5(2) at low effective stress (72 psf) was extremely small, which means that the sample did not have a logical drained strength. The reason of this behavior might be absorbing a high amount of water at a low effective stress level during the drained triaxial test. Therefore, the sample showed this very low Mohr's circle.

As illustrated in Figure 5.12, on IS-14.5 (14.5 ft-16 ft), the shear strength of soil was 1700 psf at a high effective confining stress (1440 psf), while it reduced to 965 psf at a low normal

effective stress. The drained shear strength reduction ratio between the drained shear strength of

the sample from IS-14.5 at a low confining stress to a drained shear strength at a high confining

stress was about 0.4, which meant that there was a 60% strength reduction due to reducing the

confining stress (Figure 5.14). From Mohr's circle, the effective internal friction angle of this

sample was about 22°, which supports the reliability of the 60% shear strength reduction at a low

effective confining stress condition.
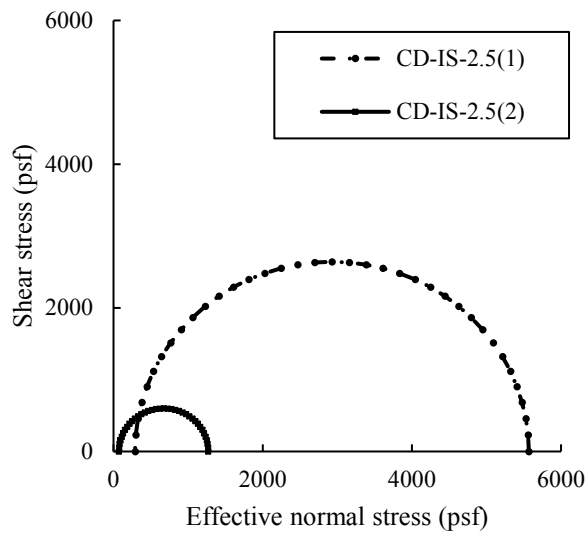
Figure 5.13 Consolidated drained effective stress Mohr's circle of samples from IS-2.5 (I-180 and Superior St.)
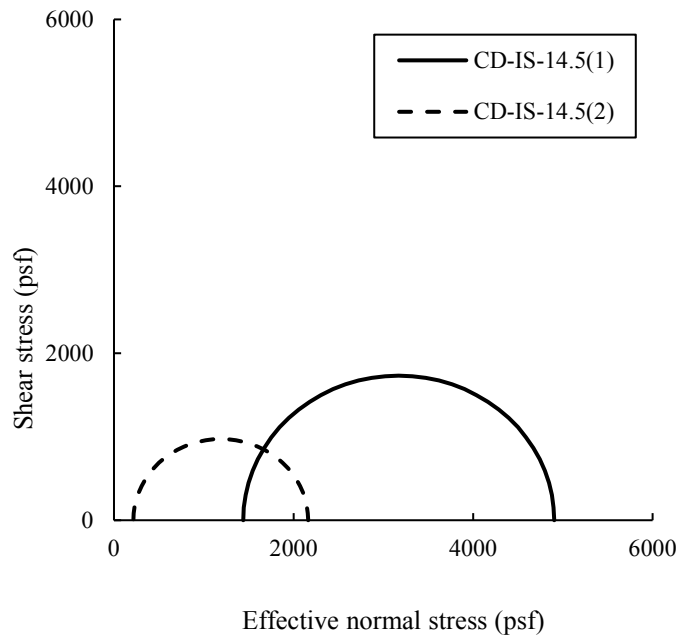
Figure 5.14 Consolidated drained effective stress Mohr's circle of samples from IS-14.5 (I-180 and Superior St.)

As illustrated in Figure 5.15, there was a sharp reduction in the shear strength of the soils at a low effective stress level for samples from North-Loup. As shown in Figure 5.16, the shear strength of the specimen from NL-4.5 (4.5ft-6ft) was reduced from 1726 psf to 572 psf when the effective confining stress was decreased from 648 psf to 216 psf. The effective internal friction angle of NL-4.5 was about 45° which is not a very reliable value. Similar to the case of samples from IS-2.5 a comparison of Mohr's circles of NL-4.5 sample shows that the Mohr's circle of CD-NL-4.5(2) at a low effective stress (216 psf) was extremely small, which means that the sample did not have a logical drained strength. The reason for this behavior might be absorbing a high amount of water at a low effective stress level during a drained triaxial test. Therefore, the sample showed this very low Mohr's circle. The triaxial test result on each sample is shown on Appendix B.
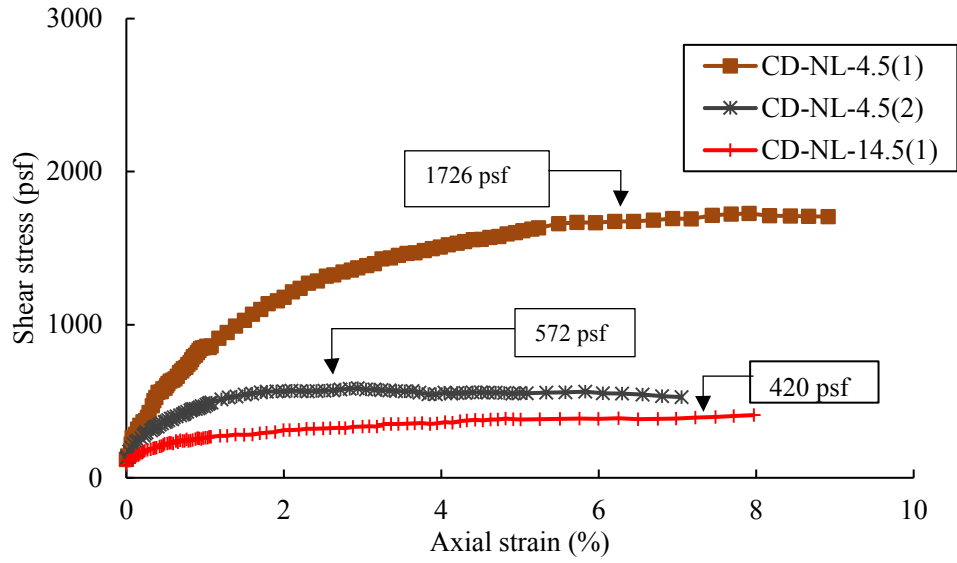
Figure 5.15 Stress-strain curves for North-Loup slope for consolidated drained triaxial test
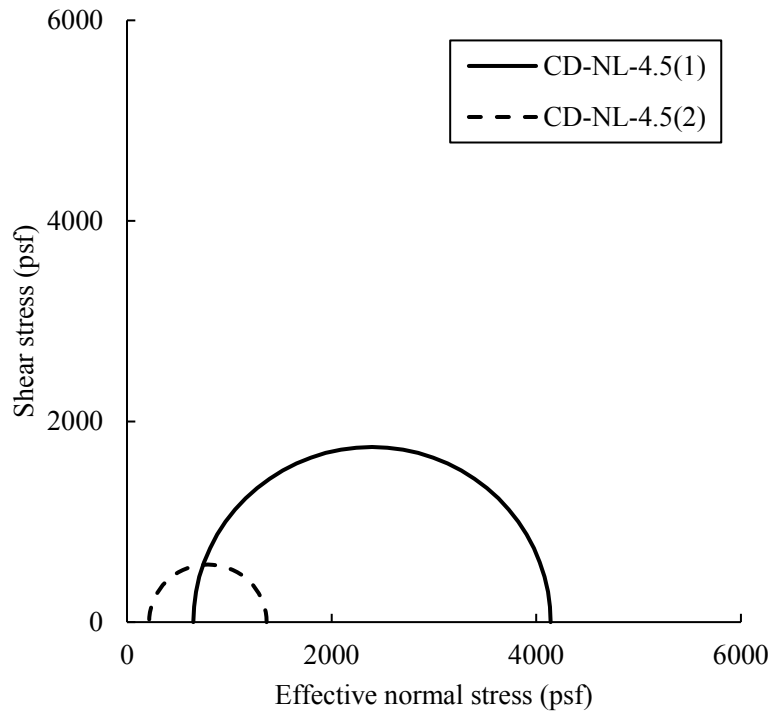
Figure 5.16 Consolidated drained effective stress Mohr's circle of samples from NL-4.5 (North-Loup)

A consolidated undrained test with pore pressure measurement (CU') was conducted on samples from IS-4.5 at shallow depth. As shown in the Figure 5.17, the undrained shear strength of soil at a low effective confining stress was not only approximately 2.3 times the drained shear strength at the same confining stress level (low effective confining stress equal to 216 psf) but also was about 1.7 times higher than the drained shear strength at a high effective confining stress (488 psf). In this regard, the drained shear strength at 488 psf effective confining stress (high effective confining stress) was 560 psf, and the drained shear strength at 216 psf effective confining stress (low effective confining stress) was 410 psf while the undrained shear strength of the soil at 216 psf effective stress was 950 psf. This high shear strength in the undrained condition is due to negative pore pressure (Figure 5.18) in overconsolidated soils. These trends for higher undrained strength for overconsolidated clays were in agreement with the results from Henkel and Skempton (1954), and Gu et al. (2016). As shown in Figure 5.18, the maximum negative pore water pressure of the CU'-IS-4.5(3) is about 280 kPa, which caused an increase in the undrained shear strength of soil. Therefore, it is not conservative to use the undrained shear strength of soil for long term stability of slopes. The effective stress based Mohr's circle from this sample is shown in Figure 5.19. The effective internal friction angle for IS-4.5 was about 22° and it supports 1.4 times reduction of the drained shear strength at high effective confining stress to low effective confining stress that was about 1.4 times.
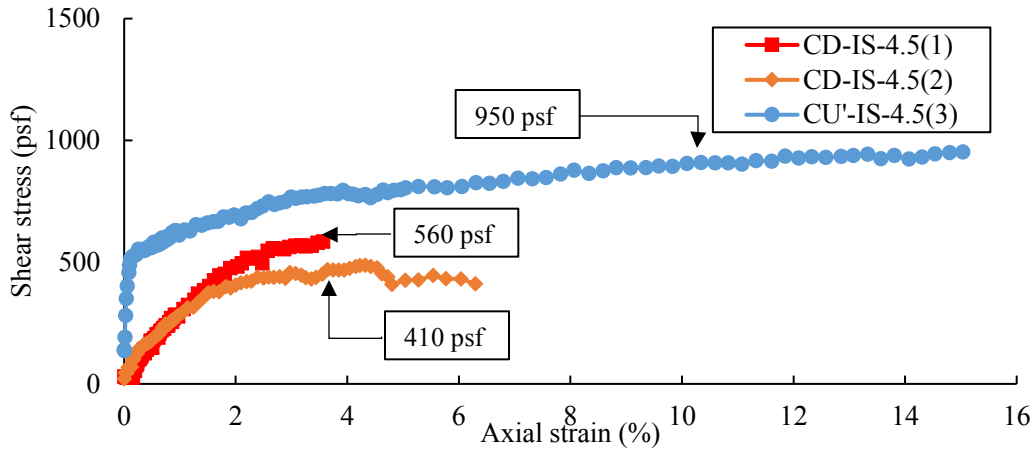
Figure 5.17 Comparison between drained and undrained stress-strain curves for I-180 and Superior St.
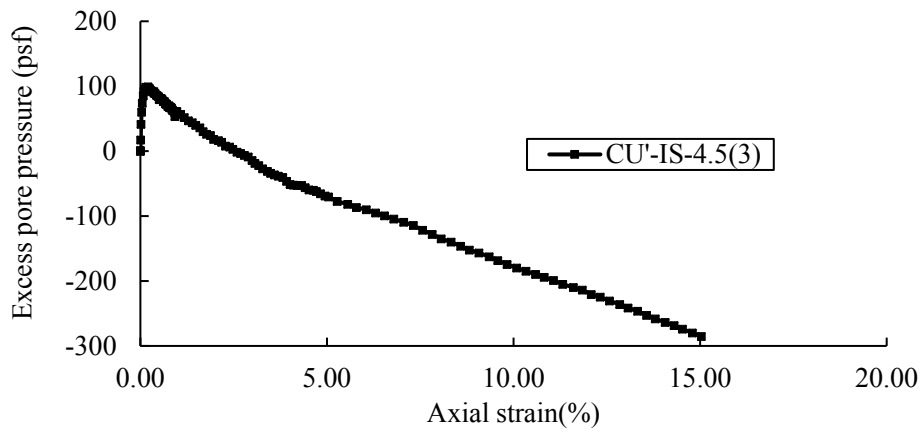
Figure 5.18 Pore pressure variation during triaxial consolidated undrained test (IS-4.5, I-180 and Superior St.)
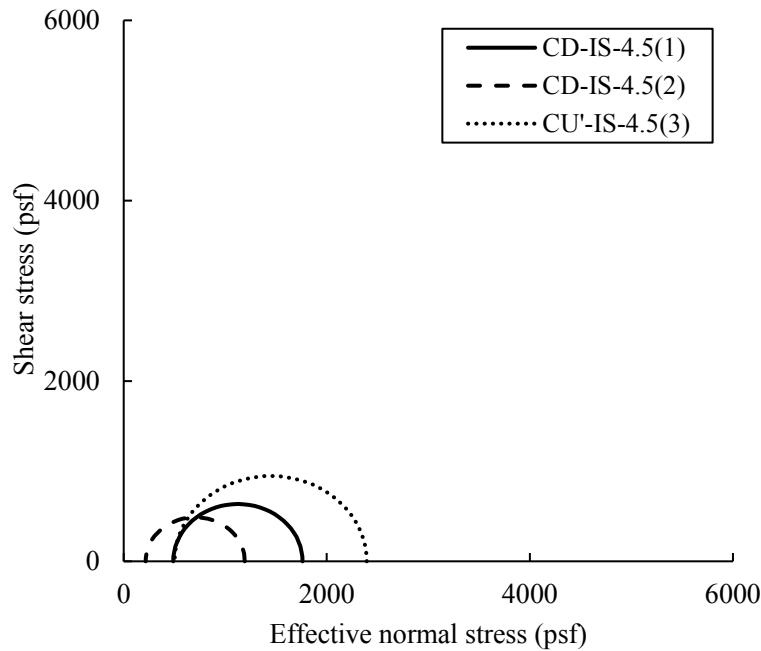
Figure 5.19 Effective stress Mohr's circle of samples from IS-4.5 (I-180 and Superior St.)

5.5.3 Volume change behavior

The volume change behavior of undisturbed samples was monitored during the triaxial tests to investigate the effect of low confining stress level on the samples during consolidation and shearing stages. The volume expansion during these stages can reduce the shear strength of the soil due to water absorption and softening.

5.5.3.1 During Consolidation stage

The volume expansion in the soil at a low stress level happened in some samples during the consolidation stage. For instance, as shown in Figure 5.19 the swell pressure of IS-14.5 (14.5 ft-16.5 ft) was about 300 psf. As shown in Figure 5.20, while consolidation pressure was 216 psf for consolidation stage the sample consolidated until swelling kicked in. As water content gets high, then swelling pressure exceeded consolidation stress, then net volume change became

swelling. The sample consolidated for about 100 minutes to -0.19% volumetric strain where it showed an approximate complete cycle of consolidation, and then it started to swell through the rest of the test to 1440 minutes to -0.021% volumetric strain. This swelled shape of the sample is shown in Figure 5.21.

Besides, conducting the triaxial consolidation test at a low effective confining stress condition showed an uncommon behavior of soil during the consolidation stage at the triaxial compression test. Figure 5.22 shows that the swelling pressure and consolidation pressure were well balanced for the specimen from NL-14.5 (North-Loup, Peoria loess) that has a swell pressure of 208 psf.
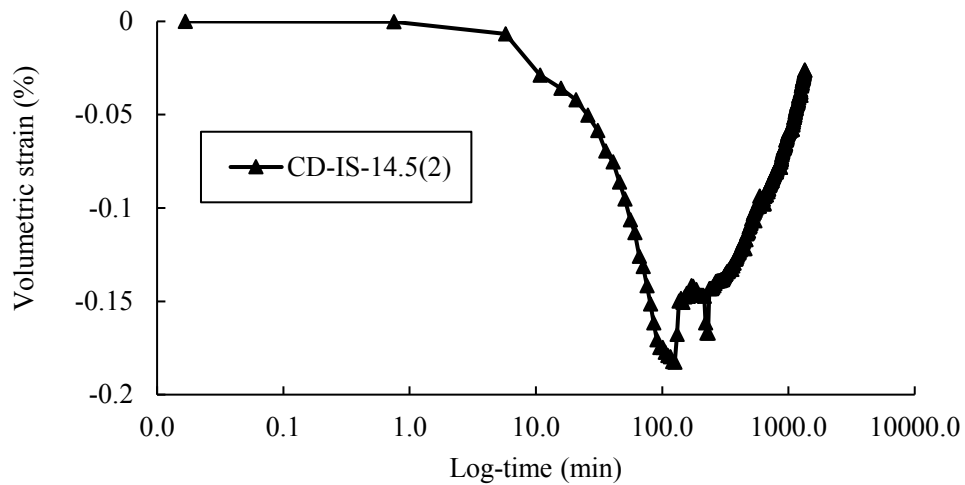
Figure 5.20 The swelling of the sample IS-14.5 (glacial till formation) at low effective stress
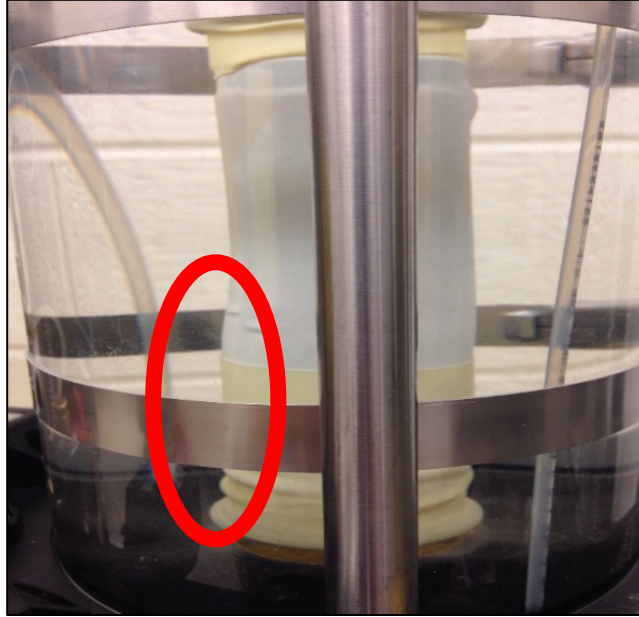
Figure 5.21 Picture of localized-swelled sample from IS-14.5 (glacial till formation) during consolidation stage in the triaxial cell
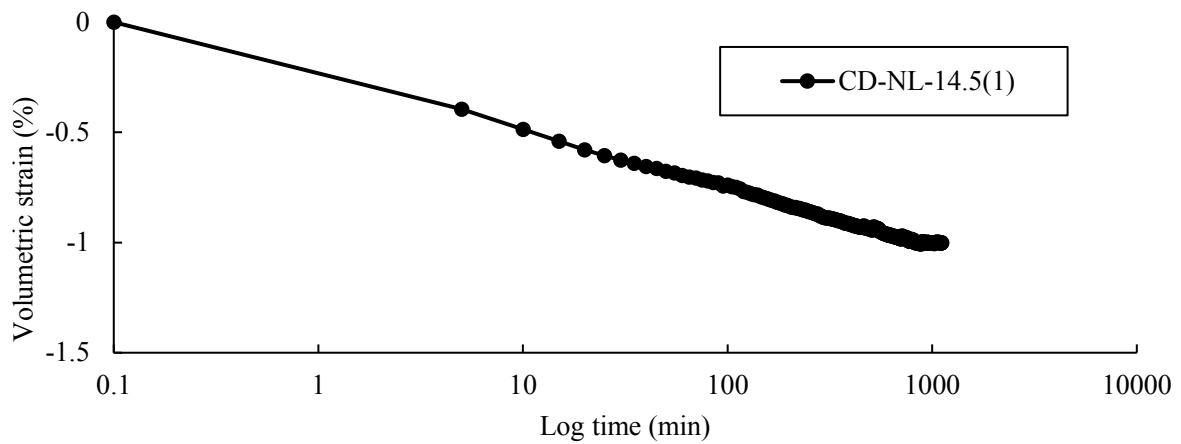
Figure 5.22 Volumetric strain of the sample IS-14.5 at low effective stress during consolidation stage

5.5.3.2 During shear stage

Figure 5.23 shows the volume change behavior of soils during the drained triaxial shearing stage. The volume change plot for other samples are presented in Appendix B. In Figure 5.23, negative values represent contraction. The Figure shows that many samples contracted during the shearing stage.
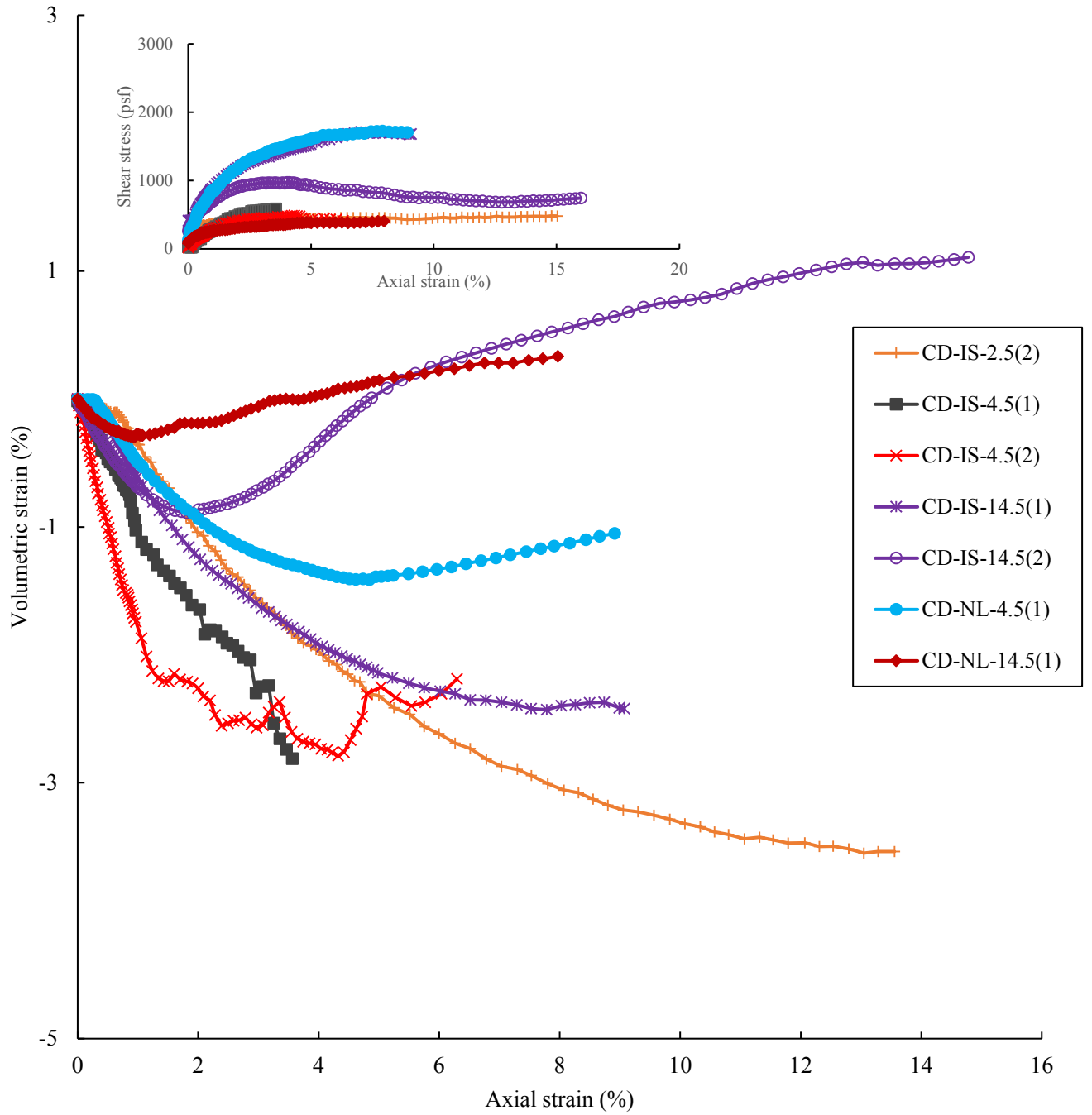
Figure 5.23 Volume change behavior during triaxial drained shearing stage (the legend of inset is similar to the main Figure)

A comparison of Figure 5.23 and Figure 5.22 (the inset of Figure 5.23) shows that after corresponding axial strain of the peak shear stress, the samples started to dilate. In other words, on the horizontal axis (axial strain), the peak stress was reached before the dilation was initiated in the samples at low effective confining stress conditions. The shear stress increased until the peak, then inter particle bonds were disintegrated, and because of the swell pressure of the samples, the soil was dilated.

5.5.4 Effect of water content

The water content has a significant effect on the fully softened shear strength of overconsolidated soils. Increasing the water content of soils may reduce the shear strength of soils down to the fully softened shear strength when soils are dispersive or have expansive minerals. Figure 5.24 shows that test samples from each Shelby tube had similar moisture contents before the triaxial test. However, the water content of all of the samples increased after the tests. This increase in water content is noTable in samples from IS-2.5 (I-180 and Superior St.) and IS-4.5 (I-180 and Superior St.), especially at low stress levels. This phenomenon may be explained due to the higher suction pressure of the samples.

As shown in Table 5.12, the initial water content of the samples was lower than the plasticity index. While at the end of the drained test, the water content of the softened soils was on average 140% and 160% higher than the plasticity index of soils from I-180 and Superior St. and North-Loup, respectively. As shown in this Table, the water content of the samples, which were tested at a low effective confining stress, was increased more than the samples that were tested under higher effective confining stress in general, because at a low effective confining condition the sample may easily swell and absorb water.

90
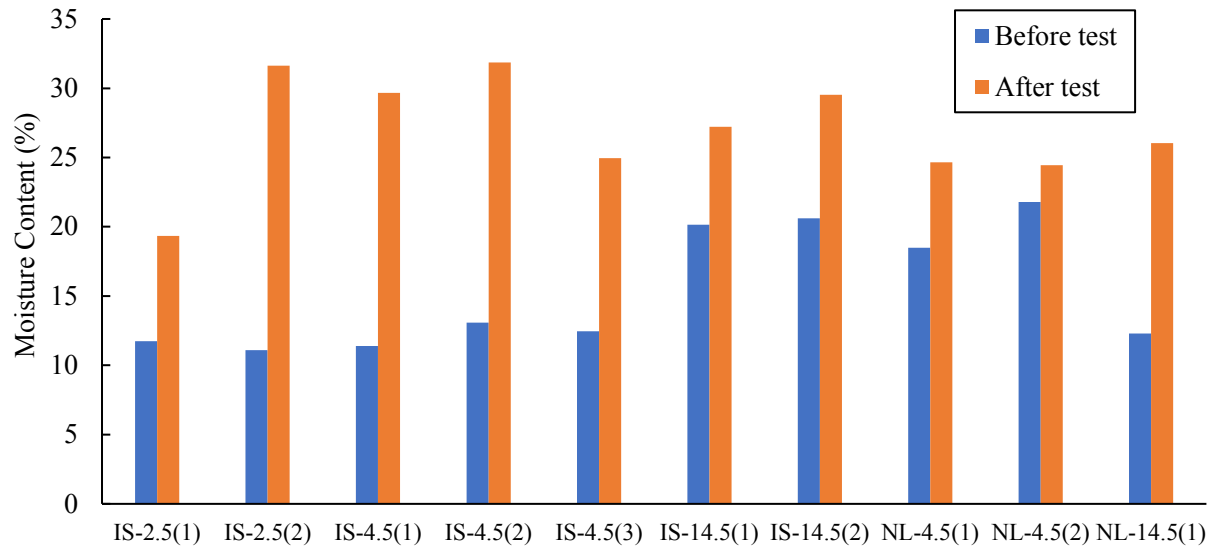
Figure 5.24 Comparison of water content of samples before and after triaxial tests

Table 5.12 Water content of the samples before and after of conducting the triaxial test

Sample Name	LL (%)	PL (%)	PI (%)	Water Content (%)	
				Before test	After test
CD-IS-2.5(1)	41.7	21.6	20.1	11.7	19.3
CD-IS-2.5(2)	45.5	23.2	22.3	11.1	31.6
CD-IS-4.5(1)	39.5	23.4	16. 1	11.4	29.7
CD-IS-4.5(2)	42.2	23.3	18.9	13.1	31.8
CU'-IS-4.5(3)	42.5	21.7	20.8	12.4	24.9
CD-IS-14.5(1)	46.2	25.1	21.1	20.1	27.2
CD-IS-14.5(2)	51.5	25	26.5	20.6	29.5
CD-NL-4.5(1)	38	17.3	20.7	18.5	24.6
CD-NL-4.5(2)	33	13.6	19.4	21.8	24.4
CD-NL-14.5(1)	29.1	22.8	6.3	12.3	26.0

5.6 Comparison between drained shear strength and unconfined compressive strength

The drained shear strength (noted as CD) and unconfined compressive strength (noted as UC) were compared to evaluate a suiTable shear strength for long-term slope stability analysis. The drained shear strength of sandy lean clayey (CL) soils from a shallow depth (IS-2.5, from I-

91

180 and Superior St.) at a low effective confining stress (72 psf) was, on average, 480 psf lower than the residual shear strength from the unconfined compression test as shown in Figure 5.25, indicating that the unconfined compression strength may not provide a conservative slope design. From the Figure 5.26, the drained shear strength of sandy lean clayey (CL) samples from IS-4.5 (from I-180 and Superior St.) was also lower than the average peak unconfined compressive strength in general. However, the consolidated undrained shear strength from this Shelby tube was close to the unconfined compressive strength. In other words, long-term stability of a slope in overconsolidated clays may not be satisfied if the undrained shear strength is considered in slope stability.
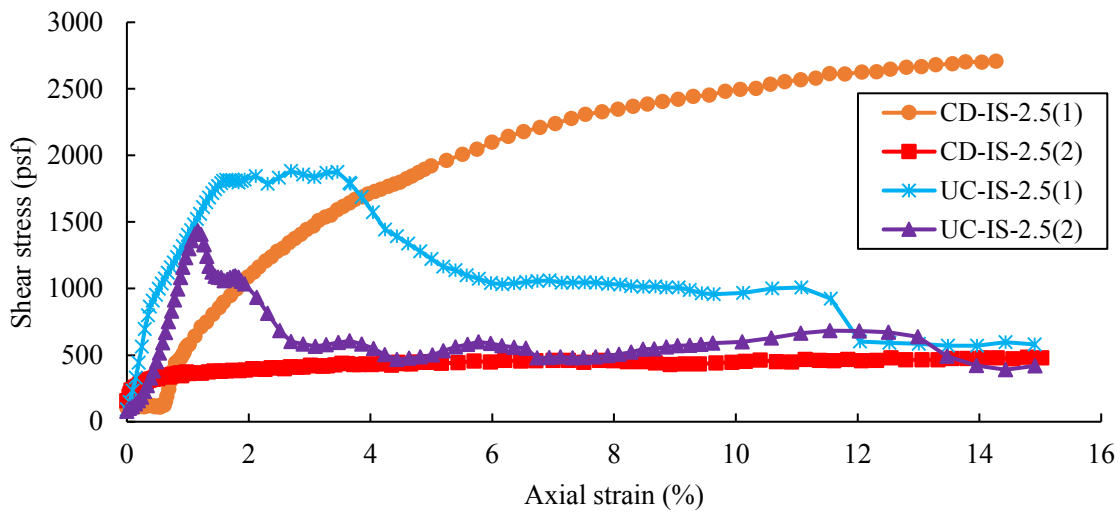
Figure 5.25 Comparison between results of unconfined compressive shear strength and triaxial drained test on loess material at shallow depth (I-180 and Superior St.)
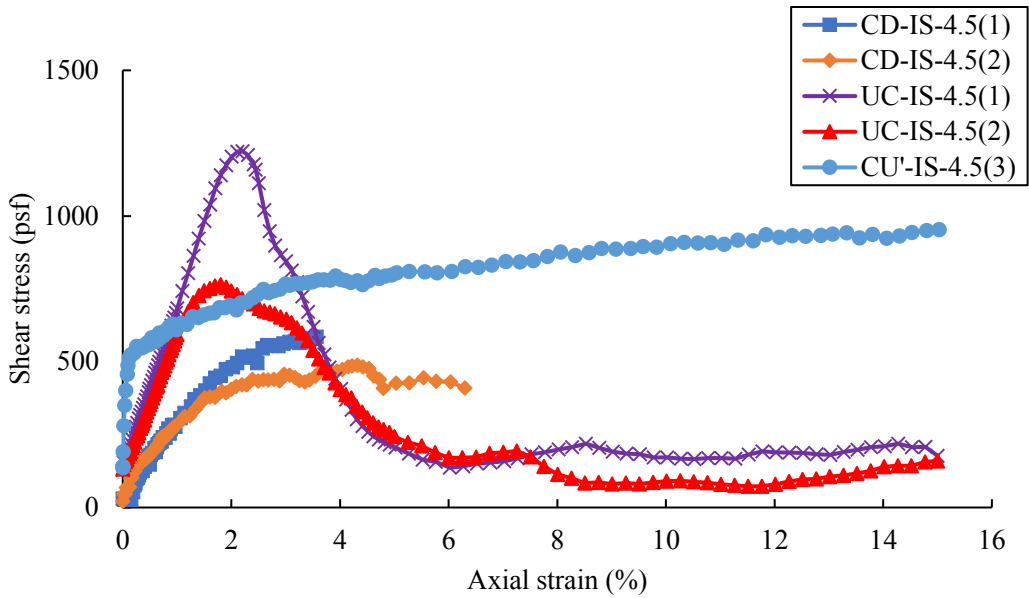
Figure 5.26 Comparison between results of unconfined compressive shear strength and triaxial drained and undrained tests on loess soil from IS-4.5 samples

For both studied sites (North-Loup and I-180 and Superior St.) in some cases such as IS-14.5 and NL-4.5, which were both clayey sand (SC), the unconfined compression shear strength of soils was lower than the fully softened shear strength from drained triaxial tests for equivalent samples, as shown in Figure 5.27 and Figure 5.28, respectively. According to gradation results, the IS-14.5 and NL-14.5 consisted of about 83% and 53% sand materials, respectively, which were mixed with clayey soils. During the unconfined compression test, the materials are not confined with the cell pressure and the failure may occur in the weak area due to cracks and fissures. Regarding the samples from NL-4.5, note that the samples had a high initial moisture content. In the presence of water, loess materials usually show low strength due to reduced cohesion in high water content. The absent of confining pressure for this collapsible soil may develop early stage failure under the unconfined compression condition.
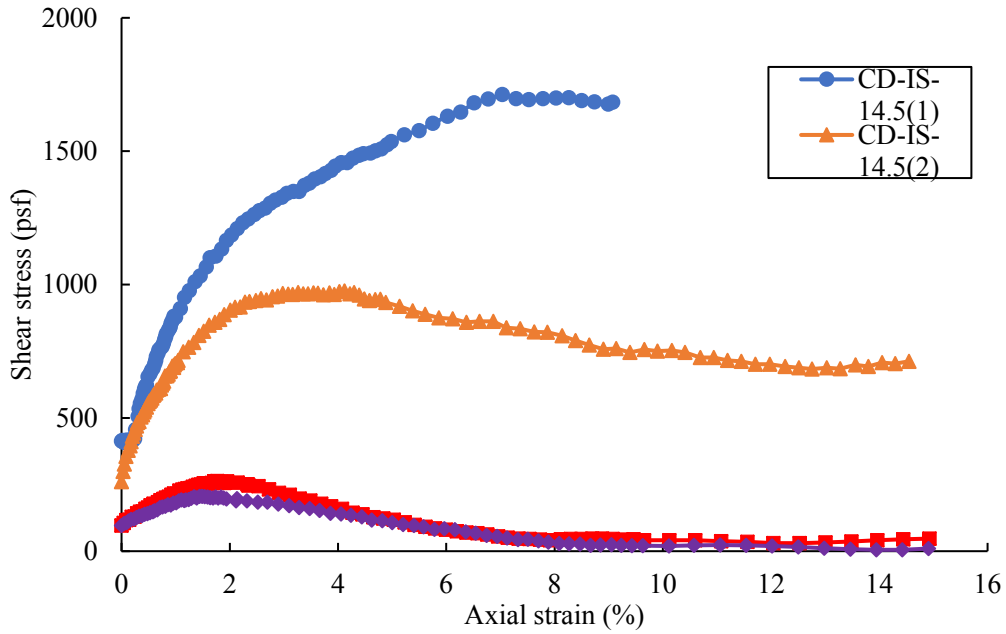
Figure 5.27 Comparison between results of unconfined compressive shear strength and triaxial drained and test on clayey sandy (SC) soils from IS-14.5 (I-180 and Superior St.) samples
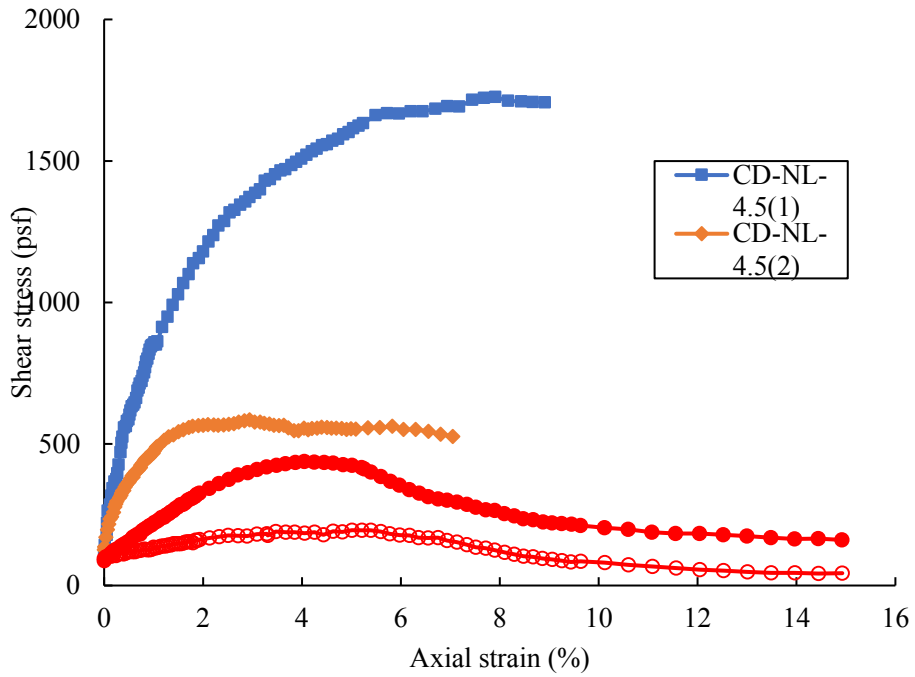
Figure 5.28 Comparison between results of unconfined compressive shear strength and triaxial drained and test on clayey sandy (SC) soils from NL-4.5 samples

5.7 Discussion

As discussed in this chapter a significant reduction in the shear strength of overconsolidated clayey soils of Nebraska was observed. Based on unconfined compression test results on overconsolidated clayey loess and glacial tills, there was a considerable reduction in the unconfined compression strength of some overconsolidated soils of Nebraska (particularly I-180 and Superior St.) from peak shear strength. In both cases studies in this research (I-180 and Superior St., and North-Loup), the average of the reduction factor (η) was 33%.

It is noted that the effect of weak layers is critical to evaluate slope stability. As discussed, there were some layers including sands, chalk layer, many cracks, and fissures, which were believed to show lower shear strength in comparison with the other layers. For example, in I-180 and Superior St. sample IS-14.5 (Figure 5.7) showed very low peak unconfined compressive strength on average about seven times lower than the other layers. It means that once the failure is initiated somewhere, then the driving stress is transferred to adjacent layers. After a while, the localized failure is spread through the entire slope, and the total failure occurs finally (Frohlich 1955, Skempton 1970). Applying the maximum shear strength from unconfined compression test in long-term stability analysis of the slopes in Nebraska, therefore, may not provide a conservative design.

The results of the consolidated drained triaxial test on overconsolidated soils in Nebraska showed that the substantial magnitude of shear strength of the soil was reduced substantially, if the confining stress acting on the soil was decreased due to cutting and constructing the slope. Therefore, this condition should be considered during the design and repair stage for slopes. The drained shear strength of samples from I-180 and Superior Street, which included IS-2.5, IS-4.5, and IS-14.5, was reduced about 82%, 52%, and 42%, respectively, when the effective confining

95

stress was reduced from 288 psf, 488 psf, and 1440 psf to 72 psf, 216 psf, and 216 psf, respectively. The drained shear strength reduction due to low effective stress for NL-4.5 from North-Loup was 66% when the effective confining stress was reduced from 648 psf to 216 psf. This condition is similar to the condition of the slope due to cutting when the overburden stress acting on the soil is removed. This condition can be amplified if the soil consisted of expansive minerals, which cause swelling especially at a low stress level. As shown in this chapter, the sample from IS-14.5 clearly swelled at a low stress level during the triaxial test. If this type of soil is exposed to the surface of the slope due to the cutting, the soil will swell eventually, actively absorb water, and then become weak. This swelling provides an ideal condition for water to percolate through the soil and reduce the shear strength of the soils. However, it is worth mentioning that the permeability of the overconsolidated soil is usually low and it may take time for water to seep through the soil and reduce the shear strength of the soil. Therefore, progressive failure due to shear strength reduction of overconsolidated soils of Nebraska is the primary factor for slope failure in this area. Severe seasonal climate changes, heavy rainfalls, type of minerals of the soils, fissures, cracks, and the permeability of the materials are the combined factors that have a significant effect on the long-term stability of slopes in Nebraska. As shown in Figure 5.29, the drained shear strength of the soil at a low effective confining stress (CD-2) was lower than the peak unconfined compressive strength of the soil.
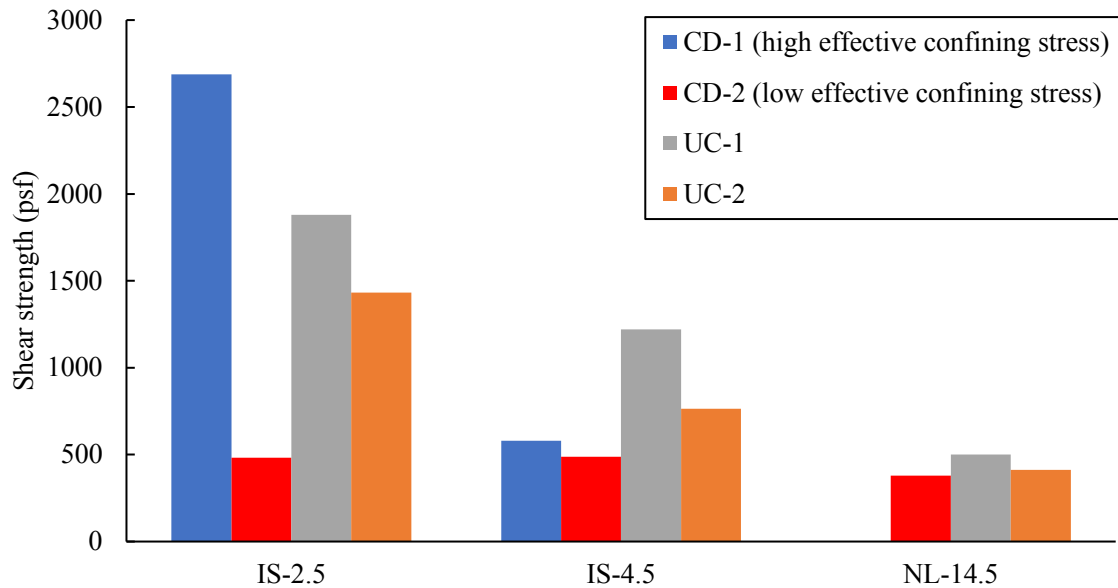
Figure 5.29 Comparison between the peak unconfined shear strength (UC) and drained shear strength (CD) of overconsolidated clayey soils from I-180 and superior St. (S) and North-Loup (R)

As shown in Figure 5.30, in some cases such as IS-14.5 the drained shear strength was higher than the unconfined shear strength, it should be noted that due to the high percentage of sand particles in this sample, an unconfined compression test might not be appropriate to use for this sample. On the other hand, it can provide evidence that when the effective confining pressure is zero the soil strength may reduce dramatically.
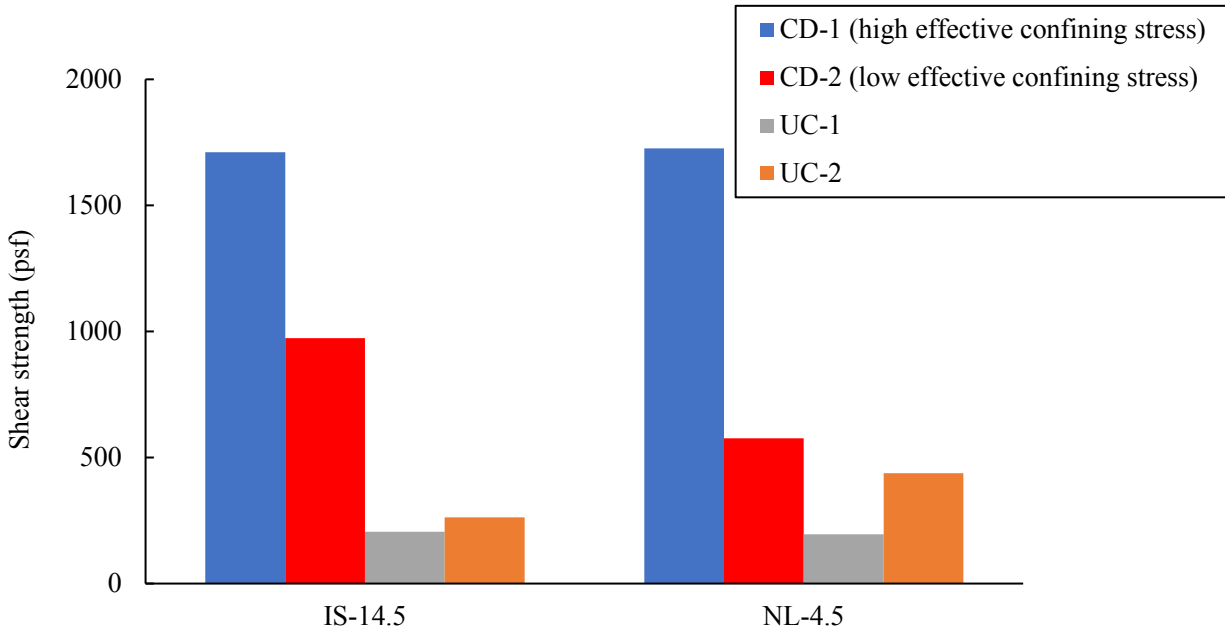
Figure 5.30 Comparison between the peak unconfined shear strength (UC) and drained shear strength (CD) of overconsolidated sandy soils from I-180 and superior St. (S) and North-Loup (R)

5.8 Summary

This study discussed the shear strength parameters of overconsolidated soils and their role in slope stability in Nebraska. Laboratory tests were conducted to evaluate the short-term and long-term shear strength of overconsolidated soil samples from failed slopes in Nebraska. A literature study on the shear strength of overconsolidated soils and clayey shales was conducted. Based on the findings of this literature survey, there is a significant reduction on shear strength of overconsolidated soils with time. Besides, expansive clay minerals induced swelling have a noTable effect on shear strength reduction of soils which cause an instability of slopes in overconsolidated clays and clayey shales.

In this study, undisturbed samples from two failure locations were used to assess the shear strength characteristics of overconsolidated soils in Nebraska. A series of unconfined compression tests, consolidated drained triaxial tests, and consolidated undrained triaxial tests were conducted.

For each test, the initial water content and final water content after conducting a triaxial test were measured to observe the changes of water content in the samples. For evaluating the swell pressure of the samples, the swell pressure test was conducted on undisturbed samples. Finally, the failure mechanism of slopes in Nebraska was discussed, and the factors contributing to this mechanism were investigated.

The major contributions, observations, and conclusions from the research are given as follows.

1. According to the results, the unconfined compression shear strength was higher than the consolidated drained shear strength of overconsolidated soils. Thus, the peak unconfined compression shear strength probably will not represent the shear strength characteristics of overconsolidated soils in Nebraska at the time of failure. Although in some cases such as IS-14.5, the drained shear strength was higher than the unconfined shear strength. It should be noted that due to the high percentage of sand particles in this sample, an unconfined compression test might not be appropriate to use for this sample. On the other hand, it can be evidence that when the effective confining pressure is zero, the soil strength may reduce dramatically. Therefore, an unconfined compression test may not be conservative to use for estimating the shear strength of Nebraskan soils in both design and retrofit stages for long-term stability of slopes.

2. The low residual unconfined compressive strength of the samples showed that slopes, which had experienced failure, might be likely to fail again. The unconfined compression test results showed that there was a fair to substantial reduction from peak strength to residual strength. In case of I-180 and Superior St. the shear strength of soils was reduced about 80% on average. The low residual unconfined shear strength

99

supports the statement that after first-time failure, where the shear strength of the overconsolidated soils are at a critical condition (residual shear strength), the slope has a high potential for further movement because the residual shear strength of the soils is negligible. This condition may be accelerated during intense rainfall.

3. High swelling pressure from shale material from Spencer slope, especially at the deep depth, showed that deep cut slopes might have higher swelling potential. Therefore, the risk of failure in these deep cut slopes is higher. However, the rate of swelling in this condition is significantly dependent on the permeability of soil, and it may take a long time for soil to swell completely.

4. Swelling at low effective stress conditions is one of the main reasons for reduction of shear strength of overconsolidated soils in cut slopes in Nebraska. In cut slopes after excavation, the stress applied to the remaining material is decreased (low effective confining stress). Therefore, relaxation of soil begins, and the available closed fissures open up due to decreased lateral pressure. As a result of rebounding, the water percolates through the soil and pore water pressure is initiated, which reduces the shear strength of materials.

5. The undrained shear strength from tiraxial test was higher than the drained shear strength of overconsolidated soils due to the negative pore water pressure in the undrained condition. Therefore, using the undrained shear strength may not be conservative in long-term stability of slopes in overconsolidated clays.

6. The water content of samples after conducting consolidated drained triaxial tests at a low confining effective stress condition was higher than the water content of the samples from the same Shelby tube at a higher effective confining pressure. This higher

final water content, which is similar to a fully saturated condition in the field, caused more softening on overconsolidated soils and reduced shear strength of soils dramatically.

7. A fully softened shear strength of materials from a drained condition at a low stress level should be considered for long-term stability of slopes in Nebraska. Using fully softened shear strength of soils at a low stress level in slope stability analysis in Nebraska provides a conservative factor of safety for the condition of shallow failure during intensive rainfalls.

Based on findings in this chapter, Nebraska specific slope design and retrofitting techniques were studied in the next chapter.

Chapter 6 Nebraska Specific Slope Design and Retrofitting Recommendations
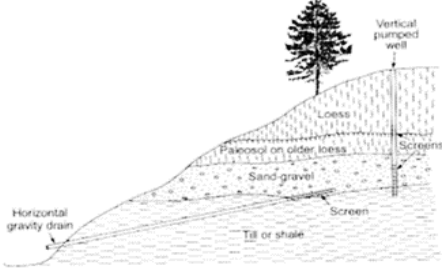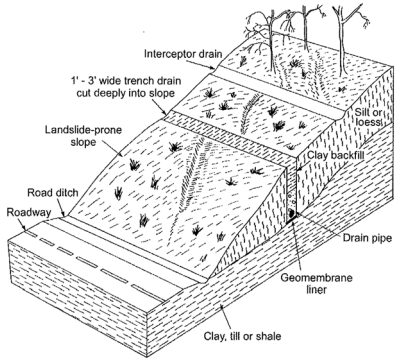
6.1 Introduction
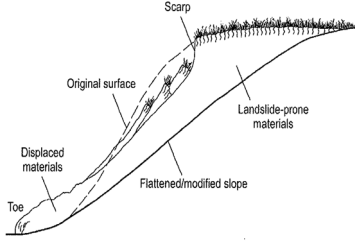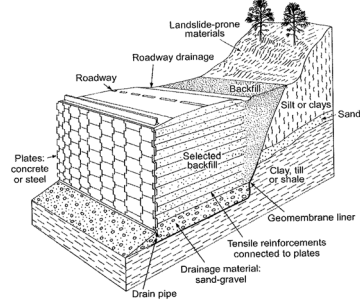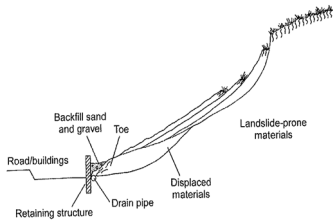
Detailed soil properties and associated failure mechanisms in Nebraska were evaluated in the previous semester. When soil strength is substantially reduced, the required slope may be significantly gentler than the current design practice of 3(H):1(V). A visual observation of the slope angle offully weathered Pierre shale and Fox Hills sandstone formation along the road side of Montana Highway 24 (close to Fort Peck dam) revealed naturally established slopes of approximately 5(H):1(V) or even gentler slopes. This gentle slope angle may interfere with property line of private land owners, and may not make economic sense. Therefore, alternative techniques were studied with summary as shown in Table 6.1.
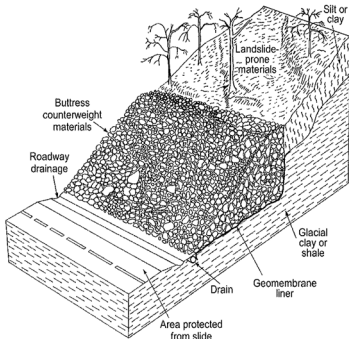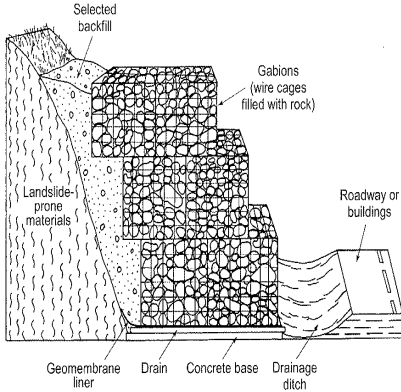
Table 6.1 demonstrates that earth anchor and remove/replace techniques are the two viable techniques that may work for Nebraska soils. Earth anchor may be good for larger slopes, and remove/replace may be good for smaller slopes. Earth anchors are designed based on the unweathered strength of intact soils and rocks at deeper depth, therefore, they are more resistant to strength degradation of soils at shallow depth. This study included the detailed procedure of anchor design in Appendix E.
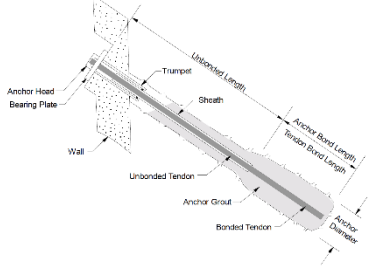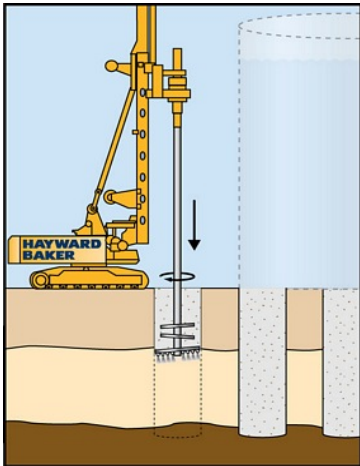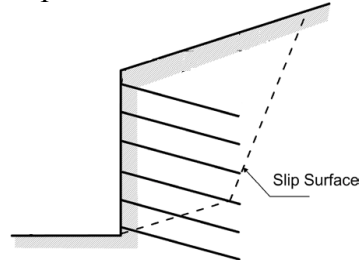
The benefits of the remove and replace technique may be bolstered if a ground modification agent is mixed and compacted with host materials during the remove and replace process. The host materials may maintain the strength for longer time because the modification agent. This research conducted verification tests to evaluate the possibility of mixing a new kind of soil modification material, biopolymer, with the host Nebraska soil. Essential findings regarding biopolymers are discussed in the next section.

Table 6.1 Retrofitting techniques with advantages and disadvantages

Technique/ References	Concept	Pros/Cons	Remark
Remove and Replace	Remove failed materials from the slope and rework the slope again with new materials	Pros: Easy, low cost Cons: May require repeated R&R if high quality materials are not available.	Popular in Midwestern states
Subsurface drainage wells (Eversoll, 2013)	Horizontal (preferred) or vertical wells drilled containing perforated pipes 1-6" diameter. Intercept perched water. 	Pros: Will reduce water buildup that is often the cause of slope failure. Cons: The drainage pipe can clog if proper screens aren't applied.	Probably effective depending on conditions. Improperly designed and maintained wells may collect water and can be a source of problems
Surface water control (Eversoll, 2013)	This refers to more than one method of collecting surface water (such as from rain) and controlling its runoff. The idea is to collect the water and direct it away from the potential slip plane. 	Pros: Directing water away from a slope will decrease the percent of precipitation that the slope will absorb. Cons: While reducing the amount of infiltration that occurs due to rain would be an effective solution, it is a major challenge to effectively divert rainfall away from a slope.	Not very effective, because controlling surface water is difficult.

Slope flattening (Eversoll, 2013)	Reduce slope angle to reduce driving force along slip plane. 	Pros: Reduces driving force, increasing stability. Cons: According to The Landslide Handbook, reducing the height of the slope increases FS by only 10-15%. The technique might also require additional slope modification. Only suiTable for rotational landslides.	This method is limited when land rights limitation applies. Can be quite costly depending on situation.
Mechanically stabilized earth (MSE) (Power et al. 2004; Eversoll, 2013; FHWA, 2007)	Alternating layers of earth and reinforcement (such as geotextiles), usually backing a retaining wall. 	Pros: Effective for steep cuts along roadways. Cheaper than concrete cantilever walls for large grade separation applications. Heavy duty, and the use of synthetic geotextiles between layers will ensure that the design is long lasting. Cons: Care must be taken to select reinforcements that have the appropriate amount of extensibility. Not very good when foundation soils are weak, which is the case in Nebraska.	Probably effective, economically and structurally sound.
Retaining structure (Power et al. 2004; Eversoll, 2013)	Restrains toe of slide from further movement. Can be concrete, stone, piles, etc. 	Pros: Resist lateral earth pressures to earth from sliding. When constructed properly, a retaining wall is sturdy and able to withstand large amounts of lateral pressure. Cons: If proper drainage isn't allowed, they can lead to buildup of groundwater.	Probably effective, structurally reliable depending on location of slip surface. Usually effective for small scale shallow slope failure.

		Not very good when foundation soils are weak, which may be the case in Nebraska.	
Buttress/ counterweight

(Power et al. 2004; Eversoll, 2013) | Increases weight at the toe by placing heavy stone or other materials to increase resisting force. Can also incorporate a drainage system.

 | Pros: This can increase strength both by applying resisting force at the toe or increasing soil strength along the shear failure plan.

Cons: May not be possible due to geometry, cost, or space limitations. | Probably effective, depending on the amount of room available for construction. |
| Gabions

(Highland, 2008; Eversoll, 2013) | Large cages filled with ~10-20cm size rock that are stacked against a slope.

 | Pros: Reinforcement material itself is simple and permeable. Result in lots of friction to resist failure.

Cons: Will require counterforts if placed on clayey soil (structural and drainage purposes). Price can be high and construction can take a long time. | Not very effective, very costly and time consuming.

Flexible structure.

Can be expensive. |
| Anchors

(Sabatini et al. 1999) | Earth is stabilized by anchoring weak layers of rock to strong rock on the surface of the slope. | Pros: Provide a large force capable of stabilizing earth above failure surface. Can be applied to both fragmented rock and soil. Reinforce the earth well enough that deep | Effective, due to its economic and structural properties.

Anchors can be re-tensioned |

		cuts for roads will remain stable. Cons: Can be aesthetically unpleasing for some old anchor heads. Newly designed heads may be eye pleasing.	when needed.
Chemical Techniques (Grouting, Chemical Mixing) (Hayward Baker, 2016)	Strengthens soils by mixing in a cement mixture into the ground. This can be done using an auger type system, as is pictured below. In addition, the same concept can be applied to strengthen surface soils using a tiller type mixer to incorporate cement into the surface soils. 	Pros: Existing soils are used as the "aggregate" to mix into the cement, so no additional materials (other than the cement itself) are needed. Works well for soft cohesive soils. Cons: Depending on the chemical used to produce the cementation, the cement can wash away after years of rain.	Probably effective, depending on the situation. Most grouting techniques are good for high permeable soils or for non-freezing temperature condition. Not very good for Nebraska soils.
Soil Nailing/ Micro Piles (Lazarte et al. 2015)	Passive (no tension is induced) reinforcements that are drilled into soil or weathered rock that transfer loads away from the slip surface in order to increase the stability of a slope. 	Pros: Good for roadway projects. Equipment used to install is relatively small, and a large number of these reinforcements can be installed relatively easily. Cons: Shorter than ground anchors, which could be a problem depending on the geotechnical conditions of the slope.	Probably effective, depending on conditions.

6.2 Soil Stabilization Using Biopolymer Additives

This research found that the strength reduction of field soils and associated slope failures may be effectively prevented by applying biopolymers to field soils. The biopolymer's high tolerance to sub-freezing temperature enhances its application potential. In addition, biopolymers are environmentally friendly and sustainable because they are essentially food additives. Applications of biopolymers are rapidly increasing (De Jong et al. 2010, Chang et al. 2015, 2016). However, they have not been widely used for the stabilization of slopes up to date. Six different biopolymers were preliminarily tested at UNL's Geotechnical Lab. The biopolymer treated soils demonstrated significant strength gain, with up to a 300% strength increase as shown in Table 6.2.

Table 6.2 The shear strength for each biopolymer treated soils (after 7 days)

Type of Bio material	Untreated	Xanthan gum	Guar gum	β-Glucan	Gellan	Lignin
Shear Strength (tsf)	2.2	3.6	3.2	3.6	6	3.6

Two promising biopolymers, Xanthan and Gellan were further tested under well-controlled, severe weathering conditions. They presented minimal strength degradation over time for glacial tills as shown in Figure 6.1 and Figure 6.2. Figure 6.1 shows the strength degradation for wet-dry cycles, and Figure 6.2 shows the strength degradation for wet-freeze-thaw-dry cyles. Results for wet-dry cycles only shows higher shear strength than for wet-freeze-thaw-dry cycles. Both Figures shows that the strength reduction stabilizes after 8 weathering cycles. Another noTable result is that the shear strength of Xanthan-treated soils after 16 weathering cycles is comparable to that of the initial unweathered strength of untreated soils. The weathered strength of untreated soils was not even in a measurable range at 16 weathering cycles. This implies that once field soils are

fortified with Xanthan, they will maintain the initial natural strength, even after an extended period of weathering cycles.
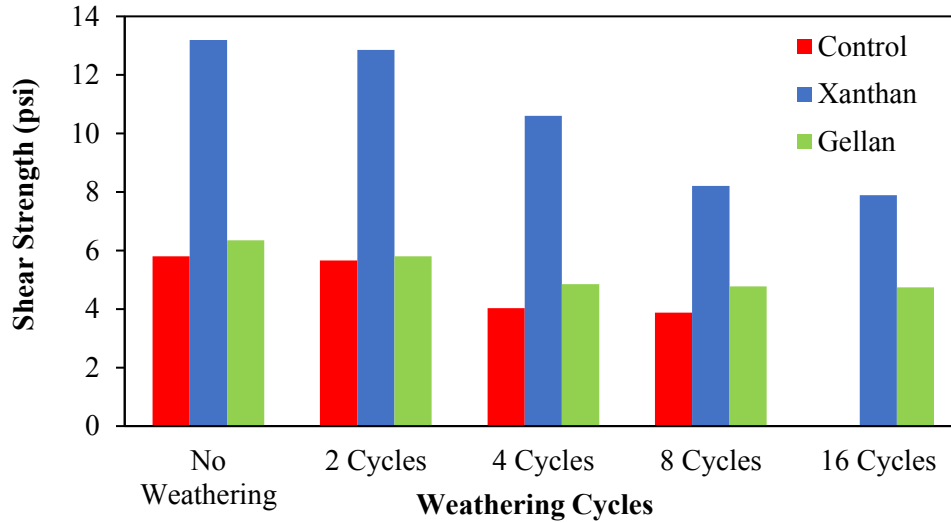
Figure 6.1 Weathering induced strength reduction of glacial tills for treated samples and untreated samples (wet-dry condition) (Note: Control samples are untreated samples)
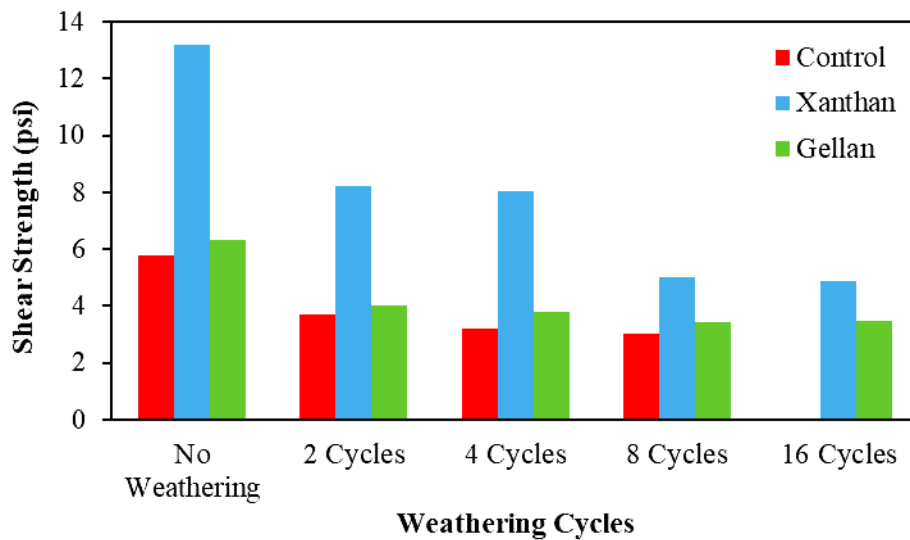
Figure 6.2 Weathering induced strength reduction of glacial tills for treated samples and untreated samples (wet-freeze-dry condition) (Note: Control samples are untreated samples)

For remolded shales, similar results were obtained as shown in Figure 6.3 and Figure 6.4. The results showed consistent results to those for glacial tills.
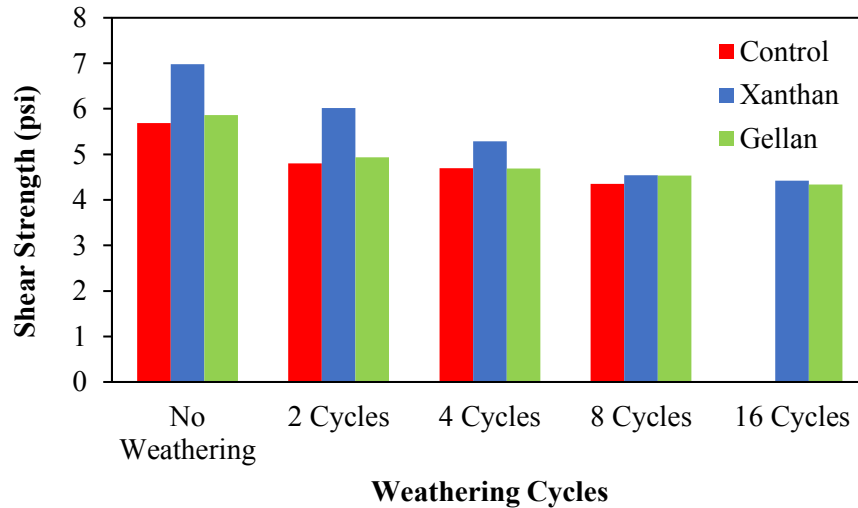
Figure 6.3 Weathering induced strength reduction of remoulded shale for treated samples and untreated samples (wet-dry condition) (Note: Control samples are untreated samples)
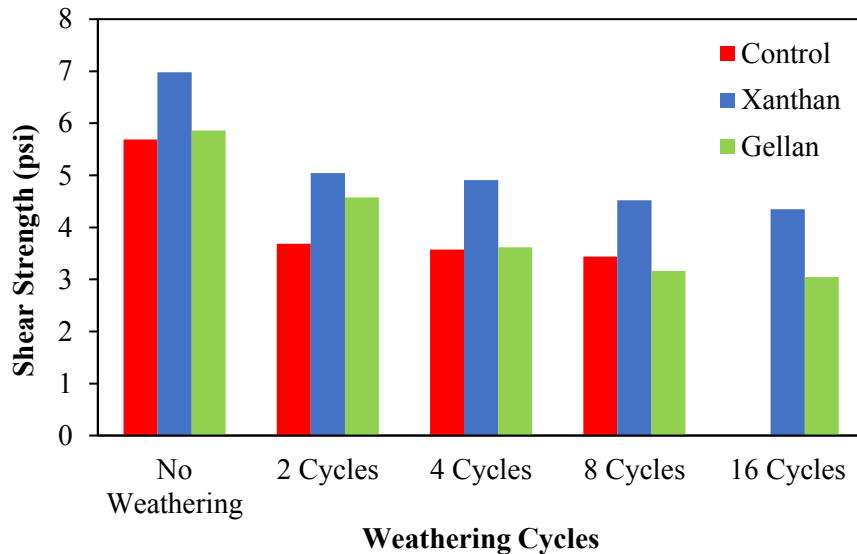
Figure 6.4 Weathering induced strength reduction of remoulded shale for treated samples and untreated samples (wet-freeze dry condition) (Note: Control samples are untreated samples)

Full detailed report is attached as Appendix D.

In addition to their strength enhancing properties, biopolymers are economical. A 1 lb. sample of biopolymer costs approximately $20-$50 and can treat approximately 1 ton of soils. Based on the promising laboratory test results, this research proposes a follow-up field application to improve failed slopes in Nebraska and subsequent performance evaluation to confirm the feasibility of the biopolymers as a cost-effective and sustainable slope stabilization/retrofitting technique. The selected biopolymers from this study can be easily applied to slopes and other geotechnical applications (such as subgrade stabilization) by either field mixing or grouting techniques.

The targeted biopolymers can be easily applied to field soils using BoMag field mixers (stabilizers and recyclers) and compactors for large-scale "Remove and Replace" projects. Flight augers and the wet-mixing technique may be used for small-scale projects. With further research regarding field application parameters (such as optimum mixing ratio of biopolymers and field soils, one for BoMag mixing and the other for auger mixing), biopolymers may become a new tool for improving problematic soils in Nebraska.

References

AASHTO. *Permanent ground anchor specification. In situ soil improvement technique*, AASHTO-AGC-ARTBA TF27 Rep., AASHTO, Washington, DC, 1990

Afolabi, A., Francis, F. A., and Adejompo, F. (2012). "Assessment of health and environmental challenges of cement factory on Ewekoro community residents, Ogun State, Nigeria." *American Journal of Human Ecology*, 1(2), 51-57.

ASTM A722. *Standard Specification for High-Strength Steel Bars for Prestressed Concrete*, American Society for Testing and Materials, Philadelphia, Penn, 2015.

Belitz, H., Grosch, W., and Schieberle, P. (1999). "Food chemistry. ed". City: Springer-Verlag. Berlin Heidelberg.

Bishop, A. W. (1955). The use of the slip circle in the stability analysis of slopes. *Geotechnique*, 7-17.

Bláhová, K., Ševelová, L., and Pilařová, P. (2013). INFLUENCE OF WATER CONTENT ON THE SHEAR STRENGTH PARAMETERS OF CLAYEY SOIL IN RELATION TO STABILITY ANALYSIS OF A HILLSIDE IN BRNO REGION. *ACTA*, 1583-1588.

Calabresi, G.; Scarpelli, G. (1985). Effects of swelling caused by unloading in overconsolidated clay. *Transportation research board*, 411-414.

Casagrande, A., and Fadum, R. E. (1940). *Notes on Soil Testing for Engineering Purposes.* Harvard University Graduate School of Engineering Publication.

Chandler, R. J. (1974). Lias clay: the long-term stability of cutting slopess. *Geotechnique*, 21-38.

Chandler, R. J. (1984). recent european experience of landslides in overconsolidated clays and soft rocks. *IV International Symposium on Landslides* , 61-81.

Chang, I., and Cho, G.-C. (2012). "Strengthening of Korean residual soil with β-1, 3/1, 6-glucan biopolymer." *Construction and Building Materials*, 30, 30-35.

Chang, I., Im, J., Prasidhi, A. K., and Cho, G.-C. (2015a). "Effects of Xanthan gum biopolymer on soil strengthening." *Construction and Building Materials*, 74, 65-72.

Chang, I., Prasidhi, A. K., Im, J., and Cho, G.-C. (2015b). "Soil strengthening using thermo-gelation biopolymers." *Construction and Building Materials*, 77, 430-438.

Chang, I., Prasidhi, A. K., Im, J., Shin, H.-D., and Cho, G.-C. (2015c). "Soil treatment using microbial biopolymers for anti-desertification purposes." *Geoderma*, 253, 39-47.

Dafalla, M. A. (2013). Effects of Clay and Moisture Content on Direct Shear Tests for Clay-Sand Mixtures. *Advances in Materials Science and Engineering*, 1-8.

Das, B. (2010). *Principles of Geotechnical Engineering, 7th Edition.* Cengage Learning.

DeJong, J. T., Mortensen, B. M., Martinez, B. C., and Nelson, D. C. (2010). "Bio-mediated soil improvement." *Ecological Engineering*, 36(2), 197-210.

Dudley, J. H. (1970). Review of collapsing soils. *Journal of the Soil Mechanics and Foundations Division*, 925-947.

Duncan J M (1996). "State of the Art: Limit Equilibrium and Finite-Element Analysis of Slopes", Journal of Geotechnical Engineering, 122:577-596

Eversoll, D. (2013). *Nebraska Landslides.* Lincoln, Nebraska: Conservation and Survey Division, School of Natural Resources, University of Nebraska, Lincoln.

Fellenius, W., "Calculation of the Stability of Earth Dams.", 2nd International Congress on Large Darns, International Commission on Large Dams, Washington, DC, 445-459, 1936.

FHWA (1999). *Geotechnical Engineering Circular No. 4. Ground Anchors and Anchored Systems*, Report No. FHWA-IF-99-015. Federal Highway Administration, Washington.

Frohlich, O. K. (1955). General Theory of Stability of Slopes. *Geotechnique*, 37-47.

Gu, C.; Wang, J.; Cai, Y.; Sun, L.; Wang, P., Dong, Q. Y. (2016). Deformation characteristics of GuGLoverconsolidated clay sheared under constant and variable confining pressure. *Soils and Foundations*, 427–439.

Henkel, D. J.; Skempton A. W. (1954). A landslide at Jackfield, Shropshire, in a heaviliy overconsolidated clay. *Geotechnique*, 131-137.

Howard, I. L., Sullivan, W. G., Anderson, B. K., Shannon, J., and Cost, T. (2013). *Design and Construction Control Guidance for Chemically Stabilized Pavement Base Layers*.

Janbu, N. (1957). Earth pressures and bearing capacity calculations by generalized procedure of slices. *Proc. Intern. Conf. Soil Mech. Foundation Eng., 4th*, (pp. 207-2012). London.

Karol, R. H., and Berardinelli, C. (2003). "Chemical grouting and soil stabilization."

Khan, M. A. (2016). *Impact of Wet-dry Cycle on Mechanical Properties of Expansive Clay Under Low Overburden Stress*.

Kim, N., Park, J., and Kim, S. (2007). "Numerical simulation of ground anchors". Computers and Geotechnics, 34(6), 498-507.

Lazarte, C. A., Robinson, H., Gómez, J. E., Baxter, A., Cadden, A., and Berg, R. (2015). *Soil Nail Walls - Reference Manual.* Geotechnical Engineering Circular No. 7.

Li, P.: Vanapalli, S.; Li, T. (2016). Review of collapse triggering mechanism of collapsible soils due to wetting. *Journal of Rock Mechanics and Geotechnical Engineering*, 256e274.

Li, Y. X.; Yang, X. L. (2015). Stability Analysis of Crack Slope Considering Nonlinearity and Water Pressure. *KSCE Journal of Civil Engineering*, 2289-2296.

Lindemann, M, (2010), "Final foundation report for Santee Spur". S54D (103), CN31918, Material and research division, Geotechnical Section, NDOR.

Lindemann, M, (2010), "Final foundation report for slide repair, highway 14 south of Verdigre and highway 84 east of Verdigre". CN M30024, Material and research division, Geotechnical Section, NDOR.

Mesri, G.; Abdei-Ghaffar, M. E. M. . (1993). Cohesion Intercept in Effective Stress-Stability Analysis. *ASCE*, 1229-1249.

Mitchell, J. K., and Soga, K. (2005). *Fundamentals of Soil Behavior.* Wiley.

Morgnestern, N. R.; Price, V. E. (1965). The analysis of the stability of general slip surfaces. *Geotechnique*, 79-93.

Peck, R. B., Hanson, W. E., and Thrornburn, T. H. (1973). *Foundation Engineering.* John Wiley & Sons.

Peterson, R., Jaspar, J. L., Rivard, P. 1. and Iverson, N. L. (1960). Limitations of Laboratory Shear Strength in Evaluating Stability of highly plastic clays. *Proceedings of the ASCE Research Conference on the Shear Strength of Cohesive Soils*, 765-791.

Petroleum, B. (2009). "Statistical review of world energy 2007." *BP, London*.

Power, M., Fishman, K., Richards, R., Makdisi, F., Musser, S., and Youd, T. L. (2004). *Seismic Retrofitting Manual for Highway Structures: Part 2 – Retaining Structures, Slopes, Tunnels, Culverts, and Roadways.* FHWA Report

Sabatini, P. J., Pass, D. G., and Bachus, R. C. (1999). *Ground Anchors and Anchored Systems.* Geotechnical Engineering Circular No. 4.

Skempton. (1964). Long-term stability of clay slopes. *Geotechnique*, 77-102.

Santee slides, planes for construction, Department of roads, State of Nebraska.

Skempton, A. W. (1970). First-time slides in overconsolidated clays. *Geotechnique*, 320-324.

Skempton, A. (1985). "Residual strength of clays in landslides, folded strata and the laboratory". *Géotechnique*, 35(1), 3-18.

Spencer, E. (1967). A method of analysis of the stability of embankments assuming parallel inter-slice forces. *Geotechnique*, 11-26.

Spencer southeast final design plan, planes for construction, Department of roads, State of Nebraska, Project NO. 281-4(122), September 2015.

Stark, T. D.; Duncan, J. M. (1991). Mechanisms of Strength Loss in Stiff Clays. . *ASCE*, 139-154.

Stas, Christina Valerie, and Fred H. Kulhawy. *Critical evaluation of design methods for foundations under axial uplift and compression loading*. Electric Power Research Institute, 1984.

Sullivan, W. G., Howard, I. L., and Anderson, B. K. (2015). "Development of Equipment for Compacting Soil–Cement into Plastic Molds for Design and Quality Control Purposes." *Transportation Research Record: Journal of the Transportation Research Board*(2511), 102-111.

Terzaghi, K. (1936). Slope Stability in natural clays. *International conference of Soil Mechanics and foundation engineering* , 161-165.

U.S. Army Corps of Engineers (2003). *Engineering and Design Slope Stability*. Engineer Manual EM 1110-2-1902, Department of the Army, Corps of Engineers, Washington, DC.

Verdigre east and south east slides, planes for construction, Department of roads, State of Nebraska, February 2013.

Warkentin, B. P., Yong, R. N. (1962). Shear strength of montmorillonite and kaolinite related to interparticle forces. *Clays and Clay Minerals*, 210-218.

Wold, R. L.; Jochim, C. L. (1989). *Landslide Loss Reduction: A Guide for State and Local Government Planning.* Colorado: FEDERAL EMERGENCY MANAGEMENT AGENCY.

Wong, R. (1998). Swelling and softening behaviour of La Biche shale. *Can. Geotech. J.*, 206-221.

Worrell, E., Price, L., Martin, N., Hendriks, C., and Meida, L. O. (2001). "Carbon dioxide emissions from the global cement industry." *Annual review of energy and the environment*, 26(1), 303-329.

Wright, S. G., Kulhawy, F. H., and Duncan, J. M. (1973). "Accuracy of equilibrium slope stability analyses". *ASCE, Journal of the Soil Mechanics and Foundations Division*, 99(10), 783-791.

Xanthakos, P. (1991). Ground anchors and anchored structures. J. Wiley & Sons, New York.

Xanthakos, P. P., Abramson, L. W., and Bruce, D. A. (1994). *Ground control and improvement*: John Wiley & Sons.

Zydron, T. and Dqbrowska, J. (2012). The influence of moisture content on shear strength of cohesive soils from the landslide area around Gorlice. *AGH Journal of Mining and Geoengineering*, 309-317.

Appendix A Summary of Unconfined Compression Tests
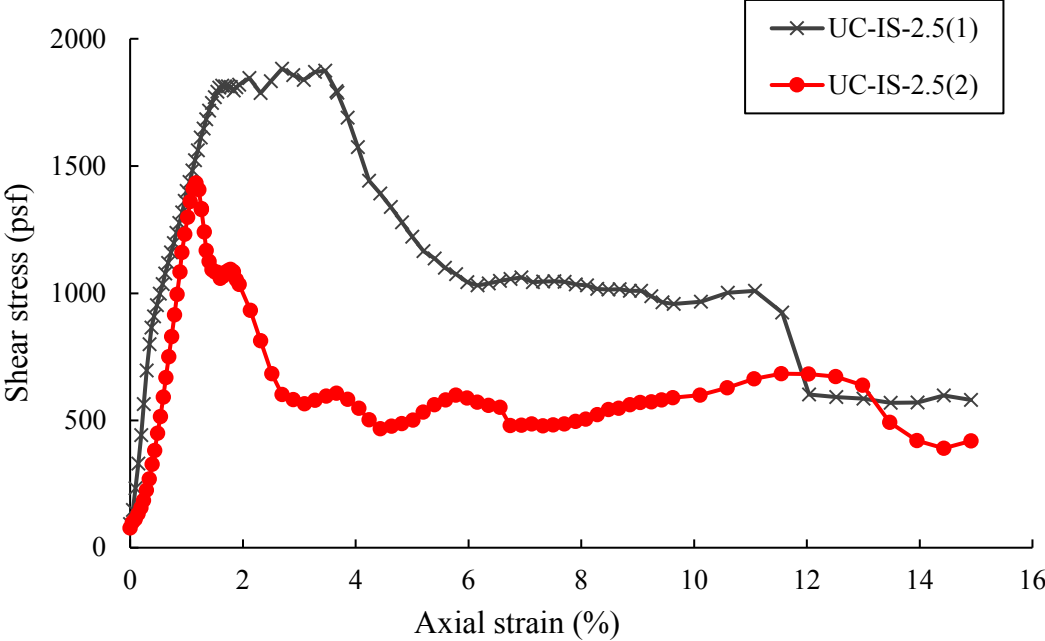
Figure A.1 Unconfined compressive test, I-180 and Superior St. (2.5 ft-4 ft)
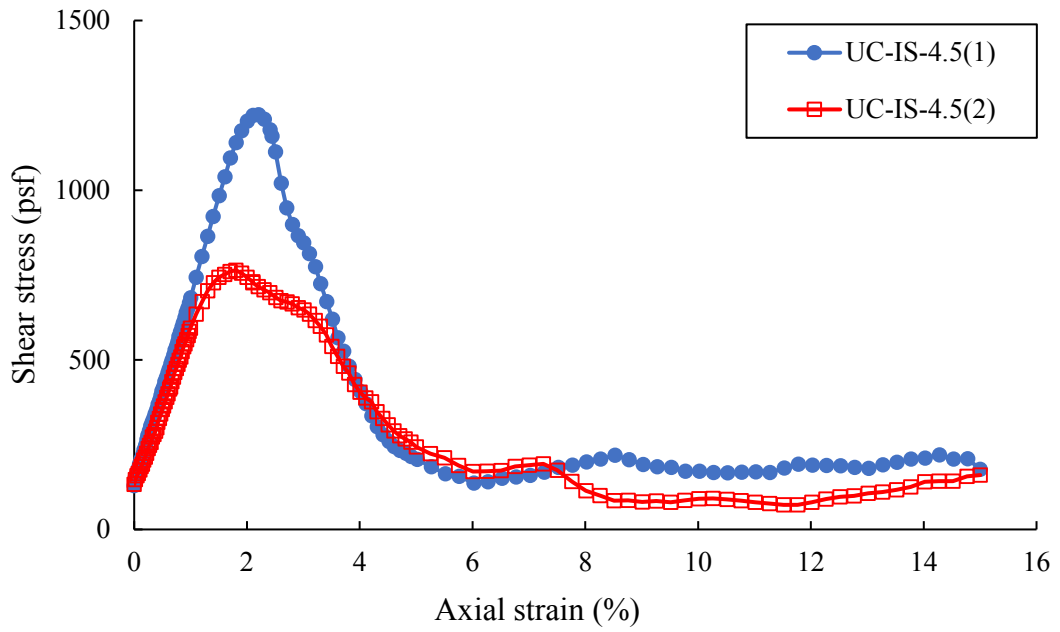
Figure A.2 Unconfined compressive test, I-180 and Superior St. (4.5 ft-6.5 ft)
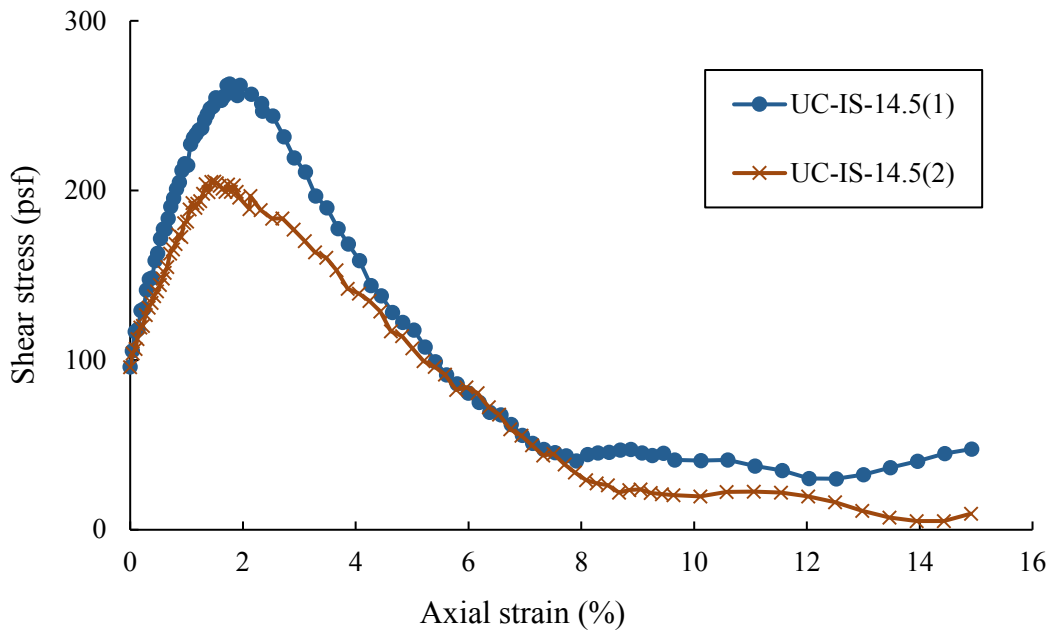
Figure A.3 Unconfined compressive test, I-180 and Superior St. (14.5 ft-16 ft)
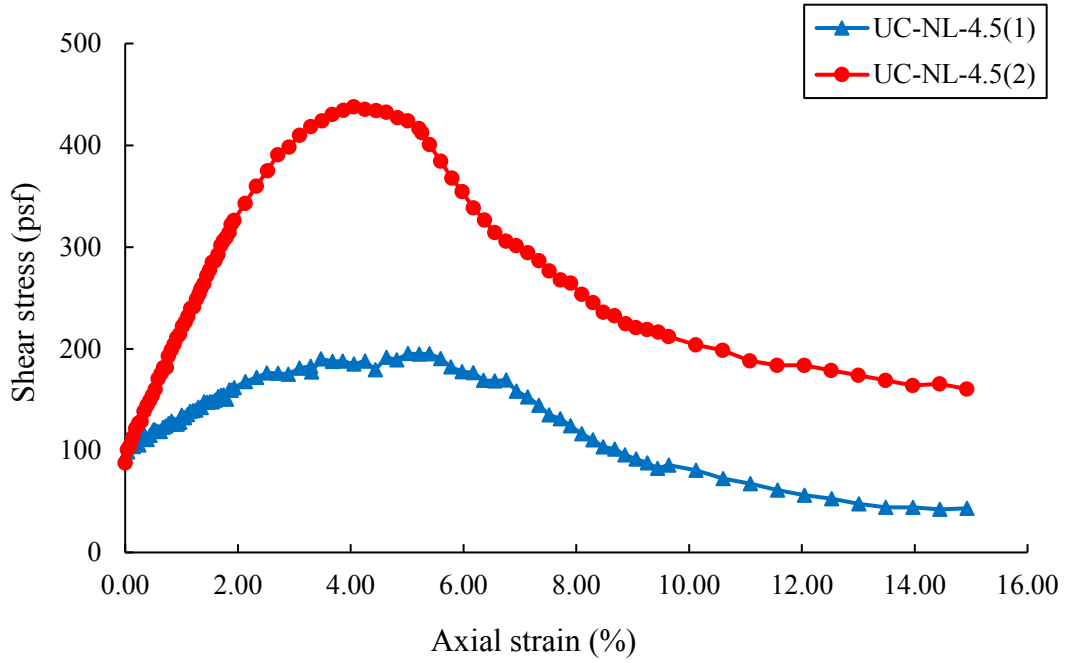
Figure A.4 Unconfined compressive test, North-Loup (4.5 ft-6 ft)
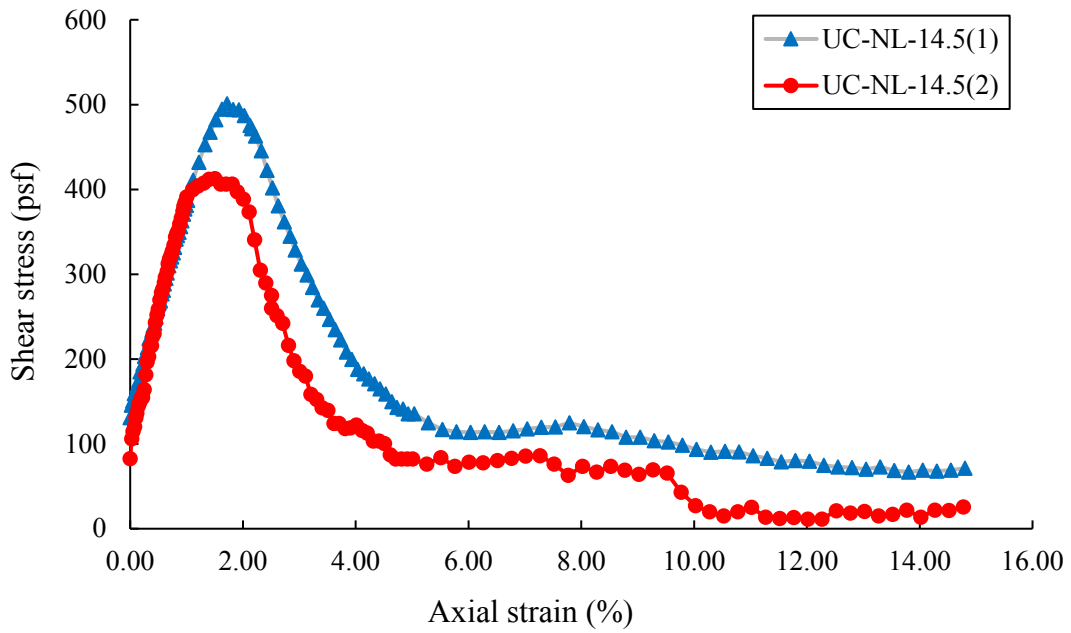
Figure A.5 Unconfined compressive test, North-Loup (14.5 ft-16.5 ft)

117

Shear stress-axial strain (triaxial)
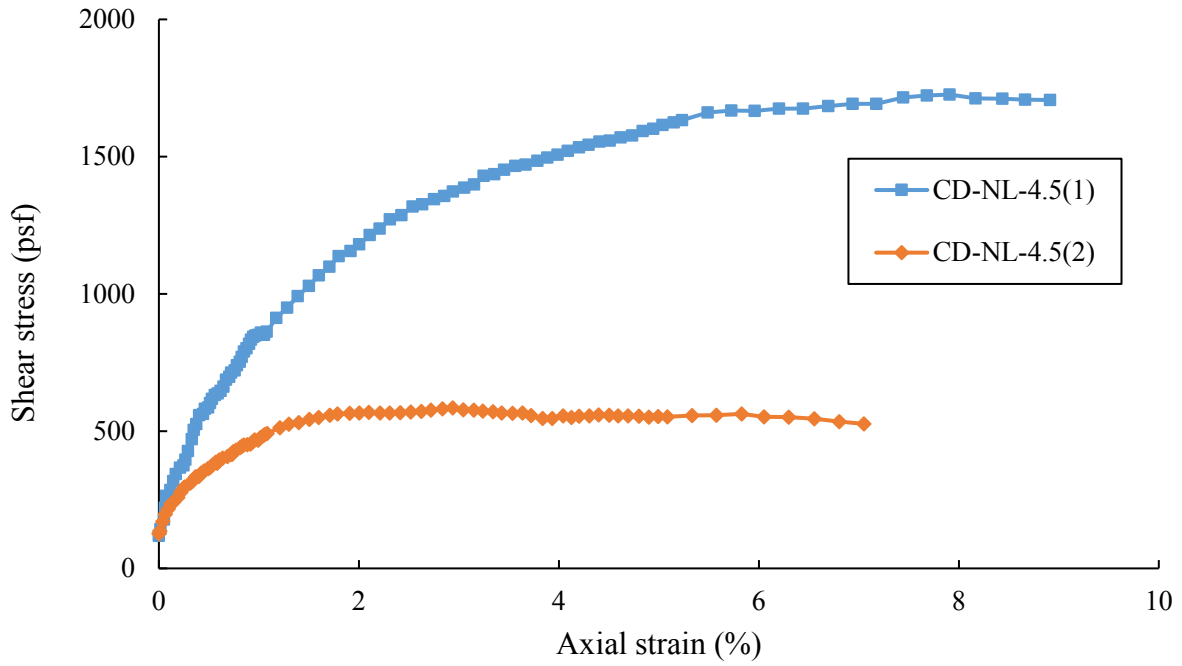
Figure B.1 Drained consolidated triaxial test, North-Loup (4.5 ft-6 ft)
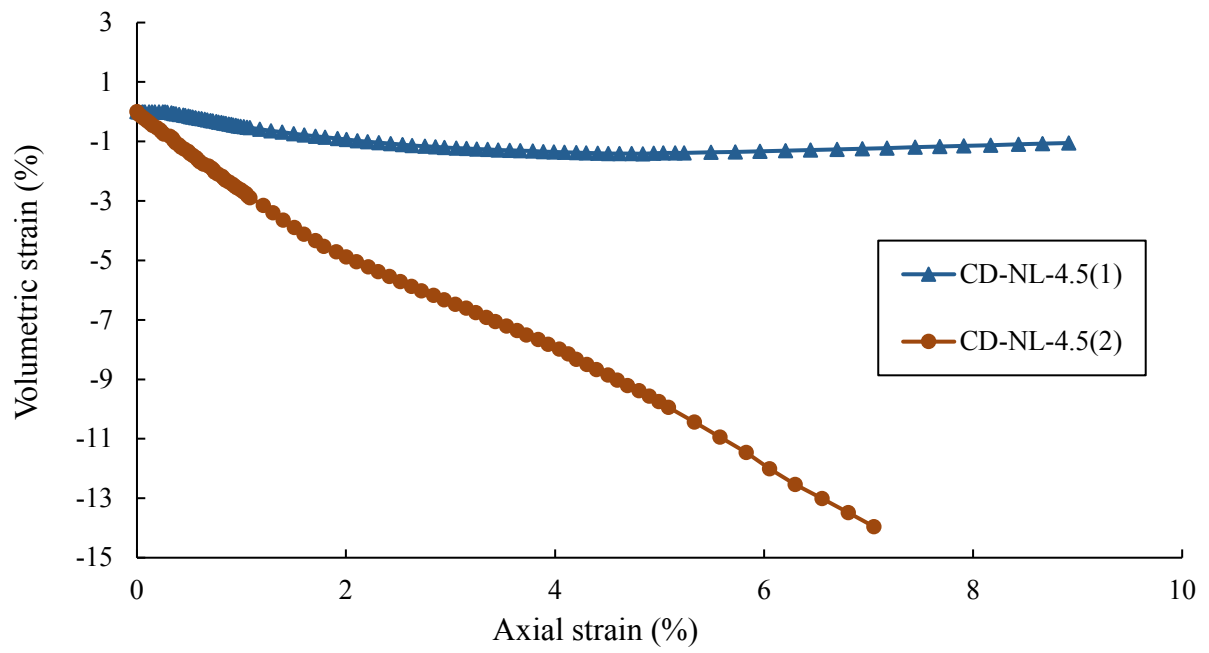
Figure B.2 Volume change behavior during shear stage at triaxial drained test, North-Loup (4.5 ft-6 ft)
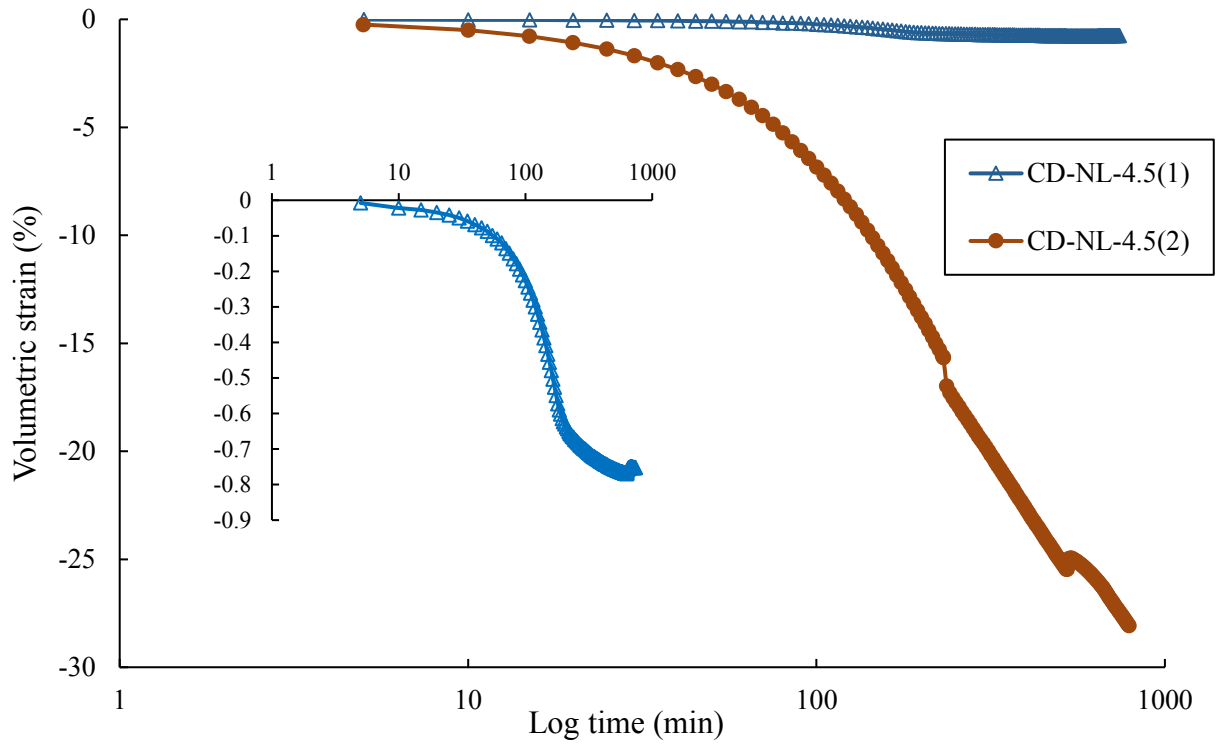
Figure B.3 Volume change behavior during triaxial-consolidation stage, North-Loup (4.5 ft-6 ft)
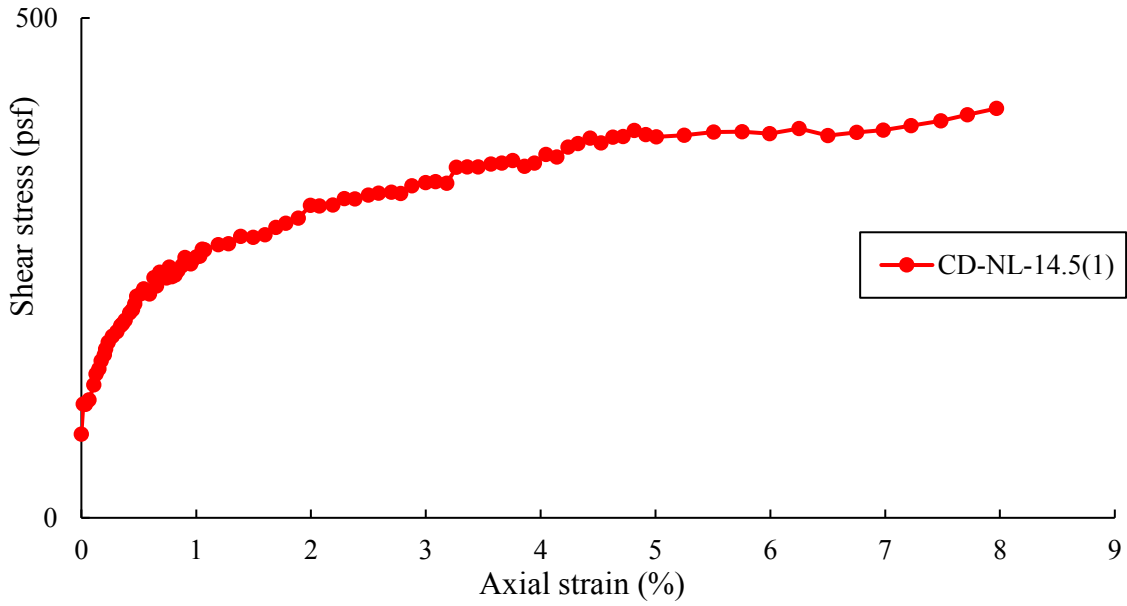
Figure B.4 Volume change behavior during shear stage at triaxial drained test, North-Loup (14.5 ft-16.5 ft)
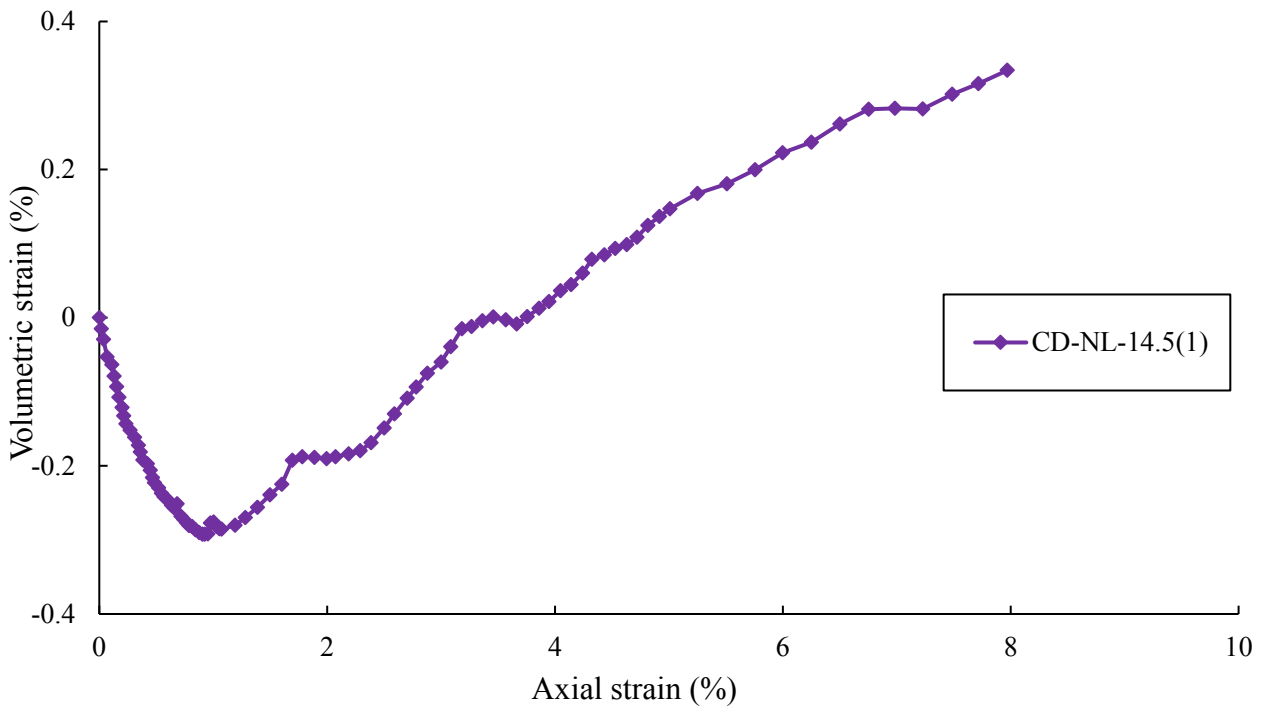
Figure B.5 Volume change behavior during shear stage at triaxial drained test, North-Loup (14.5 ft-16.5 ft)
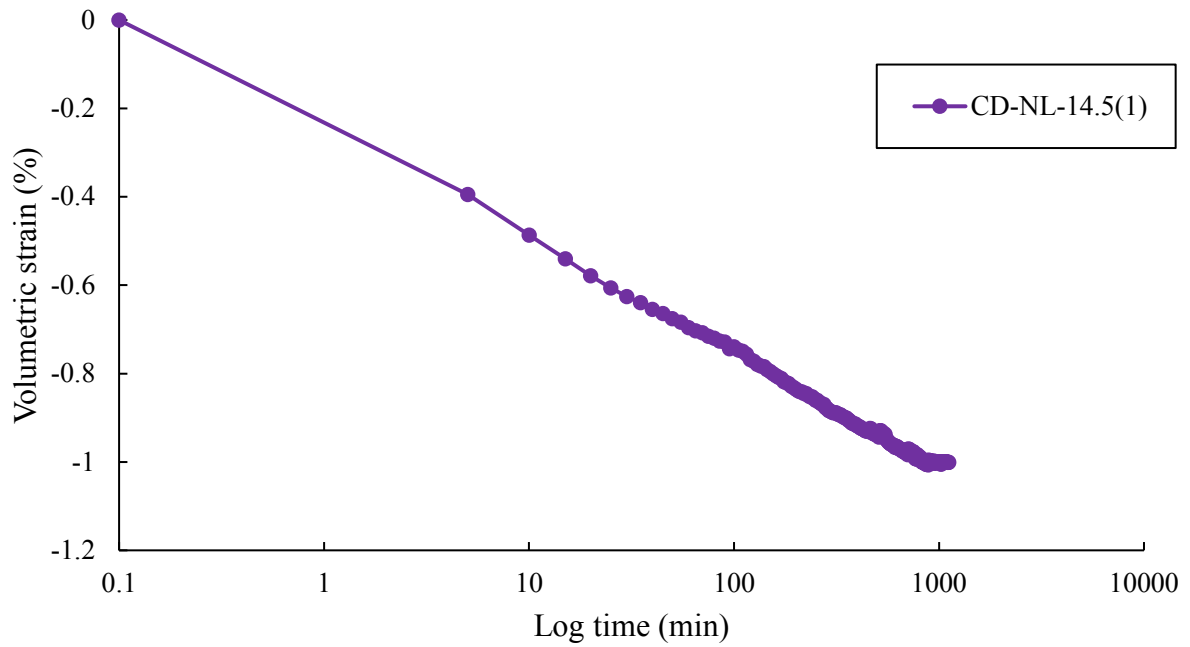
Figure B.6 Volume change behavior during triaxial-consolidation stage, North-Loup (14.5 ft-16.5 ft)
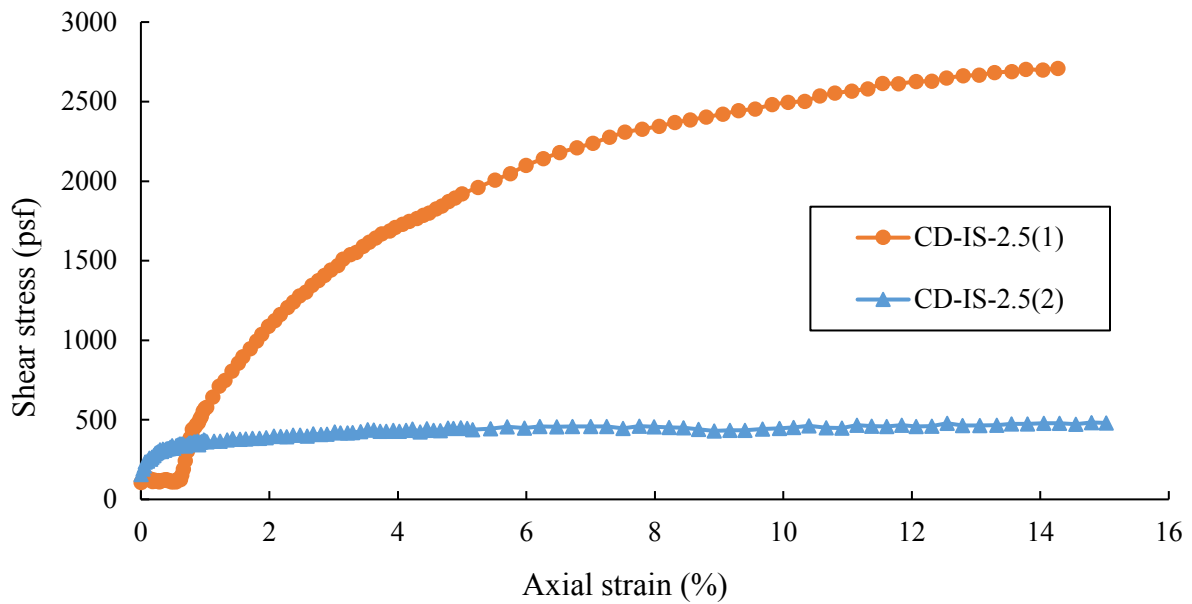
Figure B.7 Stress-strain curves, I-180 and Superior St. (*2*.5 ft- 4 ft)
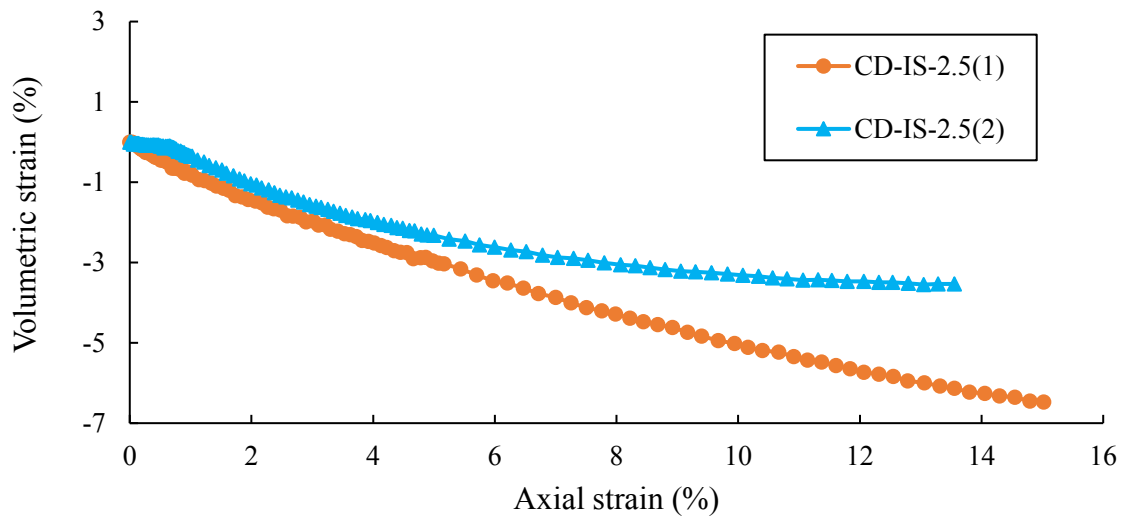
Figure B.8 Volume change behavior during shear stage at triaxial drained test, I-180 and Superior St. (2.5 ft- 4 ft)
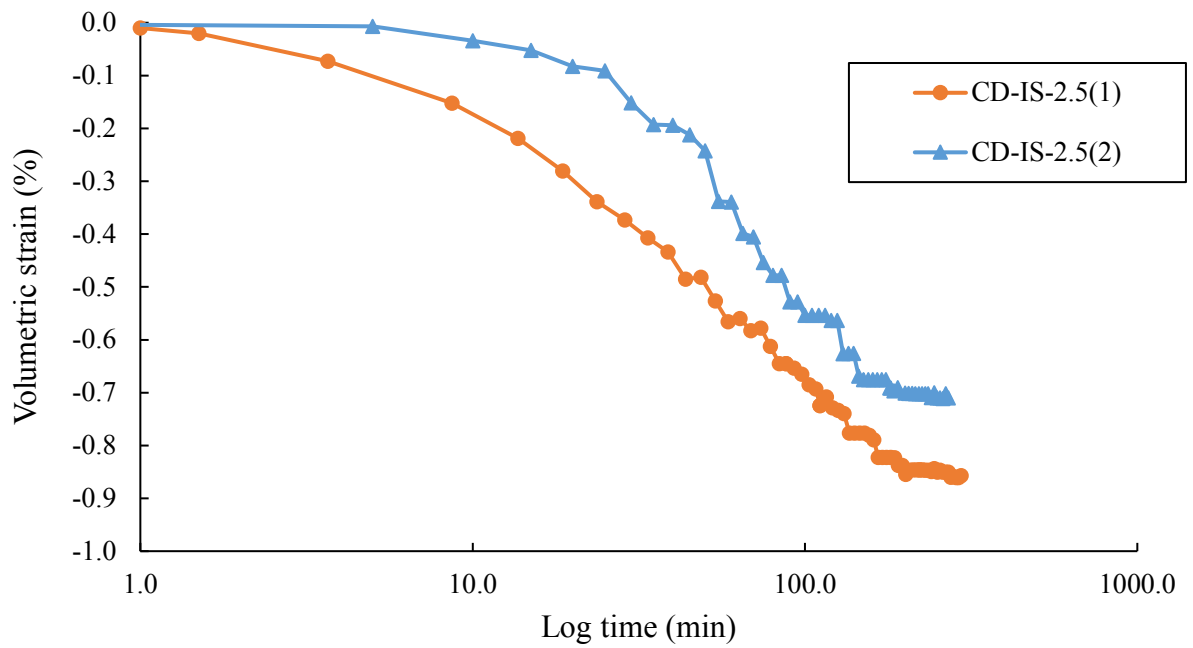
Figure B.9 Volume change behavior during triaxial-consolidation stage, I-180 and Superior St. (2.5 ft- 4 ft)
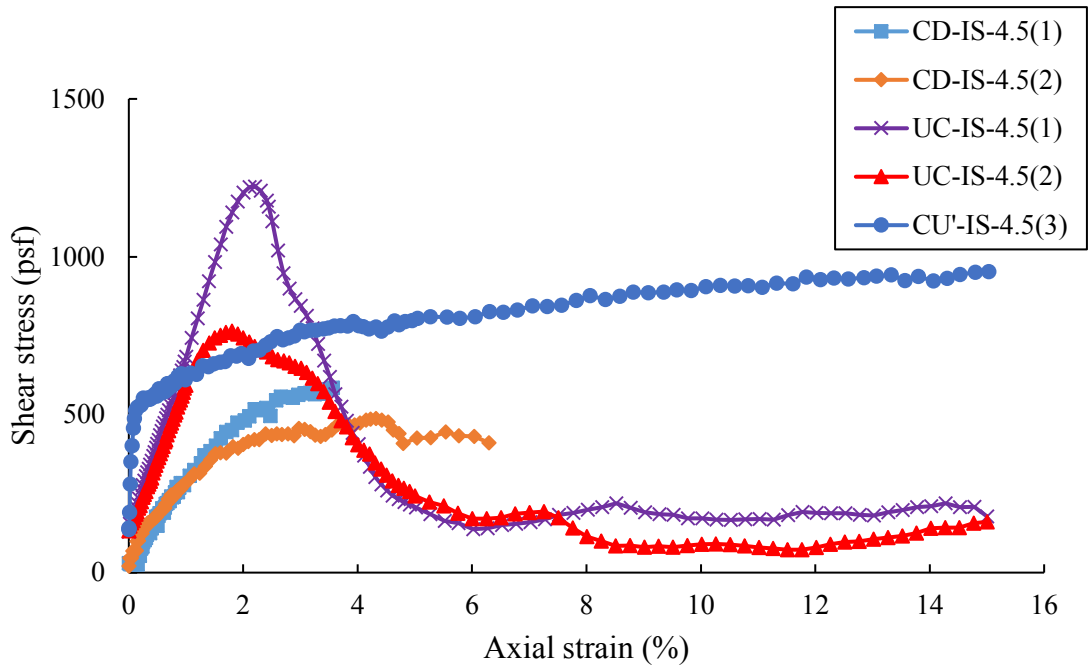
Figure B.10 Stress-strain curves, I-180 and Superior St. (4.5 ft-6.5 ft)
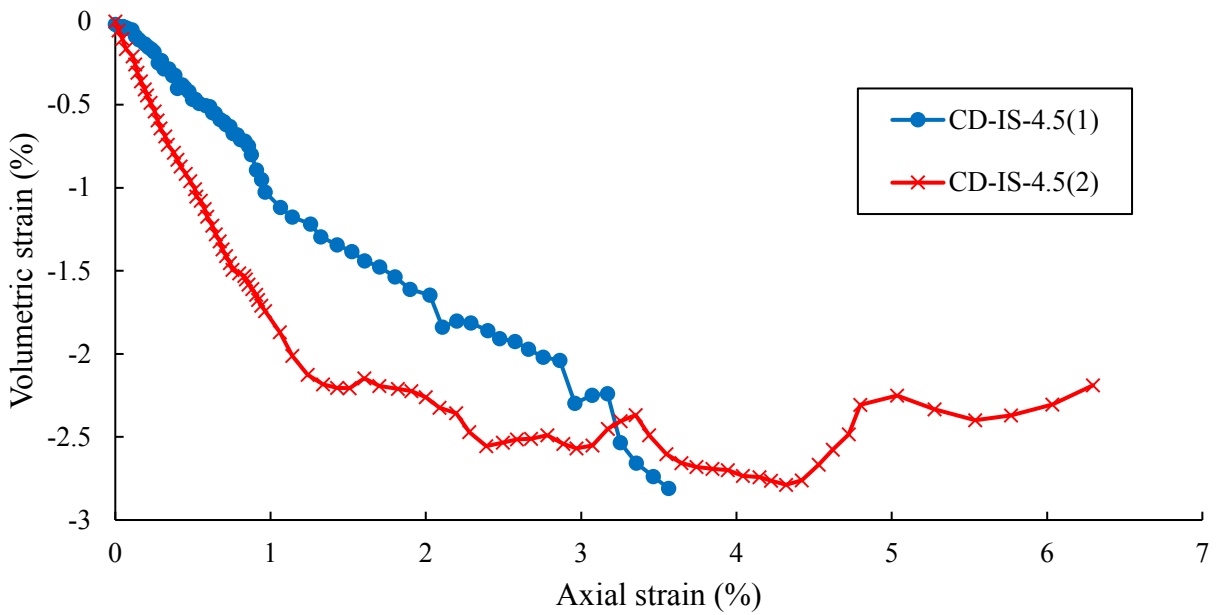
Figure B.11 Volume change behavior during shear stage at triaxial drained test, I-180 and Superior St. (4.5 ft-6 ft)

124
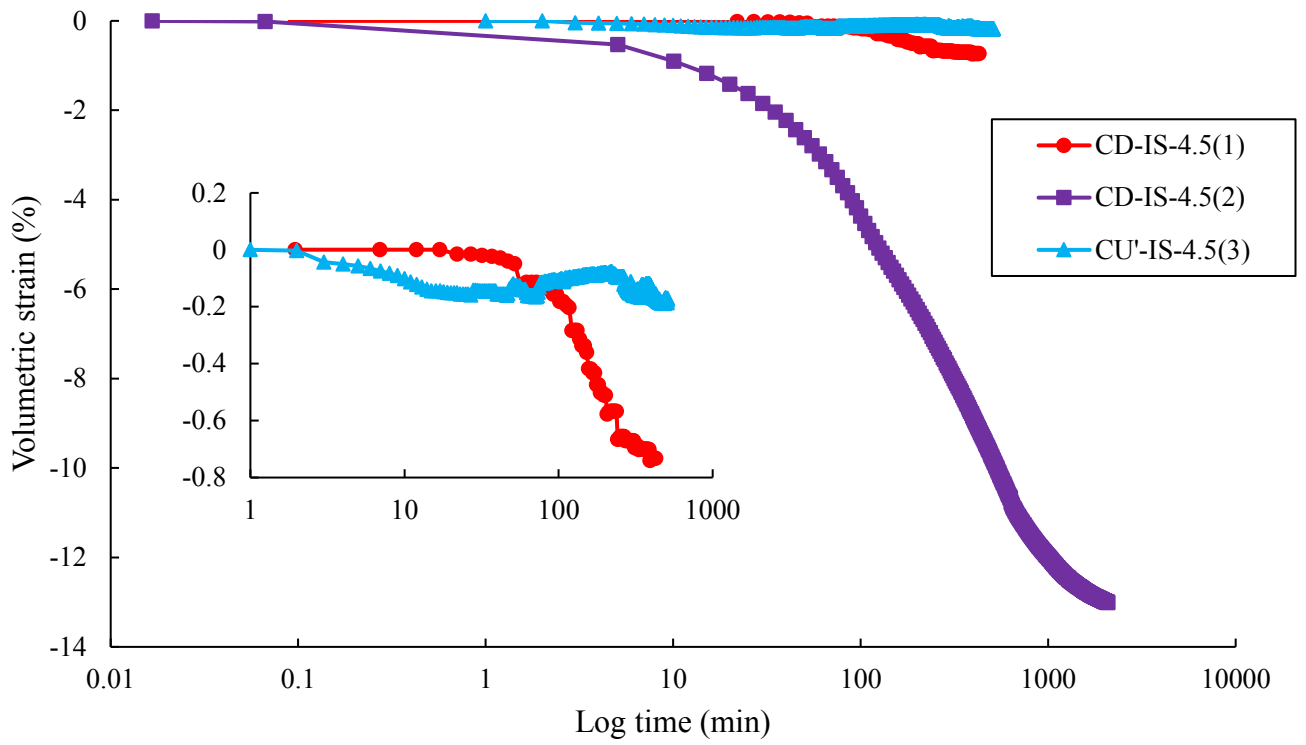
Figure B.12 Volume change behavior during triaxial-consolidation stage, I-180 and Superior St. (4.5 ft-6 ft)
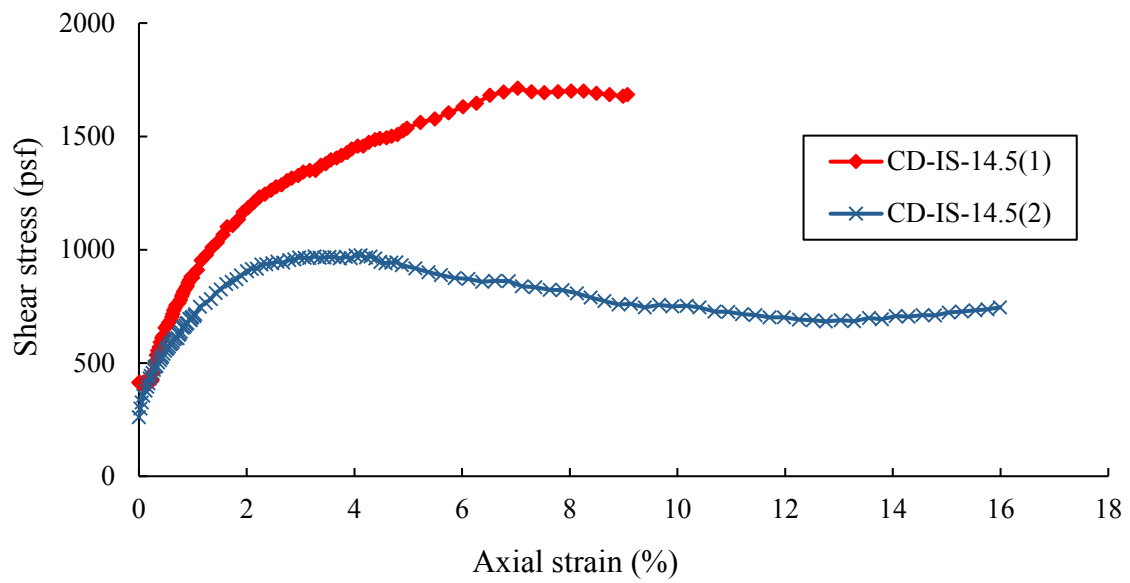
Figure B.13 Stress-strain curves, I-180 and Superior St. (14.5 ft-16 ft)

125
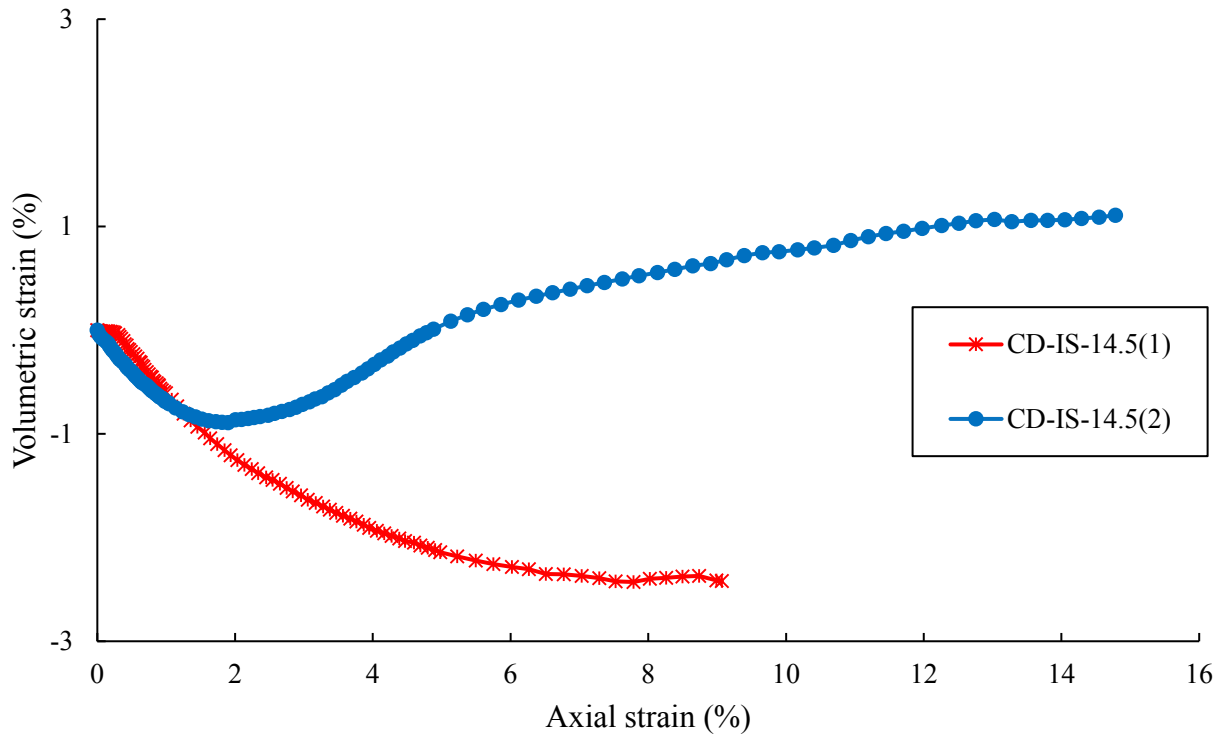
Figure B.14 Volume change behavior during shear stage at triaxial drained test, I-180 and Superior St. (14.5 ft-16 ft)
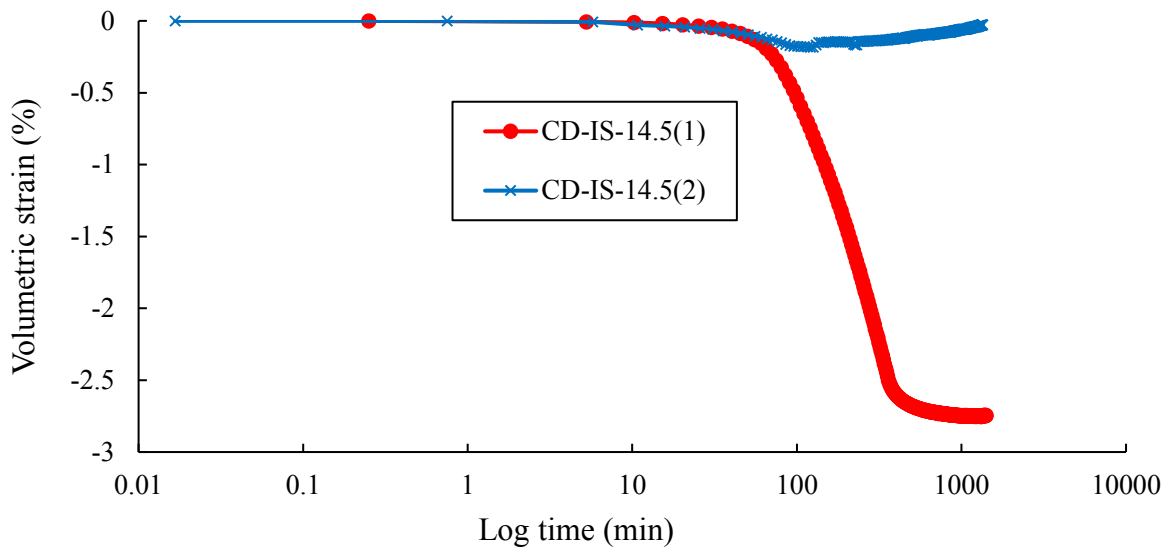
Figure B.15 Volume change behavior during triaxial-consolidation stage, I-180 and Superior St. (14.5 ft-16 ft)
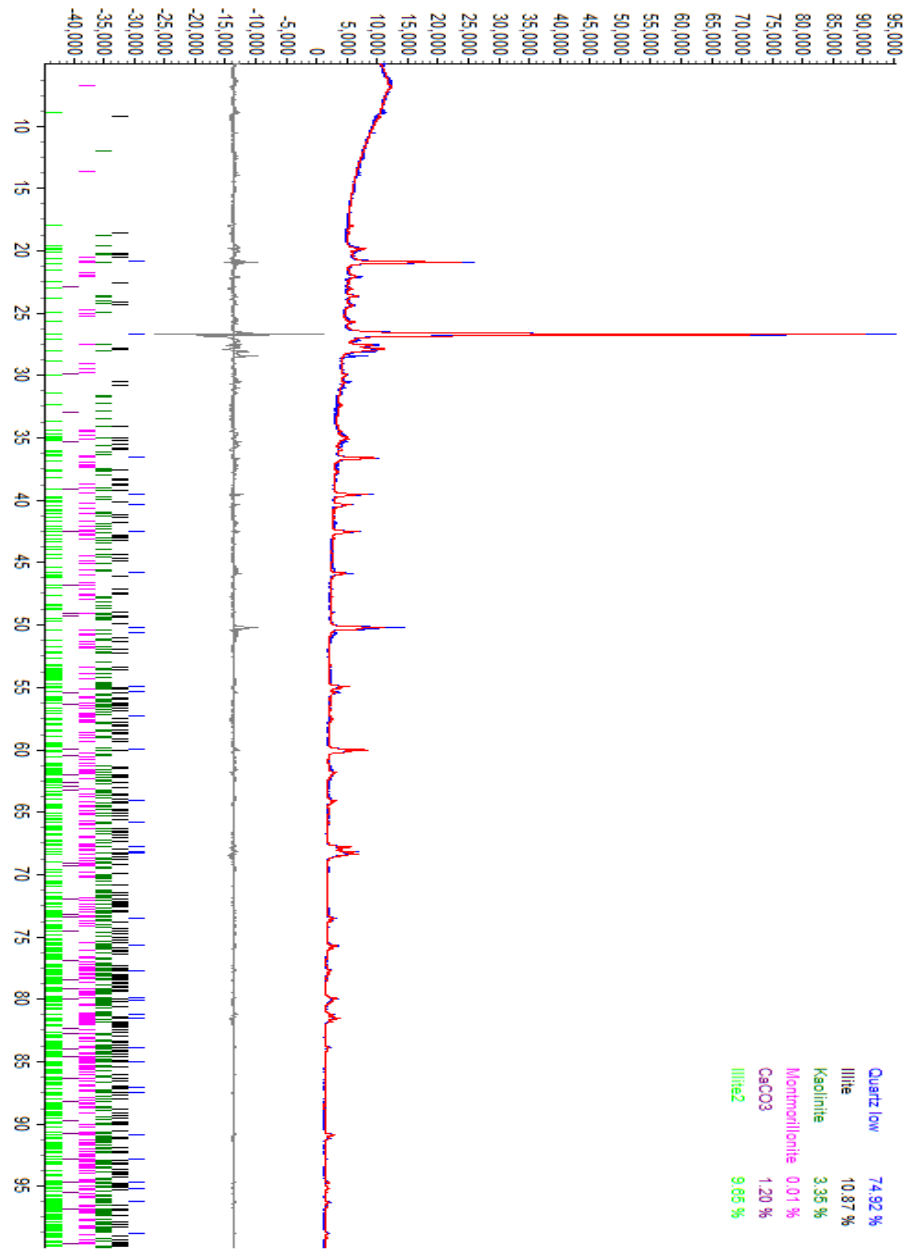
Figure C.1 XRD analysis on sample from IS-2.5, I-180 and Superior St. (2.5 ft-4 ft)
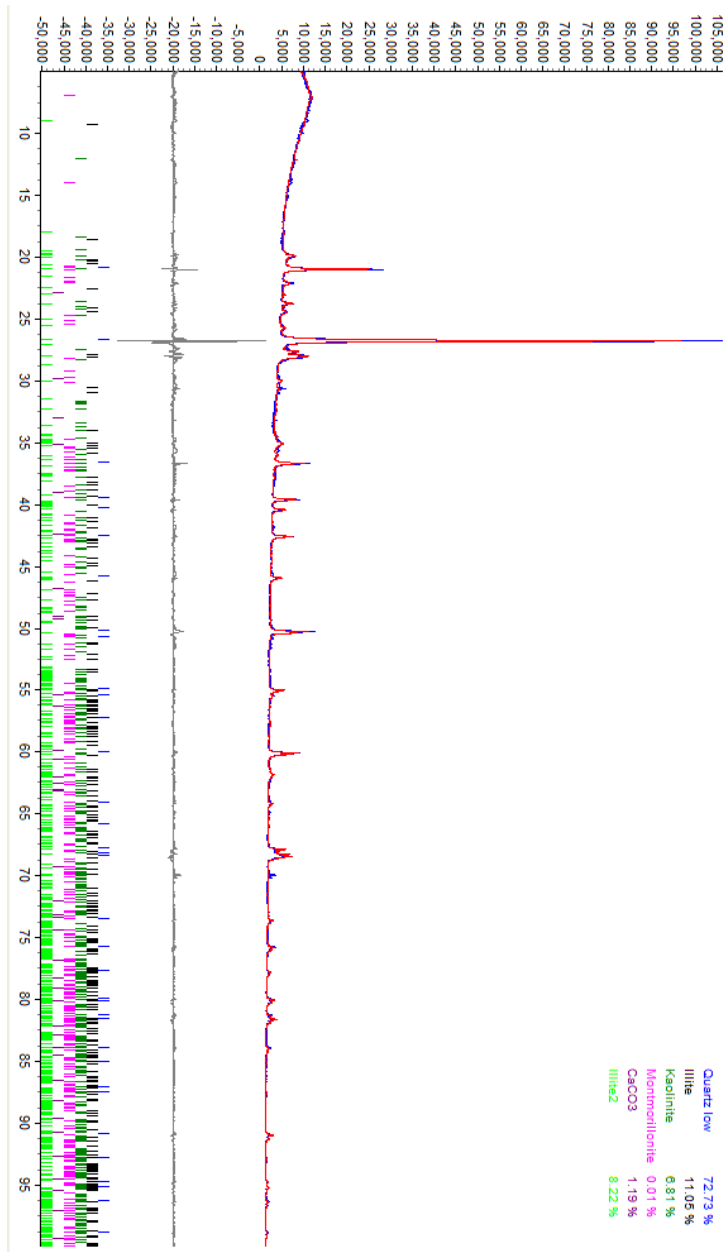
Figure C.2 XRD analysis on sample from IS-4.5, I-180 and Superior St. (4.5 ft-6.5 ft)
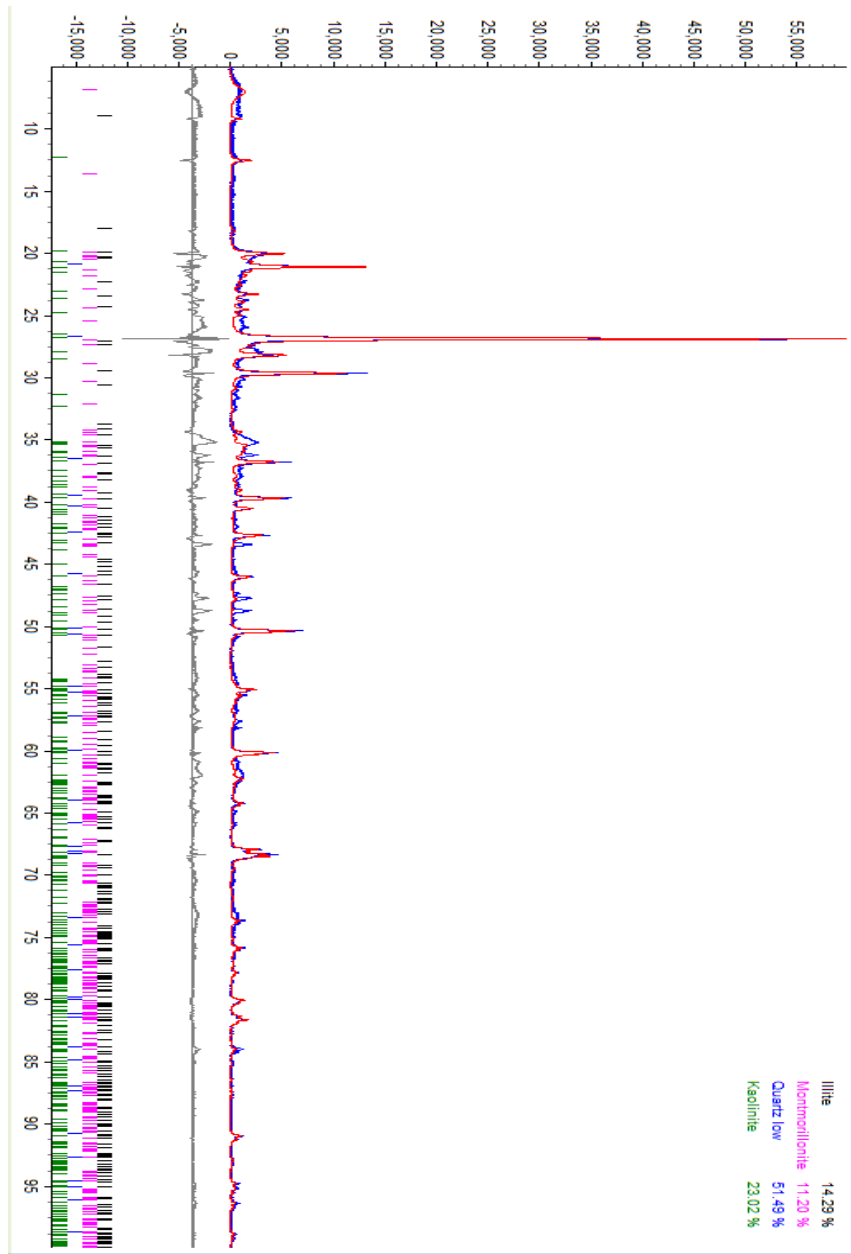
Figure C.3 XRD analysis on sample from IS-19.5, I-180 and Superior St. (19.5 ft-21.5 ft)
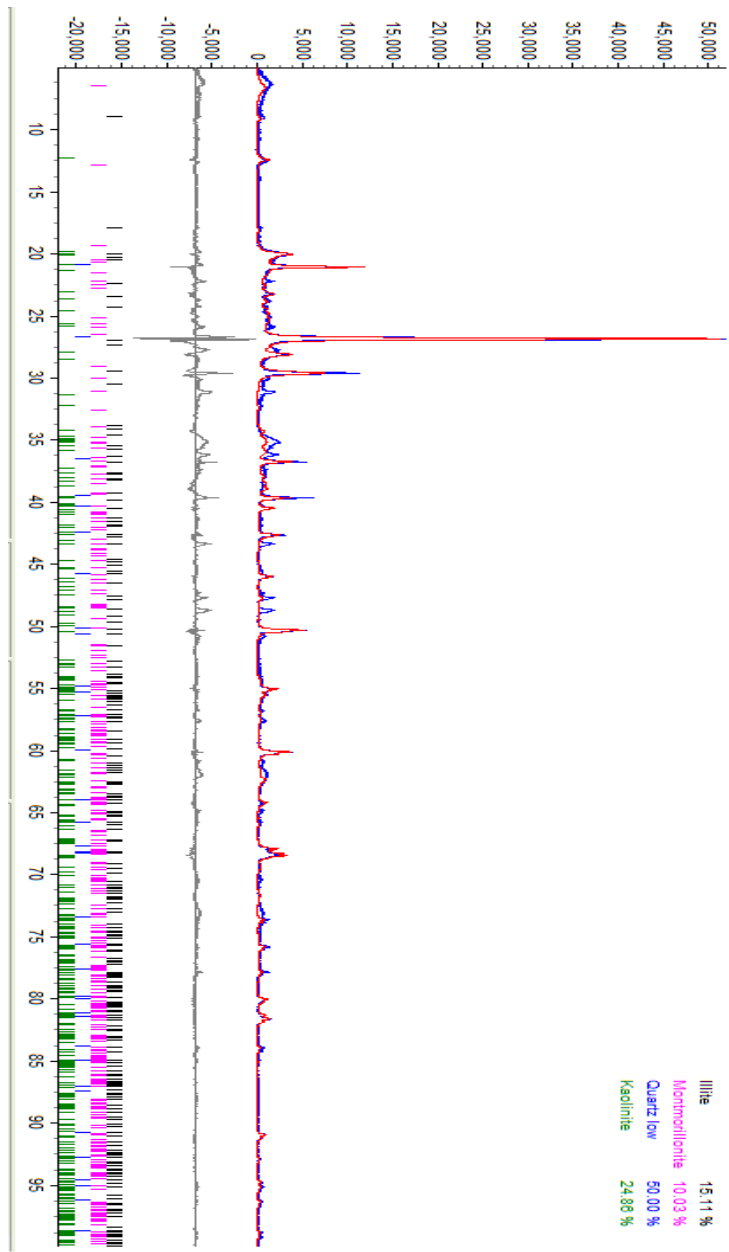
Figure C.4 XRD analysis on sample from IS-24.5, I-180 and Superior St. (24.5 ft-26.5 ft)
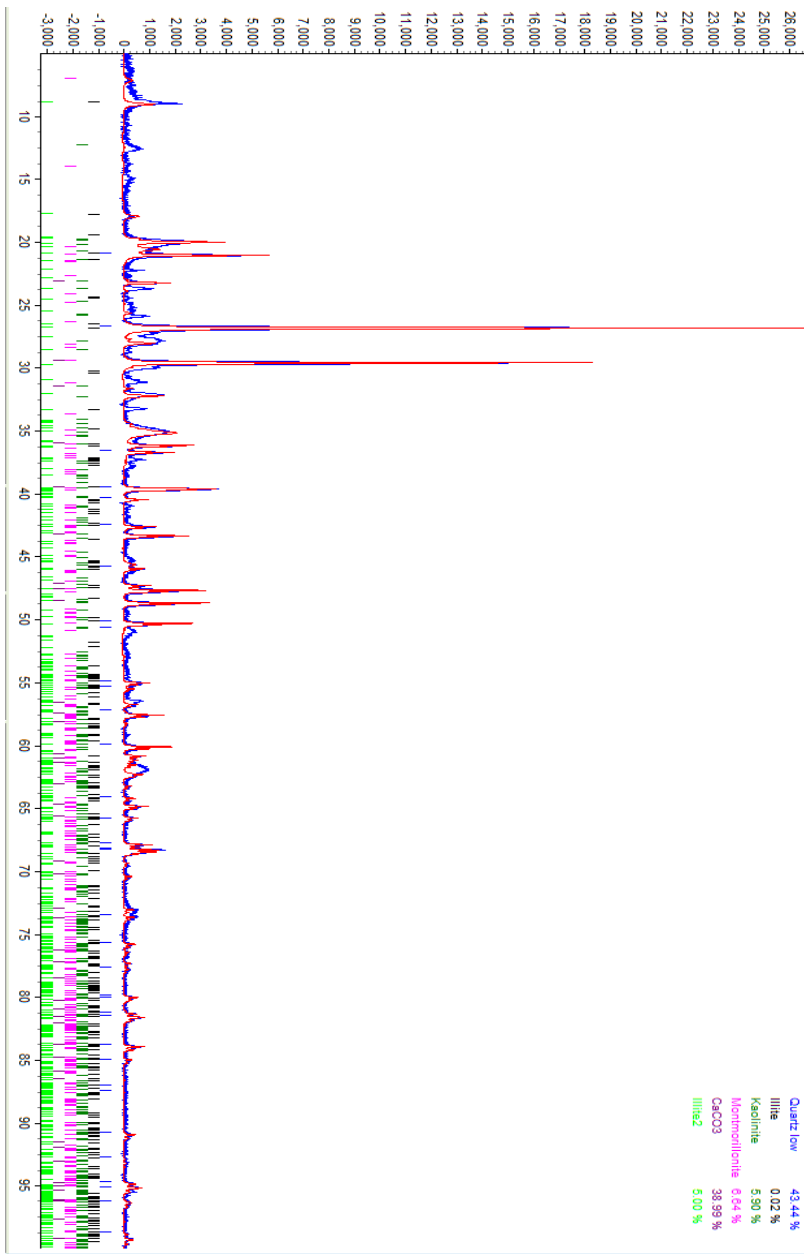
Figure C.5 XRD analysis on sample from Spencer (3 ft-4 ft).

131

Appendix D ESoil Stabilization Using Biopolymer Additives

<u>D.1 Background</u>

Chemical stabilization is one of the main methods of soil improvement and to alter the properties of soils. Several types of materials and methods can be employed for soil stabilization. One of the common approaches is the injection of synthetic materials such as micro-fine cement, epoxy, acrylmide, phenoplasts, silicates, and polyurethane (Xanthakos et al., 1994; Karol, 2003) into the pore space to bind soil particles together (DeJong et al. 2010; Karol and Berardinelli 2003; Xanthakos et al. 1994). This is accomplished using a variety of chemical, jetting, and permeation grouting techniques (DeJong et al. 2010). Among the most commonly used methods, chemical processes such as mixing with cement, fly ash, lime, lime byproducts and blends of any one of these materials have been used to alter soil properties such as strength, compressibility, hydraulic conductivity, swelling potential and volume change properties. Normally Portland cement or lime slurry is used for this purpose resulting in decreased plasticity, increased workability, reduced swelling, and increased strength.

Despite the effectiveness of aforementioned materials in improving the properties and behavior of soils, concerns have been raised with regard to adverse effects of such materials on the environment. Leaching problem associated with cement and lime stabilization has been a long-standing environmental concern. All chemical grouts except sodium silicate are toxic and/or hazardous. In 1974, acrylamide grout was associated with five cases of water poisoning in Japan, resulting in the ban of nearly all chemical grouts. Recent initiatives in certain countries propose to ban all synthetic man-made grouting materials (DeJong et al. 2010; Karol and Berardinelli 2003). Additionally, another critical concern about some of these materials is the emission of greenhouse gasses during their production. Cement has been found to be one of the world's leading causes of CO_2 emissions. With the calcination of limestone and the heat energy required in the production

of cement, approximately one ton of CO_2 is produced for every ton of cement production. It has been reported that 5% of the global carbon dioxide emissions are induced by the cement industries (Chang and Cho 2012; DeJong et al. 2010; Karol and Berardinelli 2003; Petroleum 2009; Worrell et al. 2001).

As a result of environmental concerns associated with traditional soil additives owing to their harmful nature (Afolabi et al. 2012; Chang et al. 2015b; Worrell et al. 2001); and also due to stricter environmental policies, the shift toward alternative solutions such as application of more eco-friendly materials for soil stabilization has become crucial. Among the new materials used for soil improvement, biopolymers have become an attractive option recently mainly because of their effectiveness in enhancing the properties of soils and their compatibility with the environment. Biopolymers are biodegradable polymers produced by living organisms such as algae, fungus or bacteria. They are broadly distributed in nature and serve as skeletal structure-forming substances, assimilative reserve substances, and water-binding substances (Belitz et al. 1999; Chang et al. 2015b). Biopolymers are mostly utilized in the fields of food production, agriculture, cosmetics, medicine, and pharmaceuticals (Chang et al. 2015b). Some recent studies have investigated the application of biopolymers in geotechnical engineering. Chang et al. (Chang et al. 2015a) conducted an experimental study to evaluate the effect of soil treatment using Xanthan gum. Their study showed that the Xanthan gum fibers interact directly with the charged surfaces of clayey particles; and it showed the best efficiency when it was applied to the soils with fine particles. It was also concluded that the effectiveness of Xanthan gum was increased at higher concentrations. The authors reported that the overall performance of Xanthan gum was dependent on various factors including type of soil, percentage of Xanthan gum added to the soil, mixing method, and hydration levels of soils. In another study (Chang et al. 2015b), two types of biopolymers namely

Gellan gum and agar gum were used as soil strengthening agents. Clayey and sandy soils were treated using different quantities of biopolymers as well as different treatment conditions. The results of uniaxial compressive test indicated that while both 1% Gellan and agar gum without thermal treatment improved the soil strength, thermal treatment can result in more pronounced improvement. Additionally, the study concluded that Gellan gum provided better performance than agar gum for soils with a large portion of fine contents. It has also been reported that even using a small percentage of biopolymers (e.g., 0.5-1.0%) could provide significant improvements in erodibility of soil by enhancing inter-particle cohesion (Chang et al. 2015c).

D.1.1 Experimental Plan

D.1.1.1 Materials

East Nebraska has thick deposits of glacial tills, and North East Nebraska has shales and loess. Since the majority of landslides occur in these parts of Nebraska, two types of soils (i.e., glacial till, and shale) collected from the aforementioned regions were selected for treatment. Two types of biopolymers including Xanthan gum and Gellan gum were also selected as stabilization agents. Although, there are numerous types of biopolymers available in the market, these two materials were chosen since they appeared to be among the most effective biopolymers additives according to the literature review and also preliminary test results. Xanthan gum is a polysaccharide commonly used as a food additive and rheology modifier; it is produced by fermentation of glucose or sucrose by the Xanthomonas campestris bacterium (Chang et al. 2015a). Gellan gum is a high molecular weight polysaccharide fermented from the Spingomonas elodea microbe. It has the properties of a thickening or gelling agent and is often used as a food additive (Chang et al. 2015b).

Prior to sample preparation, it was ensured that all the soils collected from the field have the particle size finer than approximately 5 mm. For the soils with larger particles, a crushing machine was used to reach the appropriate size.

D.1.1.2 Sample Preparation

Before sample preparation, all of the soil materials were kept in oven with the temperature of 105 °C for at least 48 hours to make sure they are in complete dry condition for mixing and compaction. The moisture content of soils for mixing and compaction were the selected to be same as the natural moisture content of soils in the field. This was 19.5% by mass of dry weight for the glacial till and 20.1% for the shale. For a more efficient and faster mixing process, an electric bucket mixer was employed. For stabilizing the soils, biopolymers were directly added by 1.5% dry weight and mixed with soils before adding water to the mix. Water was then gradually added, and the mixing process continued until all the particles mixed thoroughly with water and homogenous material was acquired. Figure D.1 shows the process of mixing soil, biopolymers, and water.

Figure D.1 mixing soil with biopolymers and water

For preparing test specimens, a method of compaction recently developed by Sullivan et al. was adopted (Sullivan et al. 2015). This method is called "*preparation of test specimens using the plastic mold compaction device*" and is intended to produce test specimens with approximate specimen density obtained from AASHTO T 99. This method involves the use of a plastic mold compaction device (PM device) to prepare cylindrical specimens with an approximate 2:1 height to diameter (Howard et al. 2013; Sullivan et al. 2015). This practice is intended for chemically stabilized soil materials. The PM device manufactured for the current study is shown in Figure D.2. The fixture includes a metal split-mold, collar, and base plate. The cylindrical plastic mold is 3.0 in (76.2 mm) diameter by 6.00 in (152.4 mm) tall.
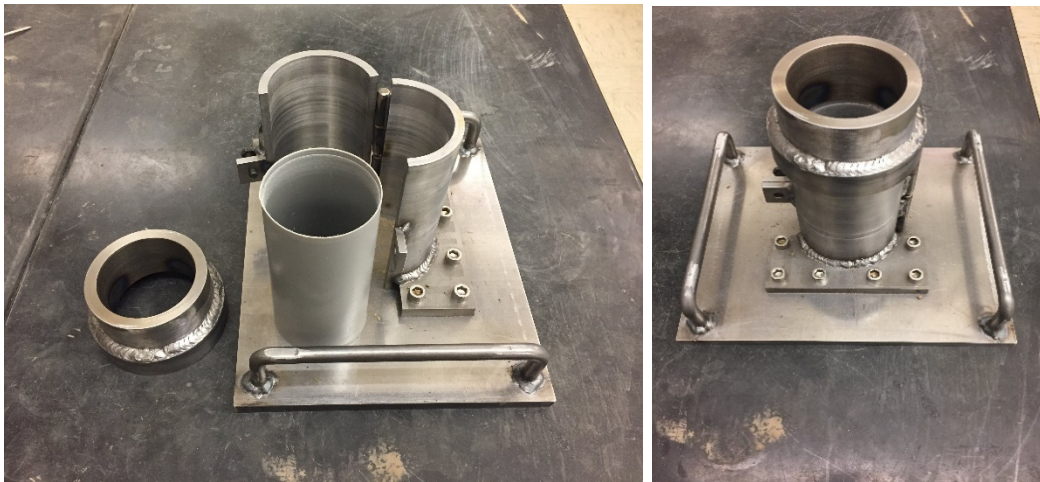
Figure D.2 Plastic mold (PM) compaction fixture

For sample compaction, the soil was compacted into the plastic mold assembly in three approximately equal layers. Each layer was compacted by five uniformly distributed blows from the rammer dropping from a height of 18 in (457 mm). The compacted sample was then removed from the plastic mold using an automatic sample extruder. Figure D.3a and D.3b demonstrate the specimens after compaction and extrusion for glacial till and shale respectively.

136
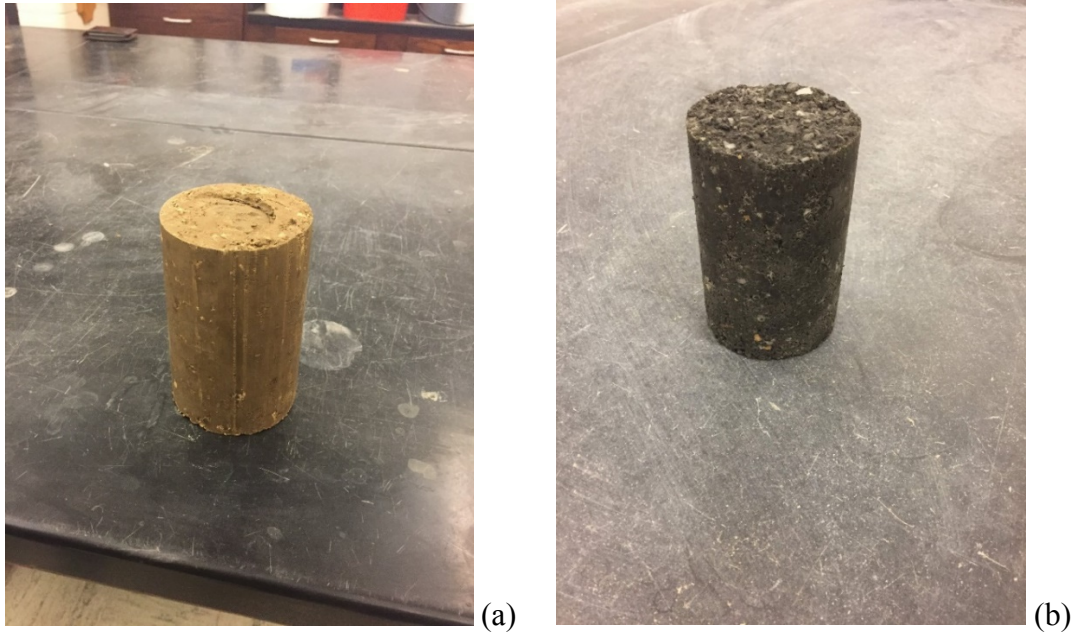
Figure D.3 (a): glacial till compacted sample (b): shale compacted sample.

To prepare specimens for weathering process and further testing, the compacted samples were cut and trimmed. In the first step, each compacted sample was split into three pieces using a hacksaw as shown in Figure D.4a. Each piece was then trimmed using a consolidation ring to obtain the final sample with 2.5 in diameter and 1.0 in height (Figure D.4b). Figure D.5 depicts the final samples after cutting and trimming for both glacial till and shale.
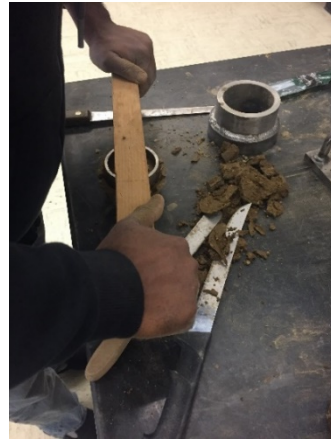
(a)	(b)

Figure D.4 Cutting and trimming compacted samples.

Figure D.5 Compacted samples after cutting and trimming

In order for the biopolymers additive to be effective in strengthening the soils, sufficient curing time should be provided before weathering and testing the samples. Therefore, after the trimming process, soil samples were placed in PVC molds to prevent sample disturbance and then were wrapped in plastic foil in order to prevent samples from losing their moisture as illustrated in Figure D.6. The soil samples were kept in curing condition for a week.

Figure D.6 Curing stabilized soil samples

One of the main targets of this experimental study was to evaluate the negative effects of wetting and freezing cycles on the strength of soils for both biopolymers stabilized, as well as untreated samples. Although it has been reported in other studies that biopolymers are effective in enhancing the properties of soil, their improving effects have not been investigated when samples are subject to various cycles of wetting, freezing, and sawing/drying. As a result, an extensive weathering plan was designed in this study to examine the behavior of soil samples with regard to different environmental conditions. The weathering plan was divided into two main groups. The first group was to simulate only wet and dry cycles in order to investigate the effect of soils exposure to water. Since Nebraska experiences significant seasonal and temperature variations, the second group was intended to simulate the condition in which soil samples are subject not only to wet, but also freezing conditions. Since it was not feasible to directly expose soil specimens to water without losing the integrity of samples, a similar procedure utilized by Khan (Khan 2016) was adopted and a special fixture was designed for this purpose. The fixture included a PVC mold

having an inner diameter with the same size as the soil specimens (i.e., 2.5 in), the outer diameter of 2.7 in, and the height of 1.6 in. The specimens were placed inside the PVC mold and two porous stones with diameters of 3.0 in and 2.5 in were placed at the bottom and top of the mold respectively to provided water infiltration and drainage. While the bottom stone completely covers both mold and specimen, the top stone was inserted inside the PVC mold to sit at the surface of the specimen. The approximate gap between the top of the mold to the top of the porous stone was about 0.3 in. This gap was considered to allow for possible volume expansion of samples due to infiltration of water. Additionally, filter papers were placed between the specimen and porous stones to prevent stones from clogging. The schematic view of the fixture is illustrated in Figure D.7, while Figure D.8 shows placement of specimen, filter papers, and porous stones. The whole fixture was then put between two hollowed polycarbonate plates and secured using four screws. The whole set which is shown in Figure D.9 then provided an efficient way to condition samples with minimum disturbance.
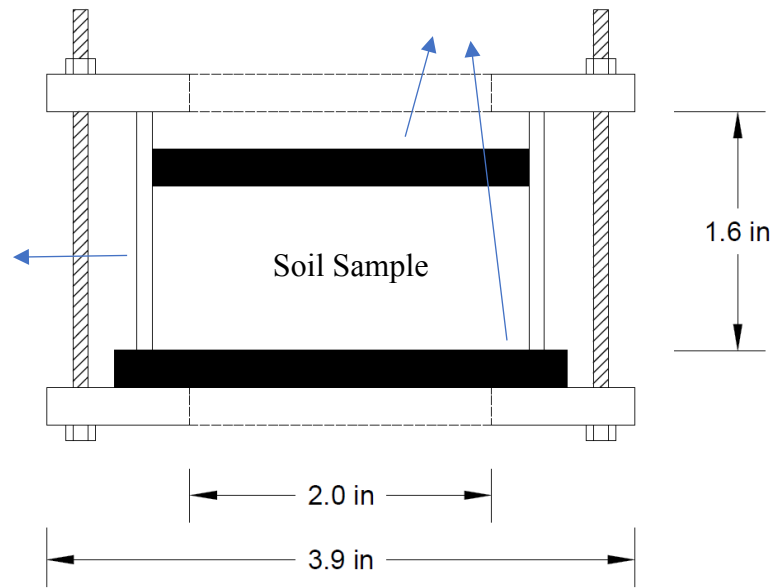
Figure D.7 The fixture used for weathering soil samples

Figure D.8 Preparing samples for weathering

Figure D.9 Securing samples in the fixture for weathering

D.1.1.3 Weathering Soil Samples

As mentioned earlier, two types of weathering conditions were selected: a) wet-dry, and b) wet-freeze-dry. For wet-dry (W-D) condition, a cycle of weathering was achieved by first placing the samples in the water bath for 24 hours and then keeping the samples for 24 hours in the oven (as shown in Figure D.10) with a temperature of 167 °F (75 °C). For wet-freeze-dry (W-F-D) condition, similar to the W-D condition, the samples were kept in the water bath for 24 hours, and then placed in the freezer for 24 hours, followed by drying in the oven at 167 °F (75 °C) for 24 hours. Four different weathering cycles including 2, 4, 8, and 16 were also chosen to see the full effect of weathering cycles on the strength of soil samples. It should be noted that one set of samples was also considered as a control group to be tested without being subjected to any weathering cycles.

Figure D.10 Water bath and oven used for weathering soil samples

D.1.1.4 Testing

After the required weathering cycles were obtained for each set of samples, the strength of

soil samples was determined using the conventional direct shear test. Considering two replicates

for each group of samples, a total of 108 specimens were prepared for testing. These included the

specimens treated with Xanthan and Gellan gums plus the original untreated soil samples. All of

the samples have also prepared for five different weathering cycles (i.e., 0, 2, 4, 8, 16). It should

be mentioned that all specimens were tested right after the last wet cycle. For the samples with no

weathering cycles, they were placed in the water bath for few hours before testing to reach the

similar of level of moisture content compared to other samples. The moisture content of samples

was determined before testing and the average results are summarized in Table D.1 and Table D.2.

After removing porous stones from the weathering fixture, soil specimens were removed from the

PVC molds and placed into the shear box. 2.9 psi (20 kpa) normal pressure was selected and kept

constant during the test. The reason for selection of relatively lower amount of normal pressure

was because the testing was meant to simulate the behavior of soil in shallow depth. A constant

shear displacement of 0.01 in/min (0.25 mm/min) was then applied until the sample failure.

143

Table D.1 Average moisture content of glacial till samples

Biopolymer	Weathering condition	No of cycles	Avg moisture content %
NA	wet-dry	0	51.8
NA	wet-dry	2	49.1
NA	wet-dry	4	50.5
NA	wet-dry	8	53.0
NA	wet-freeze-dry	0	48.2
NA	wet-freeze-dry	2	51.5
NA	wet-freeze-dry	4	49.3
NA	wet-freeze-dry	8	52.7
Xanthan	wet-dry	0	47.9
Xanthan	wet-dry	2	50.9
Xanthan	wet-dry	4	48.8
Xanthan	wet-dry	8	51.4
Xanthan	wet-dry	16	53.2
Xanthan	wet-freeze-dry	0	50.9
Xanthan	wet-freeze-dry	2	49.9
Xanthan	wet-freeze-dry	4	52.7
Xanthan	wet-freeze-dry	8	53.9
Xanthan	wet-freeze-dry	16	52.8
Gellan	wet-dry	0	48.6
Gellan	wet-dry	2	48.9
Gellan	wet-dry	4	50.4
Gellan	wet-dry	8	52.3
Gellan	wet-dry	16	51.9
Gellan	wet-freeze-dry	0	50.5
Gellan	wet-freeze-dry	2	52.1
Gellan	wet-freeze-dry	4	53.8
Gellan	wet-freeze-dry	8	50.9
Gellan	wet-freeze-dry	16	52.1

Table D.2 Average moisture content of shale samples

Biopolymer	Weathering condition	No of cycles	Avg moisture content %
NA	wet-dry	0	47.2
NA	wet-dry	2	50.9
NA	wet-dry	4	52.9
NA	wet-dry	8	53.7
NA	wet-freeze-dry	0	49.9
NA	wet-freeze-dry	2	51.5
NA	wet-freeze-dry	4	53.4
NA	wet-freeze-dry	8	52.9
Xanthan	wet-dry	0	50.6
Xanthan	wet-dry	2	49.8
Xanthan	wet-dry	4	52.3
Xanthan	wet-dry	8	52.1
Xanthan	wet-dry	16	54.0
Xanthan	wet-freeze-dry	0	51.2
Xanthan	wet-freeze-dry	2	53.6
Xanthan	wet-freeze-dry	4	53.1
Xanthan	wet-freeze-dry	8	52.9
Xanthan	wet-freeze-dry	16	52.4
Gellan	wet-dry	0	51.0
Gellan	wet-dry	2	53.8
Gellan	wet-dry	4	52.1
Gellan	wet-dry	8	49.2
Gellan	wet-dry	16	50.1
Gellan	wet-freeze-dry	0	51.1
Gellan	wet-freeze-dry	2	53.7
Gellan	wet-freeze-dry	4	49.6
Gellan	wet-freeze-dry	8	49.9
Gellan	wet-freeze-dry	16	51.5

D.1.2 Results and Discussion

Figures D.11a to D.11c present the average of direct shear test results in terms of shear strength for glacial till control samples (i.e, untreated samples), Xanthan-stabilized samples, and Gellan-stabilized samples respectively. As can be observed from these graphs, as the number of weathering cycles increases, the shear strength mostly reduces. Additionally, in all cases with the

same number of weathering cycles, samples weathered under the wet-freeze-dry condition presented lower shear strength compared to the samples weathered under the wet-dry condition. This implies that the effect of freezing is significant in loss of soil strength mainly due to the volume change that occurs during the freezing process. From these Figures, it can also be concluded that for the glacial till weathered under wet-dry condition, the highest strength loss occurs from 2 weathering cycles to 4 cycles. For the wet-freeze-dry condition however, the highest strength drop occurs from the samples with no weathering to samples with 2 cycles of weathering. This observation again highlights the significance of freezing in reducing the integrity of soil samples even during the first initial cycles. Figures D.11b and D.11c also show that the strength loss from 8 cycles to 16 cycles is insignificant for both types of weathering conditions which implies that after a certain point, the greater number of weathering cycles does not necessarily lead to reduction of soil strength. It should be noted that the testing data for control samples with 16 cycles (Figure D.11a) could not be obtained since the samples were very weak and already failed during removal from weathering fixture before testing.

(a)
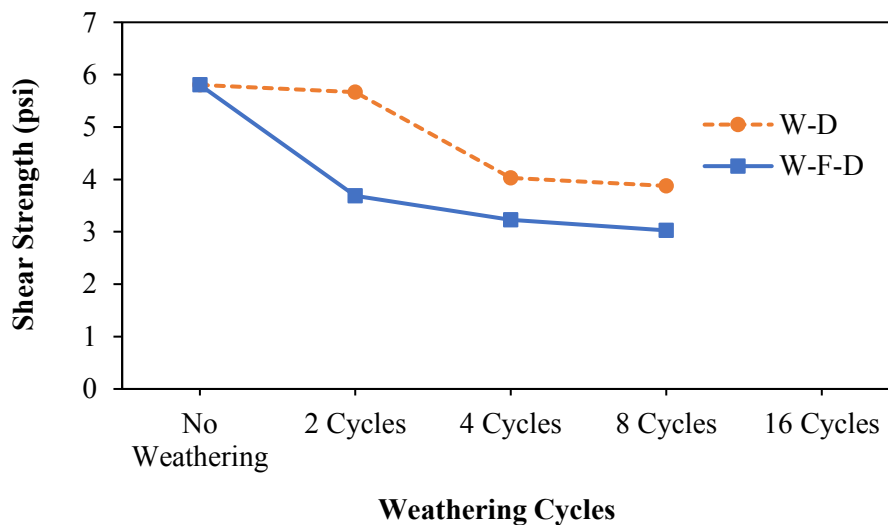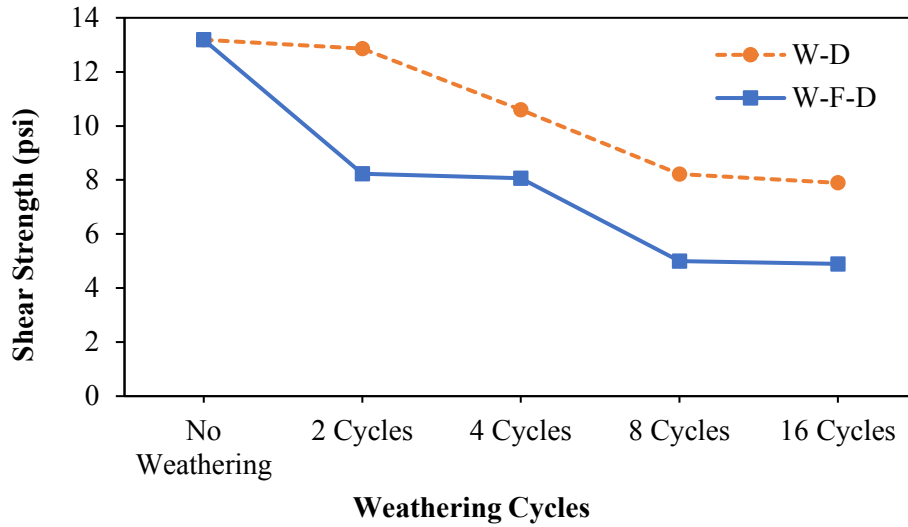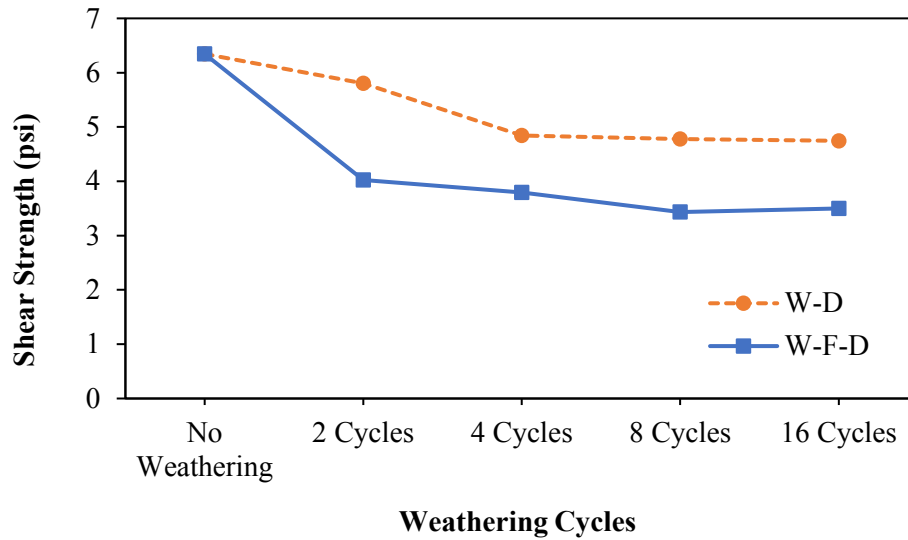
Figure D.11 Direct shear test results for glacial till (a): control samples (b) Xanthan-stabilized samples (c) Gellan-stabilized samples

The comparison between the effect of two types of biopolymers on improving the behavior of glacial till is shown in Figure D.12a for wet-dry condition, and in Figure D.12b for wet-freeze-dry weathering condition. While both biopolymers were effective to improve the strength of soils samples, Xanthan provided significantly better performance as in most cases, the glacial till

147

samples stabilized with Xanthan exhibited more than double shear strength than that of untreated or stabilized with Gellan.

(a)

(b)
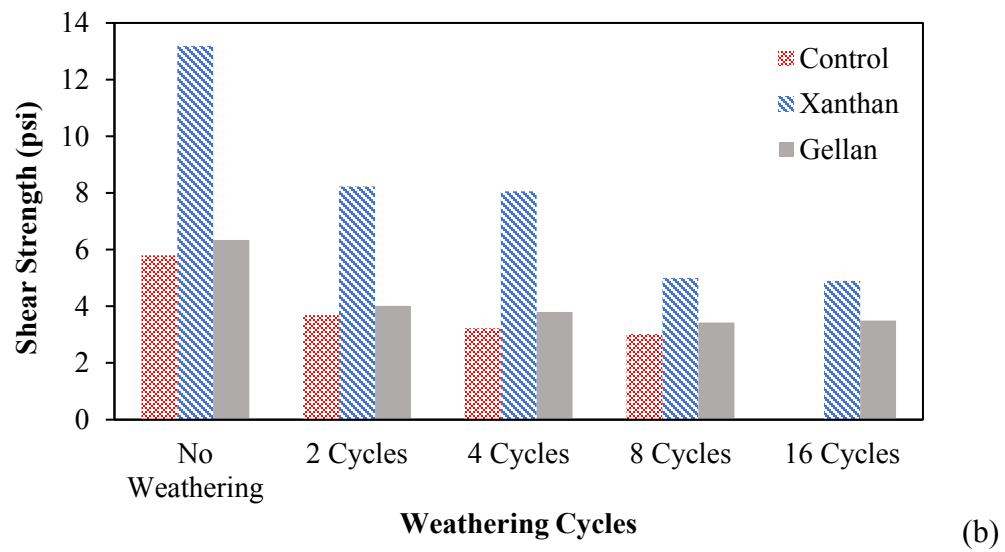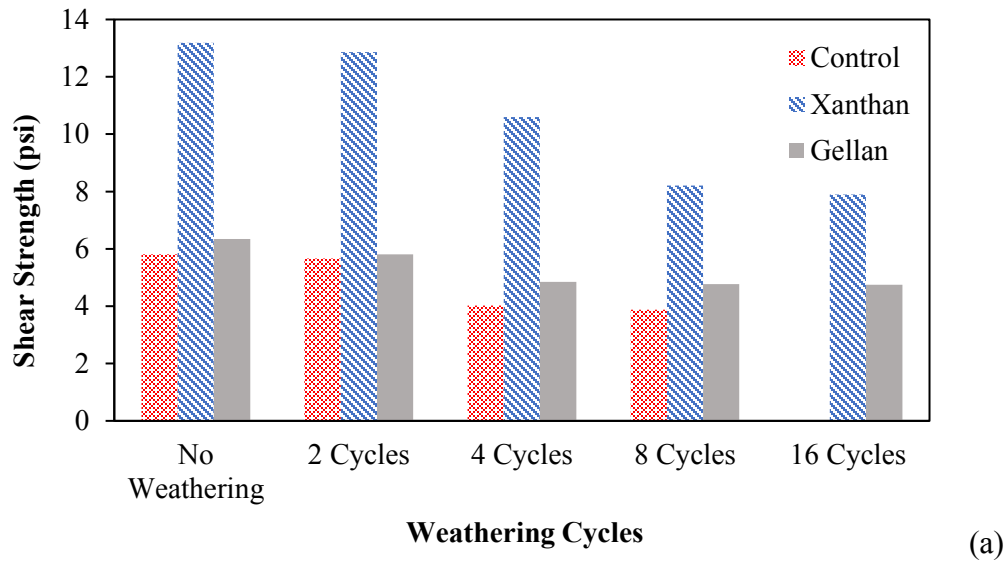
Figure D.12 Direct shear test results for glacial till (a) wet-dry condition (b) wet-freeze-dry condition

The average of direct shear test results for shale control samples, Xanthan-stabilized samples, and Gellan-stabilized samples is shown in Figures D.13a to D.13c respectively. Similar

to glacial till samples, a general decreasing trend was observed as the number of weathering increases. While samples weathered under wet-freeze-dry condition generally demonstrated lower shear strength than that of weathered under wet-dry condition, Xanthan-stabilized samples in 8 and 16 cycles showed very similar results for both types of weathering conditions (Figure D.13b). It can also be concluded from these graphs that either from 4 to 8, or from 8 to 16 cycles, the loss of strength in the samples becomes less significant.

(a)

(b)

(c)
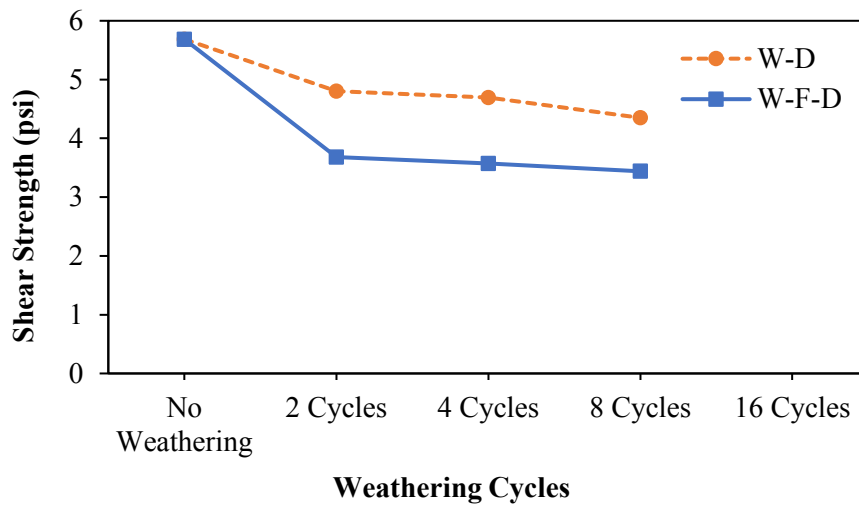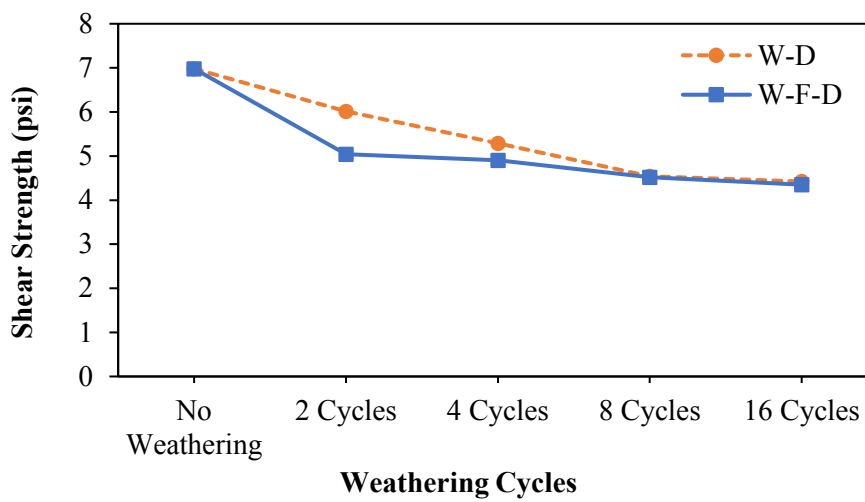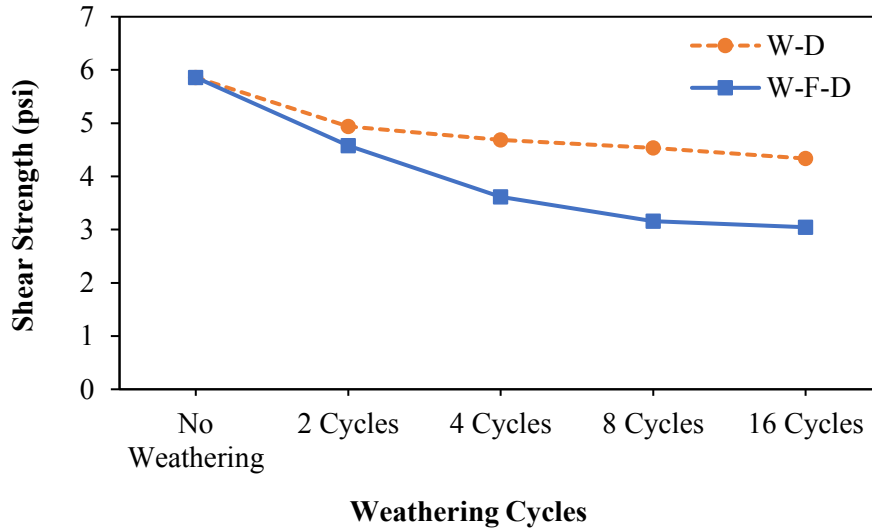
Figure D.13 Direct shear test results for shale (a): control samples (b) Xanthan-stabilized samples (c) Gellan-stabilized samples

The strengthening effect of biopolymers can also be compared in Figures D.14a and D.14b for wet-dry and wet-freeze-dry conditions respectively. In all cases, Xanthan gum was effective in enhancing the strength of soil samples, however, its improving effect on shale samples was less significant compared to glacial till. In case of Gellan gum, treated samples showed slightly better or in some cases, similar results compared to control samples. Comparing the direct shear test results on both glacial till and shale samples, it can be concluded that Xanthan gum provided a superior performance compared to Gellan gum, especially in the case of glacial till. Furthermore, except for a couple cases, wet-dry-freeze weathering condition resulted in lower shear strength than wet-dry condition for the same number of cycles.
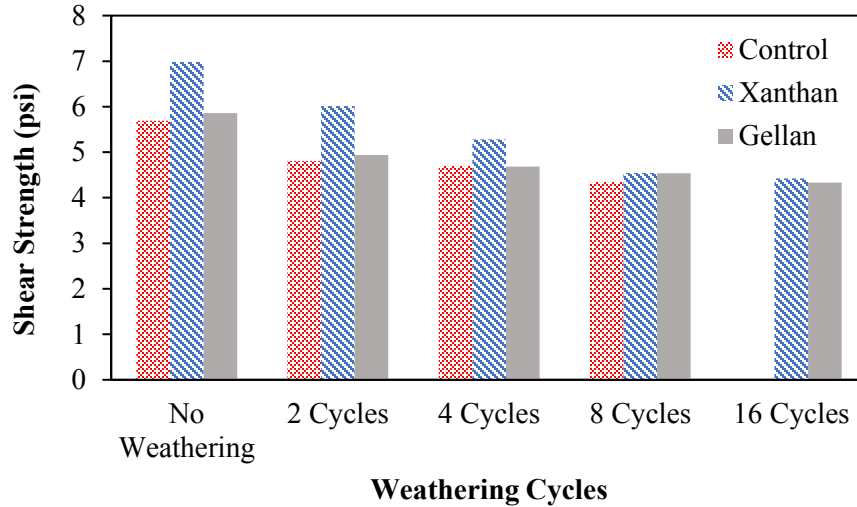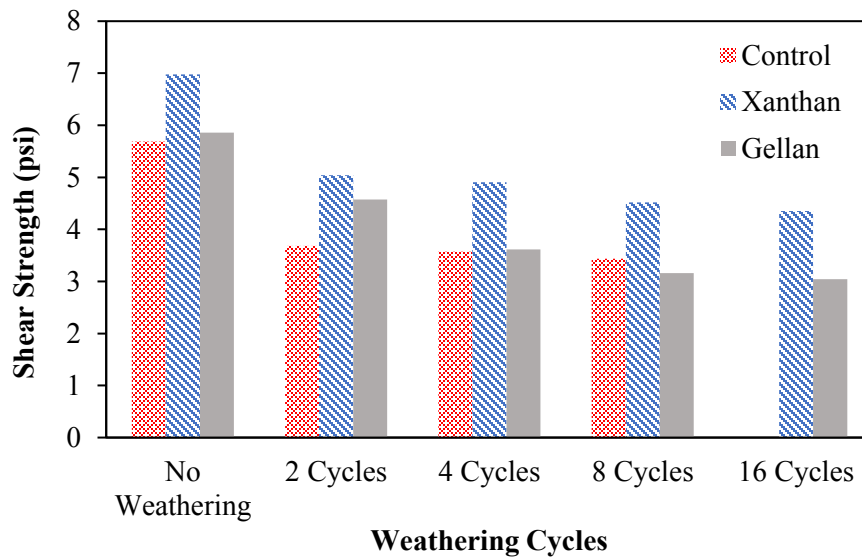
Figure D.14 Direct shear test results for shale (a) wet-dry condition (b) wet-freeze-dry condition

D.1.3 Conclusions

From the experimental results, it can be concluded that the effect of weathering on strength reduction of soil could be considerable. It also appeared that in most cases, the effect of freezing could be significant as the samples weathered under freezing condition mostly showed lower strength than that of weathered under only wet condition. Furthermore, while higher weathering

cycles generally resulted in lower shear resistance, the effect of more weathering cycles became less significant after a certain number of cycle was reached. In case of biopolymer stabilization, both biopolymers could improve the behavior of soil with Xanthan gum exhibiting superior performance compared to Gellan gum. The effect of Xanthan gum also turned out to be much more effective on glacial till samples than till samples.

Appendix E Design of Ground Anchor

E.1 General

   This chapter shows a procedure how a ground anchor may be designed for stabilizing roadside slopes in Nebraska. A hypothetical cut slope having a 1V:3H inclination is shown in Figure E.1 is considered to demonstrate the design of ground anchors. The design of anchors is preceded by slope stability analysis. Factor of safety of the slope against shear failure may be computed based on the simplified Bishop method or other proper method. Bishop method, for example, is based on limit equilibrium analysis under the assumption that slopes would fail if and only if the driving force due to natural (weight and seeping water) or manmade factors (surcharge loads) equals the resisting force that is derived from the shear strength of slope material. The Mohr-Coulomb failure criteria is employed in this case which assumes at failure soils deform plastically without increment in shear stress.
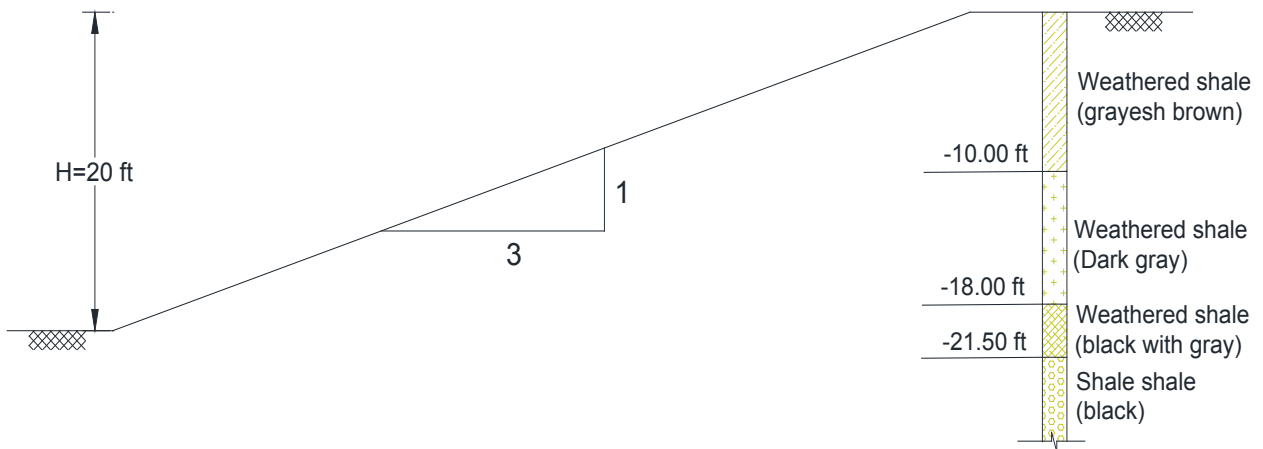
Figure E.1 Hypothetical cut slope along with soil stratification

153

E.2 Soil stratification, Properties and Groundwater Table Condition

  For the design of soil/rock anchors, a thorough understanding about the geotechnical characteristics of the site is needed. The main outputs from the geotechnical investigation are soil stratification which includes the type and thickness of soil layers, shear strength and hydraulic properties of the soil, and the piezometric heads at different location along the slope. The later one is useful to assess the pressure heads within the slope. However, these hydraulic heads are inconsistent and can vary depending on the season and construction activities. The critical piezometric heads measured at different time of the year should be considered (FHWA 1999).

  For the design example shown in Figure E.1, the assumed soil stratification is provided in the same Figure. The physical and shear strength parameters are provided in Table E.1. Hydraulic conductivity is disregarded since the worst scenario where the phreatic line is on the top of the slope is going to be considered. The groundwater Table condition is assumed to be on the surface of the slope. However, the effect of pore water pressure on the shear strength of the soil layers is assumed to be accounted within average back calculated shear strength values (s_{avg}).

Table E.1 Stratification and shear strength of soil layers

Layer	Soil Type	Thickness (ft)	Saturated unit weight, Y_{sat} (pcf)	Shear strength (s_u) (psf)
Layer-1	Weathered shale (grayish brown)	10.00	108.21	125.00
Layer-2	Weathered shale (dark gray)	8.00	114.57	188.00
Layer-3	Weathered shale (black with gray)	3.50	117.75	209.00
Layer-4	Shale (black)	15.00	124.12	272.00

E.3 Simplified Bishop's Method

The stability of the slope is analyzed based on limit equilibrium method using the simplified Bishops method (1955). This method is a more refined version of the ordinary method of slices. This is the most widely slope stability analysis technique in practice due to its relative simplicity and accuracy for circular slip surfaces. Moreover, this method is chosen since in most cases difference between various slope stability analyses methods is less than 6% (Duncan 1996). Wright et al. (1973) has also showed that the factor of safety from a simplified Bishop's method is within 5% of factor of safety computed from finite element procedures. The Bishop's method includes the effect of interslice normal forces while it ignores interslice shear stresses. Factor of safety in this method is computed based on iteration. Figure E.2 shows a typical slice and forces acting on it.
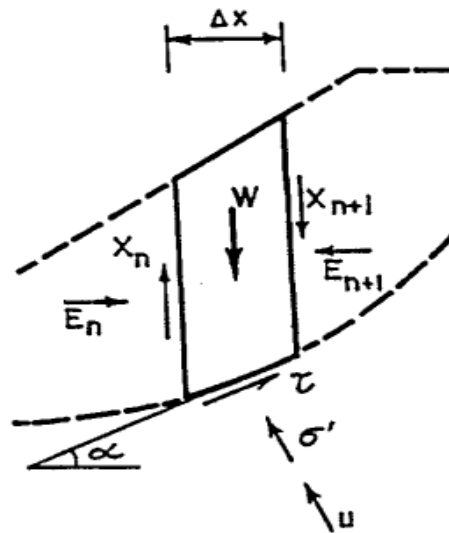
Figure E.2 Forces and stresses acting on a single slice

The interslice forces X_n and X_{n+1} are neglected and equilibrium of the vertical forces yield the factor of safety equation shown in equation 2. However, this method only satisfies moment and vertical forces equilibrium. Forces in the horizontal directions do not satisfy equilibrium conditions.

$$F_s = \frac{\sum \text{maximum resisting force on the base of slice}}{\sum \text{driving forces on base of slice}} \tag{1}$$

$$F_s = \frac{\sum\left[(c'\Delta x + (W - u\Delta x)\tan\phi')\frac{1}{M_\alpha}\right]}{\sum W \sin\alpha} \tag{2}$$

where F_s = Factor of Safety, c'= cohesion, W= weight of a slice, u = pore water pressure at the base of a slice, Δx = is slice width, and M_α is given by:

$$M_\alpha = \cos\alpha + \frac{\sin\alpha\tan\phi'}{F_s} \tag{3}$$

Weight of a slice is computed by the following equation:

$$W = \gamma\Delta x h \tag{4}$$

where γ = unit weight of soil; h = slice height. The weight is given in a unit of force per unit length.

E.4 Critical Slip Surface

Determining the critical slip surface at which the factor of safety of the slope would be minimum is cumbersome job if one tries to do all calculations by hand. This is due to the reason that the center of the circular slip surface should be varied several times before reaching the most critical position. But the position of the critical slip surface can be easily determined with the help of computer software like GEOSLOPE. For the example considered in this chapter, the critical

slip surface with the factor of safety 1.0 for the given slope geometry and material properties based on simplified Bishop's method was found to be as the one shown in Figure E.3. The radius of the critical slip surface is 50 ft.
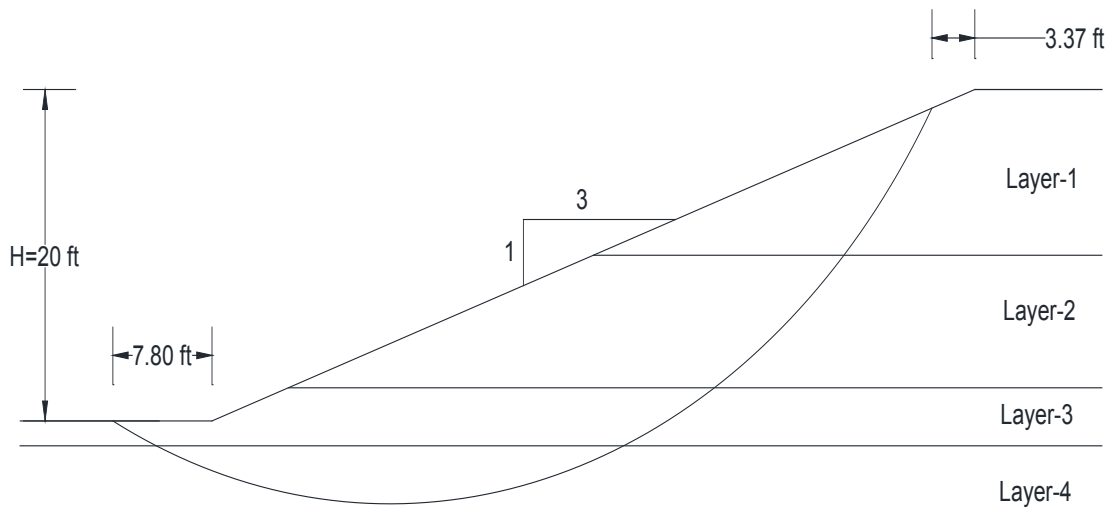
Figure E.3 Critical slip surface

E.5 Shear Strength Parameters

Prior to the computation of factor of safety, it is mandatory to know the appropriate values of shear strength parameters. For overconsolidated soils constituting cut slopes, the recommended shear strength parameters are those obtained from drained shear strength tests (FHWA 1999). However, for the analysis explained in this report, the back analyzed undrained shear strength is considered as a substitution for shear strength that can be computed from drained shear strength parameters which might be difficult to accurately pin point their magnitudes for failed slopes. The undrained shear strength obtained from back analysis can indirectly tell what the shear strength of the soils should be, so that the slope will be in critical stage. Drained shear strength along the critical slip surface can be obtained based on the general Mohr-Coulomb failure criterion shown in Equation 5 below.

$$\tau = c' + \sigma'_n \tan \phi' \tag{5}$$

where τ = drained shear strength along failure plane; c' = cohesion; σ'_n = effective normal stress on failure plane; ϕ' = effective angle of friction.

The overall effect of cohesion, effective angle of internal friction and overburden pressure can be represented by an average shear strength obtained from back analysis. It is suiTable to substitute this representative shear strength based on the equation shown below.

$$\tau = s_{avg} = c \tag{6}$$

where s_{avg} = average back calculated shear strength; c = cohesion that represent average shear strength s_{avg}. The overall effect of friction, confining pressure are altogether included in the cohesion. Hence, in Equation 6, $\phi' = 0$.

Based on the above assumption, the factor of safety equation given in Equation 2 will be modified as:

$$F_s = \frac{\sum \left[(c\varDelta x) \frac{1}{\cos\alpha} \right]}{\sum W \sin\alpha} \tag{7}$$

Factor of safety is obtained directly from Equation 7 without the need for iteration.

Assuming the slip surface shown in Figure E.3 is among the potential slip surfaces assumed throughout the trial and error procedure of determining critical slip surface, slicing and factor of safety analysis for this slip surface will be discussed in this section.

E.6 Slicing and Factor of Safety Computation

Slicing of the slope material above the assumed slip surface should consider the overall curvature of the slip surface and stratification. It is advantageous to make sure that there is no slice base that traverse two distinct soil layers. For the assumed slip surface in this example, 26 slices having an average width of 2.5 ft (0.76 m) have been adopted. Figure E.4 shows the slicing of the slope material. The slicing and determination of the necessary dimensions and inclination of each slice from the horizontal is done using AutoCAD tool. A sample analysis is done for slice no. 10 on how to determine the resisting and driving forces on the base of this slice. A complete Table showing the same analysis for the entire 26 slices is shown at the end of this Appendix.
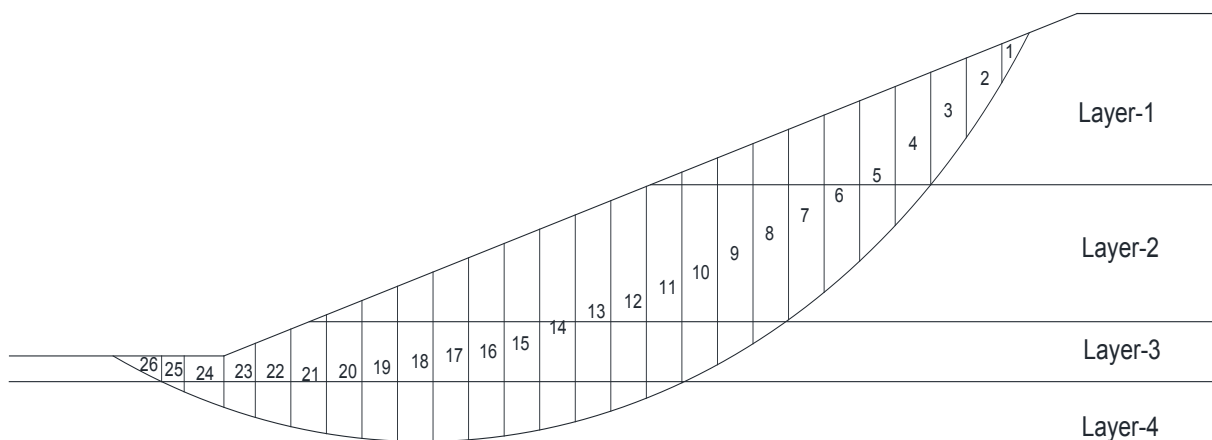
Figure E.4 Slicing of slope material

Global factor of safety for the entire slices should be calculated by adding all resisting forces on the base of each slice and then divide by summation of all the driving forces on each

slice base. Based on this technique, the factor of safety of the slip surface shown in Figure E.4 was calculated to be 1.03, which indicates the slope is at critical condition and needs some retrofitting method to retain its stability again. Design factor of safety was taken to be as 1.30 (U.S. Army Corps of Engineers' Slope Stability Manual 2003). Ground anchors will be used to raise the factor of safety which was obtained as 1.03 to the design factor of safety which is 1.30. The analysis and design of ground anchor will be discussed in next section.

Sample Example: (Slice No. 10)

Input

$\Delta x = 2.50$ ft

$h = 12.19$ ft

$c_u = 209$ psf

$\alpha = 22.91^o$

$\gamma = 117.75$ pcf

Output

$W = \gamma \Delta x h = 117.75 * 2.50 * 12.19 = 3588.43$ lb/ft

$\text{Resisting force} = (c\Delta x)\dfrac{1}{\cos \alpha} = (209 * 2.50) * \dfrac{1}{\cos(22.91)} = 567.245$ lb/ft

$\text{Driving force} = W \sin \alpha = 3588.43 * \sin(22.91) = 1396.92$ lb/ft

---

E.7 Design of Ground Anchor

The anchor design discussed hereinafter addressed estimation of the required anchor load, anchor inclination, horizontal spacing, identification of suiTable tendon type, estimation of fixed and free anchor length. Type A anchors will be considered in this example. These anchors are suiTable in rocks as well as stiff cohesive soils. Since much soil layers are weathered shales, this

anchor type will be good choice. The effective diameter of grout would be the same as drill hole diameter for Type A anchors.

E.7.1 Anchor Inclination

Anchors are installed in inclined position to expedite anchor hole drilling and grouting. Furthermore, anchors might be constructed and inclined to make sure they are embedded in suiTable ground. Many contractors consider 15° inclination as a minimum inclination for proper grouting (Xanthakos 1991). But, the effect of overburden will be smaller if a low inclination is adopted for soils where shear strength is dictated by friction besides cohesion. Maximum anchor inclination can go up to 45° when a suiTable ground cannot be reached less than 35 ft (10 m). Most soil anchors are installed at 15° to 30° from the horizontal. The minimum suiTable anchor inclination, which is 15° is considered.

E.7.2 Anchor Load and Spacing

The anchor load is computed based on required design factor of safety. The design factor of safety was considered as 1.30. Since the anchors are assumed to prestressed grouted anchor which will function as active anchor, the anchor load that is going to be transferred to the soil/rock will decrease the driving force in equation 8 below. The effect of normal component of the anchor load on the resisting force is neglected. The same design technique is depicted in FHWA (1999).

$$F_s = \frac{\sum \text{maximum resisting force on the base of slice}}{\sum \text{driving forces on base of slice} - T_a} \tag{8}$$

where T_a is anchor load parallel to slip surface as shown in Figure E.5.

Summation of resisting forces was obtained as 16,522.66 lb/ft while the summation of driving forces was calculated to be 16,106.29 lb/ft. The required anchor load is then computed by substituting resisting and driving forces along with the deign factor of safety in equation 8 as follows:

$$1.30 = \frac{16,522.66}{16,106.29 - T_a}$$

$$T_a = 16,106.29 - \frac{16,522.66}{1.30} = 3,396.55 \text{ lb/ft}$$

Therefore, the required anchor load tangent to the slip surface is 3,396.55 lb/ft (50 kN/m). Two rows of anchors spaced at equal spacing from the toe to the intersection of the slip surface with the slope above the toe. This anchor load can be easily computed using "Anchor" option in GeoSlope. Figure E.6 shows the vertical spacing of anchors and their orientation.
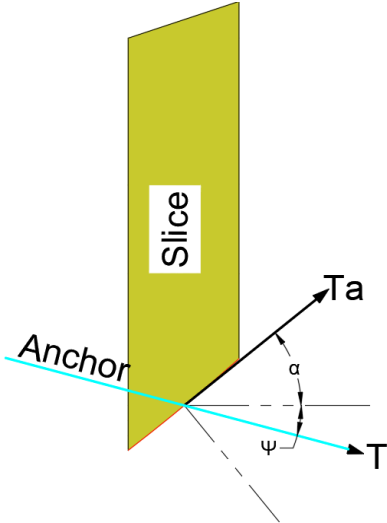
Figure E.5 Anchor load and component of anchor load tangent to slip surface
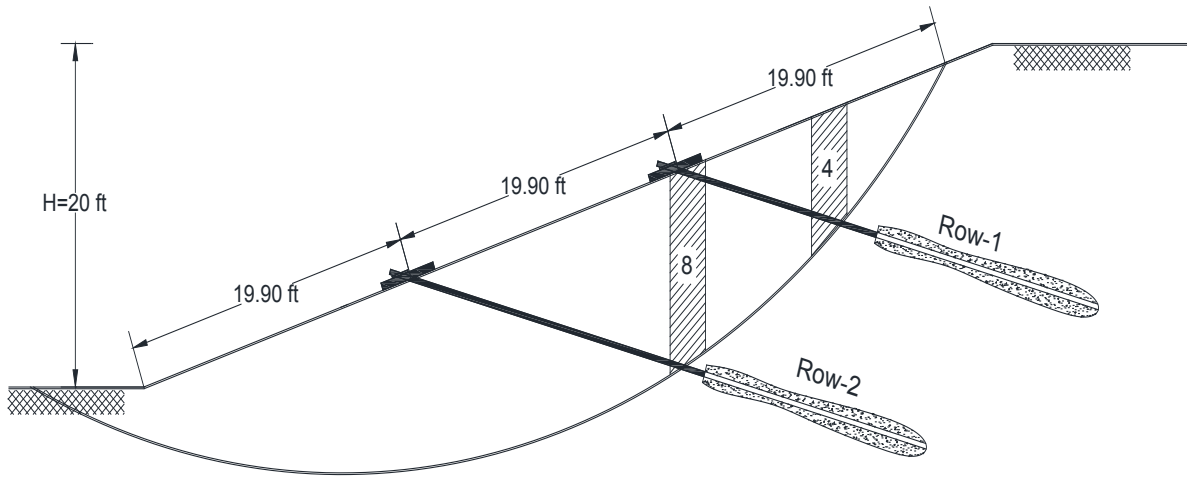
Figure E.6 Anchor orientation for trial-1

The anchors pass through slice no. 4 and 8 in this case. The inclinations of the tangent for slice no. 4 and 8 from the horizontal are $\alpha = 43.59^o$ and $\alpha = 29.30^o$ respectively. The inclination of the anchors was fixed at $\psi = 15^o$. Thus, required design anchor load per unit length can be estimated by:

$$T = \frac{T_a}{cos(\alpha+\psi)} \tag{9}$$

where T = design anchor load per unit length.

However, the component of the anchor load parallel to the slip surface, i.e T_a, should be split between each anchor. To make the design anchor load uniform among the anchors, the following equations are proposed to obtain the distribution of the component of the design anchor load on the slip surface.

$$T_{a1} = \left[\frac{cos(\alpha_1+\psi)}{cos(\alpha_1+\psi)+cos(\alpha_2+\psi)}\right] T_a \qquad (10)$$

$$T_{a2} = \left[\frac{cos(\alpha_2+\psi)}{cos(\alpha_1+\psi)+cos(\alpha_2+\psi)}\right] T_a \qquad (11)$$

The design anchor loads for each row can be now calculated since component of anchor load parallel to the slip surface, inclination of base of slice and anchor from the horizontal are known. The components of the design anchor load for each slice are computed as:

$$T_{a1} = \left[\frac{\cos(43.59+15)}{\cos(43.59+15)+\cos(29.30+15)}\right]3396.55 = \left[\frac{0.521}{0.521+0.715}\right]3396.55 = 1431.71\,\text{lb/ft}$$

$$T_{a2} = \left[\frac{\cos(29.30+15)}{\cos(43.59+15)+\cos(29.30+15)}\right]3396.55 = \left[\frac{0.715}{0.521+0.715}\right]3396.55 = 1964.833\,\text{lb/ft}$$

The design load is calculated by using Equation 8 as:

$$T = \frac{T_a}{cos(\alpha+\psi)} = \frac{1431.71}{cos(43.59+15)} = \frac{1964.833}{cos(29.30+15)} = 2748.00\,\text{lb/ft} = 40.10\,\text{kN/m}$$

The horizontal spacing should be selected between 5-9 ft (1.5-3 m) to ensure no overlapping of stressed zone along the bond length of the anchors (minimize group effect). A horizontal spacing of 9 ft is selected for the first trial as the required anchor load is relatively small. Thus, the design anchor load required from a single independent anchor can be calculated as follows:

$$T_d = T * s \qquad (12)$$

164

where s is spacing of anchors in the horizontal direction.

Based on Equation 12, the required design load for a single anchor will be 2748.00* 9 = 24,732 lb (110.00 kN).

E.7.3 Fixed and Free Length

Fixed (bond) length is governed by the shear strength of the soil-grout interface and effective diameter of the grout. The ultimate skin friction resistance at the soil-grout interface can be calculated as follows:

$$Q_{\text{uf}} = \pi D L_a \tau_f \tag{13}$$

where Q_{uf}= ultimate skin friction at soil-grout interface; D = effective diameter grout; L_a= fixed length; τ_f= interface shear strength between soil and grout.

The interface shear strength using the back calculated shear strength (s_{avg}) can be computed as follows:

$$\tau_f = \alpha s_{avg} \tag{14}$$

where α = empirical reduction factor.

The typical values of reduction factor are from 0.5 to 0.66. The maximum value of α = 0.66 is used for further analyses. The free length spans the length from the face of the slope to the beginning of the bond length. It includes the distance from the face of the slope to the slip surface and some additional penetration length. The minimum free length for bar tendons should be 3 m

(FHWA 1999). Based on the recommendation of FHWA, the penetration length should be 1.5 m or 0.2H whichever is larger. Where H is the height of the slope. The former distance is a function of the specific location of the anchor on the slope. From the AutoCAD draft, the free length of Row-1 anchors will be 15 ft + 5 ft = 20 ft (>3 m ok!) and Row-2 has 20.5 ft + 5 ft = 25.5 ft (>3 m ok!). Where 5 ft is additional allowance of penetration length after the slip surface into the suiTable/stable ground (in this case 1.5 m was considered since 0.2H (H=20 ft) is less than 1.5 m). The total length of an anchor is calculated by adding up the free length and fixed (bond) length as follows:

$$L = L_f + L_a \tag{15}$$

where L = total length of anchor; L_f = free length.

From equilibrium stand point the total anchor design load should be equal to the ultimate skin friction resistance at the grout-ground interface. Figure E.7 illustrates free length and fixed length for anchors.
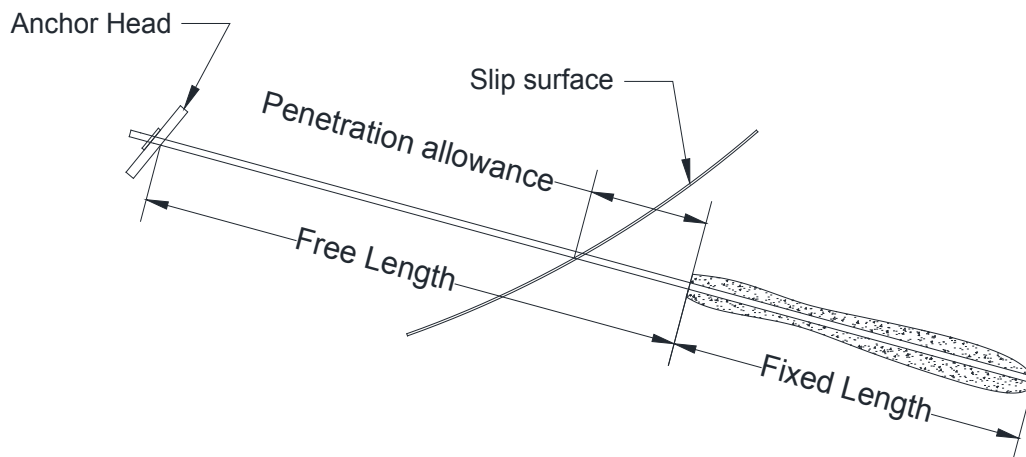
Figure E.7 Components of ground anchors

166

Thus, the bond length can be computed by equating Equation 12 with Equation 13.

$$T_d = Q_{uf} \qquad (16)$$

$$L_a = \frac{T_d}{\pi D \tau_f} \qquad (17)$$

The fixed length (bond length) is commonly selected between 3-10 m (Xanthakos 1991). On the other hand, FHWA recommends 4.5-12 m. In this case, FHWA recommendation has been implemented. The design anchor load is the same for both rows of anchors, however, the shear strength of the soil layers that they are likely to traverse are different. Shear strengths of all soil layers which are within 12 m from the slip surface are compared and the minimum is considered. For instance, for Row 1 anchors, the shear strength is taken to be the minimum of the layer-2 and layer-3 as these anchors will cross these layers. Similarly, for Row-2, the minimum of Layer-3 and 4 are considered. Assuming the drill hole diameter as well as the grout diameter to be 9 (type A anchor), the bond lengths are calculated as follows ($D = 9$ in.):

$$L_a(Row-1) = \frac{24732}{\pi(9/12)(0.66)(188)} = 84.60 \text{ ft} = 25.80 \text{ m} \gg 12 \text{ m} \dots\text{length should be reduced}$$

$$L_a(Row-2) = \frac{24732}{\pi(9/12)(0.66)(209)} = 76 \text{ ft} = 23.16 \text{ m} \gg 12 \text{ m} \dots\dots \text{ length should be reduced}$$

Computed fixed anchor lengths are so big due to low shear strength of the layers which is going to raise the required total anchor length to be very high as well as make grouting operation quite difficult. Therefore, the number of rows of anchors should be increased as well as the horizontal spacing should be lowered. *Trial-2* starting from determination of anchor loading, spacing and fixed length is discussed herein after.

Step-1: Determine total required tangent component of design anchor load

$$F_s = \frac{\sum \text{maximum resisting force on the base of slice}}{\sum \text{driving forces on base of slice} - T_a}$$

$$1.30 = \frac{16,522.66}{16,106.29 - T_a}$$

$$T_a = 16,106.29 - \frac{16,522.66}{1.30} = 3,396.55 \text{ lb/ft}$$

Step-2: Fix the number of anchor rows (i.e in this trial, it is going to be three) and determine the inclination of the slice bases from the horizontal.

$$\alpha_1(slice - 3) = 47.70^o \qquad \alpha_2(slice - 6) = 36.11^o \qquad \alpha_3(slice - 10) = 22.91^o$$

Step-3: Inclination of anchors fixed at 15°, $\psi = 15^o$

Step-4: Determine distribution of tangent components of the anchor load for each anchor

$$T_{a1} = \left[\frac{cos(\alpha_1 + \psi)}{cos(\alpha_1 + \psi) + cos(\alpha_2 + \psi) + cos(\alpha_3 + \psi)}\right] T_a = \left[\frac{0.459}{1.876}\right] 3396.55 = 831.032 \text{ lb/ft}$$

$$T_{a2} = \left[\frac{cos(\alpha_2 + \psi)}{cos(\alpha_1 + \psi) + cos(\alpha_2 + \psi) + cos(\alpha_3 + \psi)}\right] T_a = \left[\frac{0.628}{1.876}\right] 3396.55 = 1137.011 \text{ lb/ft}$$

$$T_{a3} = \left[\frac{cos(\alpha_3 + \psi)}{cos(\alpha_1 + \psi) + cos(\alpha_2 + \psi) + cos(\alpha_3 + \psi)}\right] T_a = \left[\frac{0.789}{1.876}\right] 3396.55 = 1428.506 \text{ lb/ft}$$

Step-5: Determine design anchor load per unit length (perpendicular to slope plane)

$$T = \frac{T_a}{cos(\alpha+\psi)} = \frac{831.032}{cos(47.70+15)} = \frac{1137.011}{cos(36.11+15)} = \frac{1428.506}{cos(22.91+15)} = 1810.53 \text{ lb/ft}=26.42 \text{ kN/m}$$

Step-6: Fix the horizontal spacing and calculate the design anchor load (unit of force). In this trial spacing is assumed as 5 ft.

$$T_d = T * s = 1810.53 * 5 = 9052.65 \text{ lb} = 40.26 \text{ kN}$$

Remark: design anchor load almost decreased by half.

Step-7: Determine fixed anchor length using Equation 7.17 for each anchor rows

$$L_{a1} = \frac{T_d}{\pi D \tau_{f1}} = \frac{9052.65}{\pi(9/12)(0.66)(188)} = 30.96 \text{ ft} = 9.45 \text{ m} < 12 \text{ m.. satisfy the requirement}$$

$$L_{a2} = \frac{T_d}{\pi D \tau_{f2}} = \frac{9052.65}{\pi(9/12)(0.66)(188)} = 30.96 \text{ ft} = 9.45 \text{ m} < 12 \text{ m.. satisfy the requirement}$$

$$L_{a3} = \frac{T_d}{\pi D \tau_{f3}} = \frac{9052.65}{\pi(9/12)(0.66)(209)} = 27.85 \text{ ft} = 8.50 \text{ m} < 12 \text{ m.. satisfy the requirement}$$

Step-8: Determine total length of each rows of anchors using Equation 7.15

$$L_1 = L_{f1} + L_{a1} = (9.20 + 5) + 30.96 = 45.16 \text{ ft} = 13.80 \text{ m}$$

$$L_2 = L_{f2} + L_{a2} = (16.47 + 5) + 30.96 = 52.43 \text{ ft} = 16.00 \text{ m}$$

$$L_3 = L_{f3} + L_{a3} = (20.88 + 5) + 27.85 = 53.73 \text{ ft} = 16.40 \text{ m}$$

Bond length requirement for all rows is now satisfied. Additionally, the depth from the center of the top row anchor's bond length up to the ground surface should be checked if it is greater than or equal to 4.5 m to prevent grout leakage during installation of anchor bond length

(FHWA 1991). Thus, for the uppermost ground anchor (i.e Row-1), the distance from the center of the grout to the ground surface was obtained as 12.50 ft (3.81 m < 4.5 m) as shown in Figure E.8.

Therefore, all anchor rows should be lowered down to meet this requirement. Since the inclination of the anchors is gentle (15°), all anchors are lowered by 14.76 ft (4.5 m) below the top breakpoint of the slope. Trial-3 was done in the same manner using the steps followed for Trial-2 without increasing the number of anchor rows but lowering them down to meet the 4.5 m depth requirement. After going through all steps, the following lengths of each anchor rows were calculated.

Figure E.8 Anchor configuration for Trial-2

Bond length:

$$L_{a1} = \frac{T_d}{\pi D \tau_{f1}} = \frac{8041.05}{\pi(9/12)(0.66)(188)} = 27.50 \text{ ft} = 8.40 \text{ m} < 12 \text{ m} \dots \text{ satisfy the requirement}$$

$$L_{a2} = \frac{T_d}{\pi D \tau_{f2}} = \frac{8041.05}{\pi(9/12)(0.66)(209)} = 24.74 \text{ ft} = 7.54 \text{ m} < 12 \text{ m} \dots \text{ satisfy the requirement}$$

$$L_{a3} = \frac{T_d}{\pi D \tau_{f3}} = \frac{8041.05}{\pi(9/12)(0.66)(272)} = 19.01 \text{ft} = 5.80 \text{ m} < 12 \text{ m} \ldots\ldots \text{ Satisfy the requirement}$$

Total length:

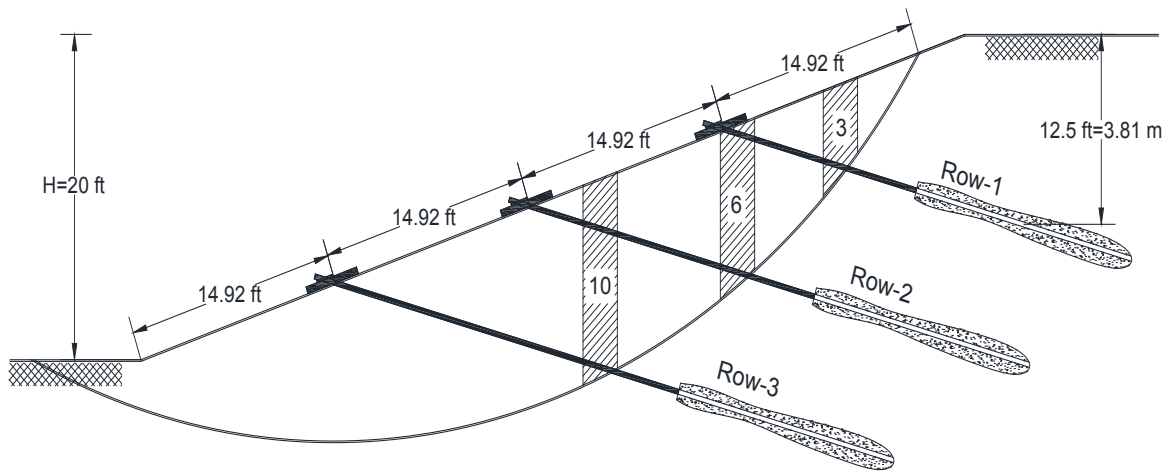$$L_1 = L_{f1} + L_{a1} = (13.30 + 5) + 27.50 = 45.8 \text{ ft } = 14.00 \text{ m}$$

$$L_2 = L_{f2} + L_{a2} = (19.25 + 5) + 24.74 = 52.00 \text{ ft } = 15.85 \text{ m}$$

$$L_3 = L_{f3} + L_{a3} = (21.16 + 5) + 19.01 = 45.17 \text{ ft } = 13.80 \text{ m}$$

Now, the depth from ground surface to the center of the nearest anchor bond length was calculated as 16.61 ft (5.0 m> 4.5 m satisfy the requirement). Figure E.9 shows the final configuration of the anchors designed based soil-grout interface strength criterion. The updated design load for trial-3 was found to be 8041.05 lb (35.76 kN).
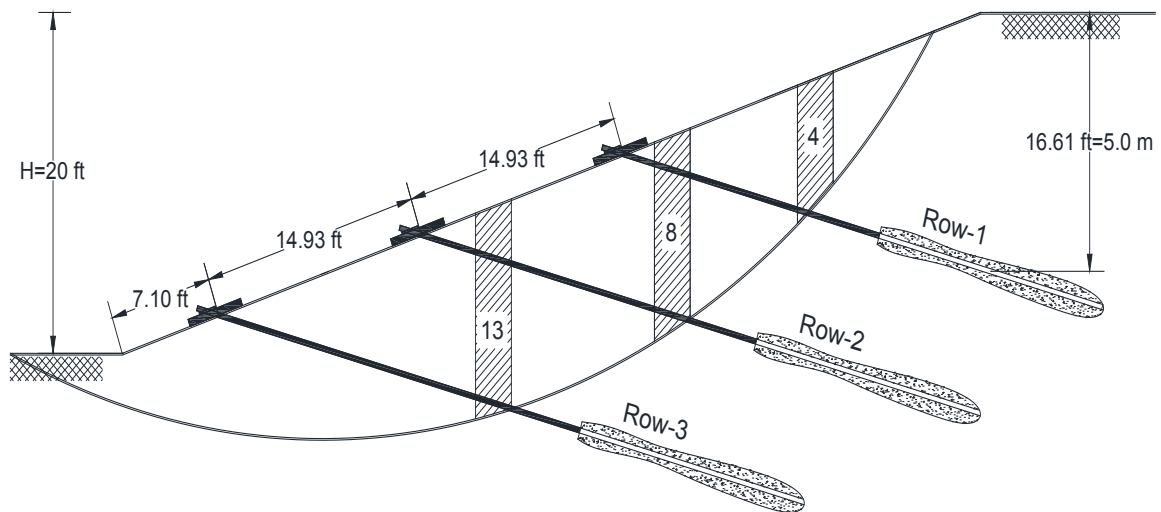
Figure E.9 Anchor configuration for Trial-3 (final)

E.7.4 Tendon Type and Size

The commonly used anchor tendon types are: bars, wires, or strands used in either as a single unit or as a group. Individual assessment and evaluation are required to decide the type of

tendon to be used for a specific purpose. The choice of tendon type is mainly influenced by the cost, easiness of fabrication, transportation and handling in the site, requirement of corrosion protection, required design load, and allowable stress levels (Xanthakos 1991). The major engineering variables for the different types of tendons are: cross-sectional area, ultimate strength and relaxation loss. Table E.2 shows the relative comparison of the different types of tendons. Figure E.10 also shows plain bars, threaded bars and strands having different cross-sectional area going from left to right respectively.

For retrofitting of slopes in Nebraska, it is generally recommended to use bar tendons as the slopes are shallower and less capacity anchors would be demanded. Moreover, considering their stiffness and relatively lower cost, they could be an ideal choice for relatively shallower slopes. The relaxation loss expected may not be very high considering the lesser amount of anchor load that is going to be transferred to the ground.

Table E.2 Relative comparison of bar, wires and strand tendons

Bars	Wires & Strands
✓ Plain or threaded ✓ Simplest type of tendon ✓ Shallow/low capacity installation ✓ More easily protected against corrosion ✓ Stiff (in certain condition can be used as a drill rod) ✓ Easy for prestressing	✓ Higher tensile strength ✓ Easy for storage, manufacturing and transportation ✓ Higher elasticity ✓ Lower creep loss ✓ Strands are more accepTable and nowadays popular among designers and contractors

✓ Lower cost	

Since the design load obtained in the previous section is too low, the minimum prestressing bar grade has been adopted. From ASTM A722, 150 ksi grade bar having a nominal diameter of 26 mm was picked. Details of this bar is given below:

Bar grade: 150 ksi

Nominal diameter: 1 in. (26 mm)

Ultimate stress f_{pu}: 150 ksi (1035 MPa)

Nominal cross-sectional area A_{ps}: 0.85 in.^{2} (548 mm^2)

Ultimate strength $f_{pu}A_{ps}$: 127.5 kips (568 kN)

60 % of ultimate strength $0.6f_{pu}A_{ps}$: 76.5 kips (341 kN)

Figure E.10 Tendons for ground anchors: plain bars, threaded bars, strands from left to right

Per FHWA (1999) recommendation, the design load should not exceed 60% of the specified minimum tensile strength. The design anchor load was calculated as 9649.26 lb (42.92

kN). Thus, since 60% of the ultimate strength of the bar selected is greater than the expected design load, the design is satisfactory.

E.7.5 Check for Bond Strength between Grout and Prestressing Bar

The pull-out resistance at the grout-tendon interface is another factor that govern the overall capacity of ground anchors. Like the pull-out resistance mobilized between grout and soil interface, the gout-tendon interface resistance is also given by a similar equation as shown below (Kim 2007):

$$Q_{up} = \pi n D_e L_a f_{ub} \tag{18}$$

where Q_{up} = ultimate pull-out resistance; n = number of strands; D_e = effective diameter of strand; L_a = bond length; f_{up} = ultimate bond stress between grout and strand.

The maximum bond stress between grout and strand was computed from an empirical relation given in AASHTO 1990 as follows:

$$f_{up} = 4.8\sqrt{f_{ck}}/d \tag{19}$$

where f_{up} = maximum bond stress; f_{ck} = ultimate grout strength in MPa (compressive); d = diameter of strand.

The ultimate grout strength f_{ck} was considered as 20 MPa (Kim 2007). The diameter of the bar used is 26 mm. Therefore, the maximum bond stress will be:

$$f_{up} = 4.8\sqrt{20}/0.026 = 826 \ \text{kPa}$$

For the minimum bond length (i.e 12.21 m), the ultimate pull-out resistance is obtained using Equation 18 as follows:

$$Q_{up} = \pi(0.026)(12.21)(826) = 824 \text{ kN}$$

For a FS=2, the design pull-out resistance would be 412 kN. Comparison of the design pull-out resistance with the design anchor load clearly shows that the bond strength between grout and prestressing bar is quite enough to resist the tensile design load of 42.92 kN. Hence, design is adequate to prevent bond failure between grout and tendon selected.

Appendix A

Slice No.	α_i	Δx	h_i	unit weight, kN/m^3	W_i	Length (l_i)	$W_i \sin\alpha_i$	c_i'	$c_i'\Delta x_i$	$\sec\alpha_i$	$(c_i'\Delta x_i)(\sec\alpha_i)$
1	56.50	1.93	1.14	108.21	238.09	3.49	*198.47*	*125.00*	*241.25*	*1.81*	*436.77*
2	52.16	2.50	3.53	108.21	954.96	4.07	*753.89*	*125.00*	*312.5*	*1.63*	*509.10*
3	47.70	2.50	5.61	108.21	1517.66	3.71	*1122.08*	*125.00*	*312.5*	*1.49*	*464.11*
4	43.59	2.50	7.38	114.57	2113.82	3.45	*1456.87*	*188.00*	*470*	*1.38*	*648.67*
5	39.75	2.50	8.77	114.57	2511.95	3.25	*1605.56*	*188.00*	*470*	*1.30*	*611.13*
6	36.11	2.50	9.89	114.57	2832.74	3.09	*1668.71*	*188.00*	*470*	*1.24*	*581.63*
7	32.64	2.50	10.76	114.57	3081.93	2.97	*1661.52*	*188.00*	*470*	*1.19*	*558.04*
8	29.30	2.50	11.43	117.75	3364.78	2.87	*1645.90*	*209.00*	*522.5*	*1.15*	*599.06*
9	26.06	2.50	11.91	117.75	3506.08	2.78	*1539.54*	*209.00*	*522.5*	*1.11*	*581.57*
10	22.91	2.50	12.19	117.75	3588.51	2.71	*1396.28*	*209.00*	*522.5*	*1.09*	*567.20*
11	19.83	2.50	12.41	124.12	3850.75	2.66	*1305.65*	*272.00*	*680*	*1.06*	*722.82*
12	16.81	2.50	12.35	124.12	3832.13	2.61	*1107.70*	*272.00*	*680*	*1.04*	*710.32*
13	13.84	2.50	12.20	124.12	3785.58	2.57	*905.10*	*272.00*	*680*	*1.03*	*700.31*
14	10.90	2.50	11.92	124.12	3698.70	2.55	*699.06*	*272.00*	*680*	*1.02*	*692.48*
15	8.00	2.50	11.50	124.12	3568.38	2.52	*496.37*	*272.00*	*680*	*1.01*	*686.68*
16	5.11	2.50	10.95	124.12	3397.72	2.51	*302.48*	*272.00*	*680*	*1.00*	*682.71*
17	2.24	2.50	10.28	124.12	3189.82	2.50	*124.61*	*272.00*	*680*	*1.00*	*680.52*
18	-0.62	2.50	9.52	124.12	2954.00	2.50	*-31.95*	*272.00*	*680*	*1.00*	*680.04*
19	-3.49	2.50	8.56	124.12	2656.11	2.50	*-161.61*	*272.00*	*680*	*1.00*	*681.26*
20	-6.37	2.50	7.51	124.12	2330.31	2.52	*-258.41*	*272.00*	*680*	*1.01*	*684.22*
21	-9.26	2.50	6.35	124.12	1970.37	2.53	*-316.90*	*272.00*	*680*	*1.01*	*688.97*
22	-12.18	2.50	5.03	124.12	1560.78	2.56	*-329.13*	*272.00*	*680*	*1.02*	*695.64*
23	-14.95	2.21	3.66	124.12	1003.94	2.29	*-258.86*	*272.00*	*601.12*	*1.03*	*622.16*
24	-17.94	2.79	2.57	124.12	889.96	2.93	*-273.99*	*272.00*	*758.88*	*1.05*	*797.62*
25	-20.60	1.58	1.81	124.12	354.95	1.69	*-124.83*	*272.00*	*429.76*	*1.07*	*459.08*
26	-23.70	3.42	0.79	117.75	318.14	3.73	*-127.81*	209.00	*714.78*	*1.09*	*780.54*
							16106.29				**16522.66**

176